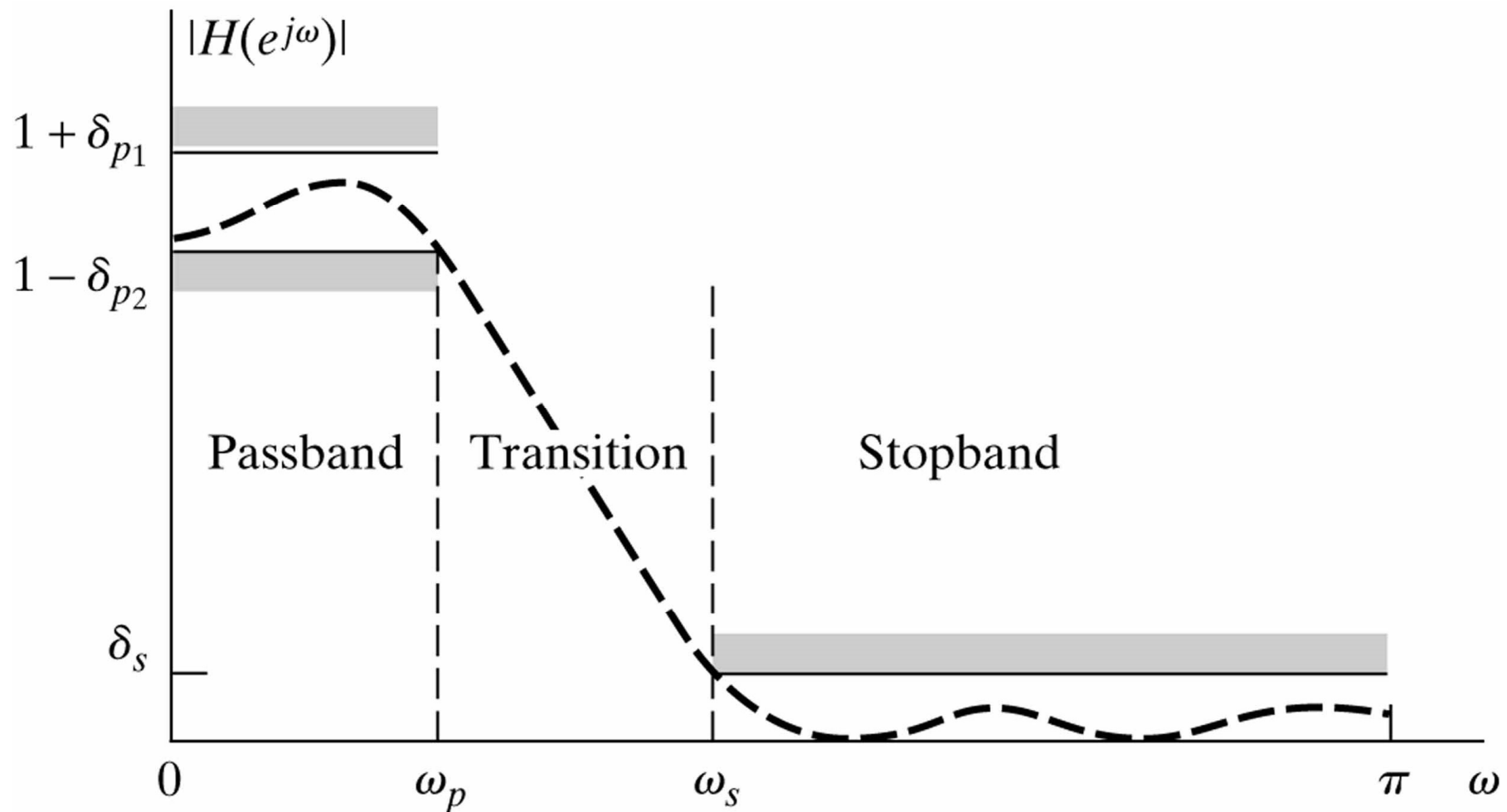
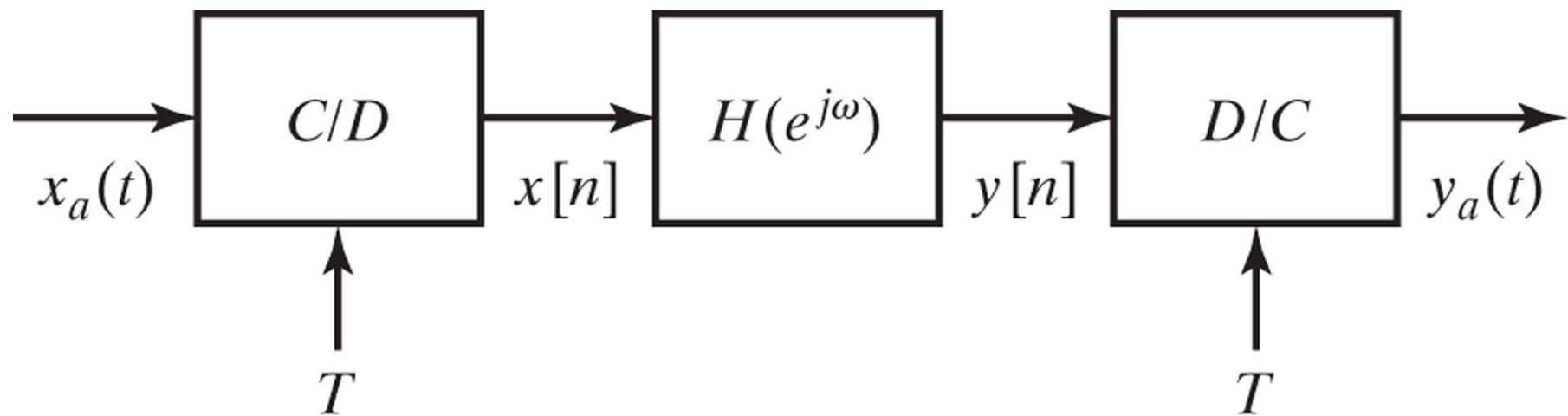


**Figure 7.1** Lowpass filter tolerance scheme.



**Figure 7.2** Basic system for discrete-time filtering of continuous-time signals.



**Figure 7.3** Illustration of aliasing in the impulse invariance design technique.

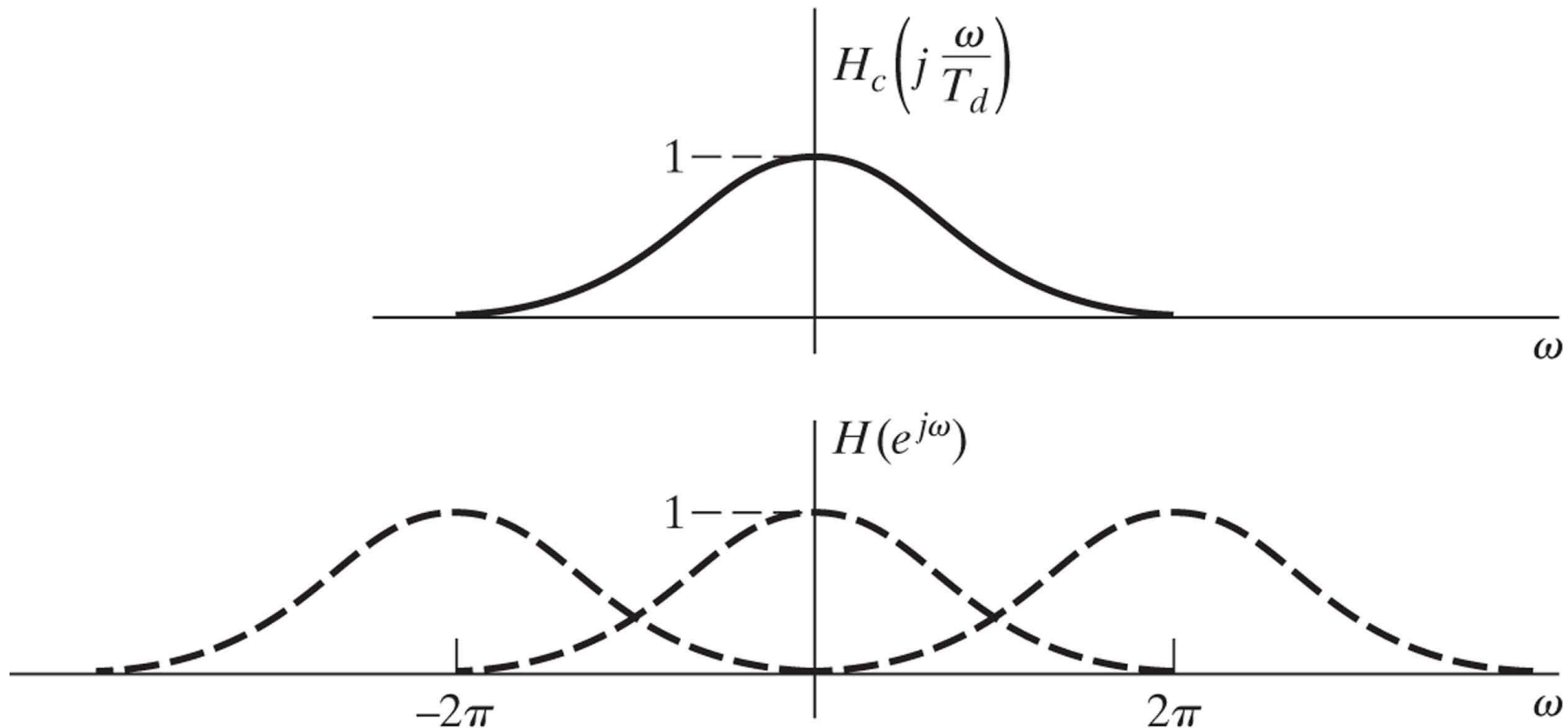


**Figure 7.4** s-plane locations for poles of  $H_c(s)H_c(-s)$  for 6<sup>th</sup>-order Butterworth filter in Example 7.2.

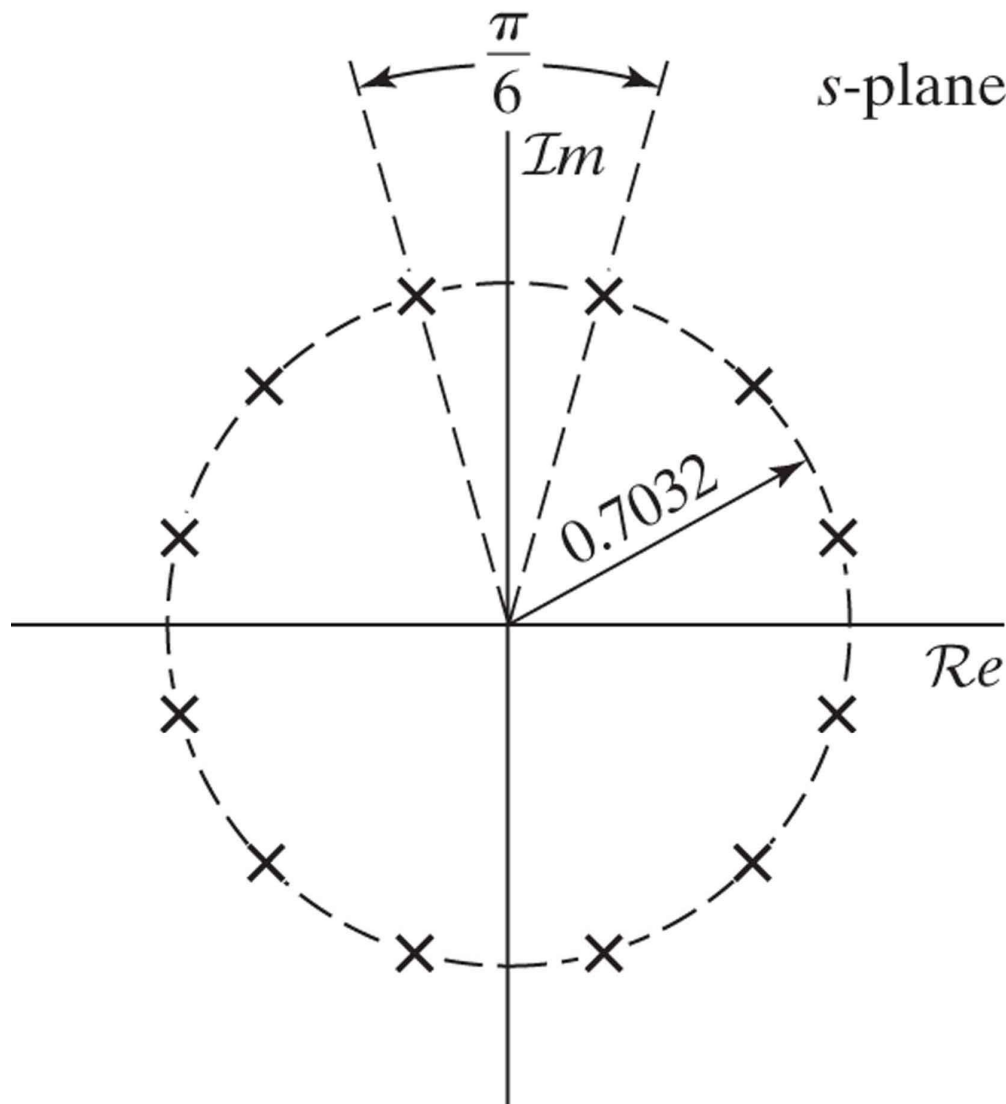


**Figure 7.5** Frequency response of 6<sup>th</sup>-order Butterworth filter transformed by impulse invariance. (a) Log magnitude in dB. (b) Magnitude. (c) Group delay.

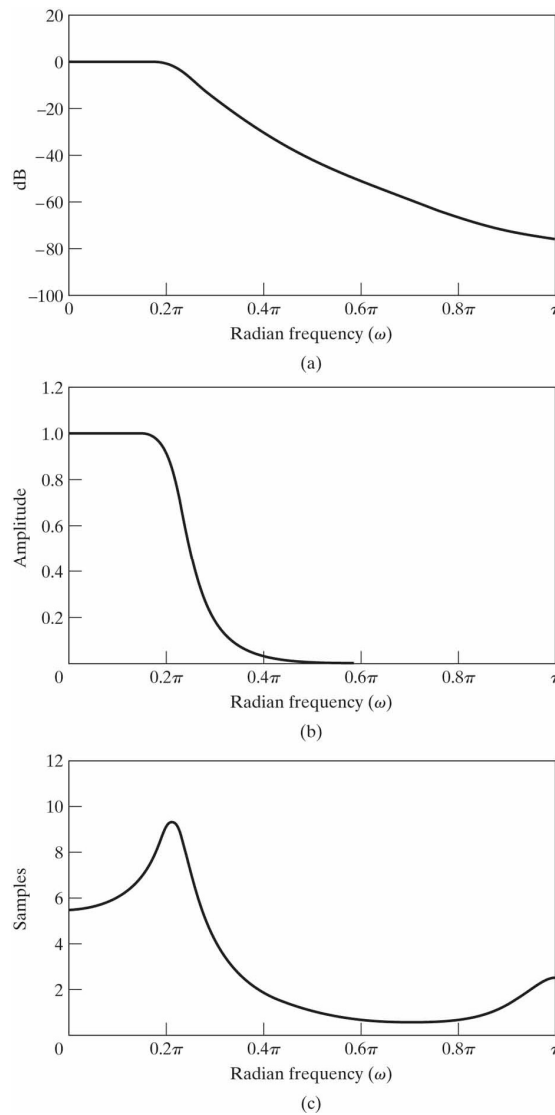


**Figure 7.6** Mapping of the  $s$ -plane onto the  $z$ -plane using the bilinear transformation.

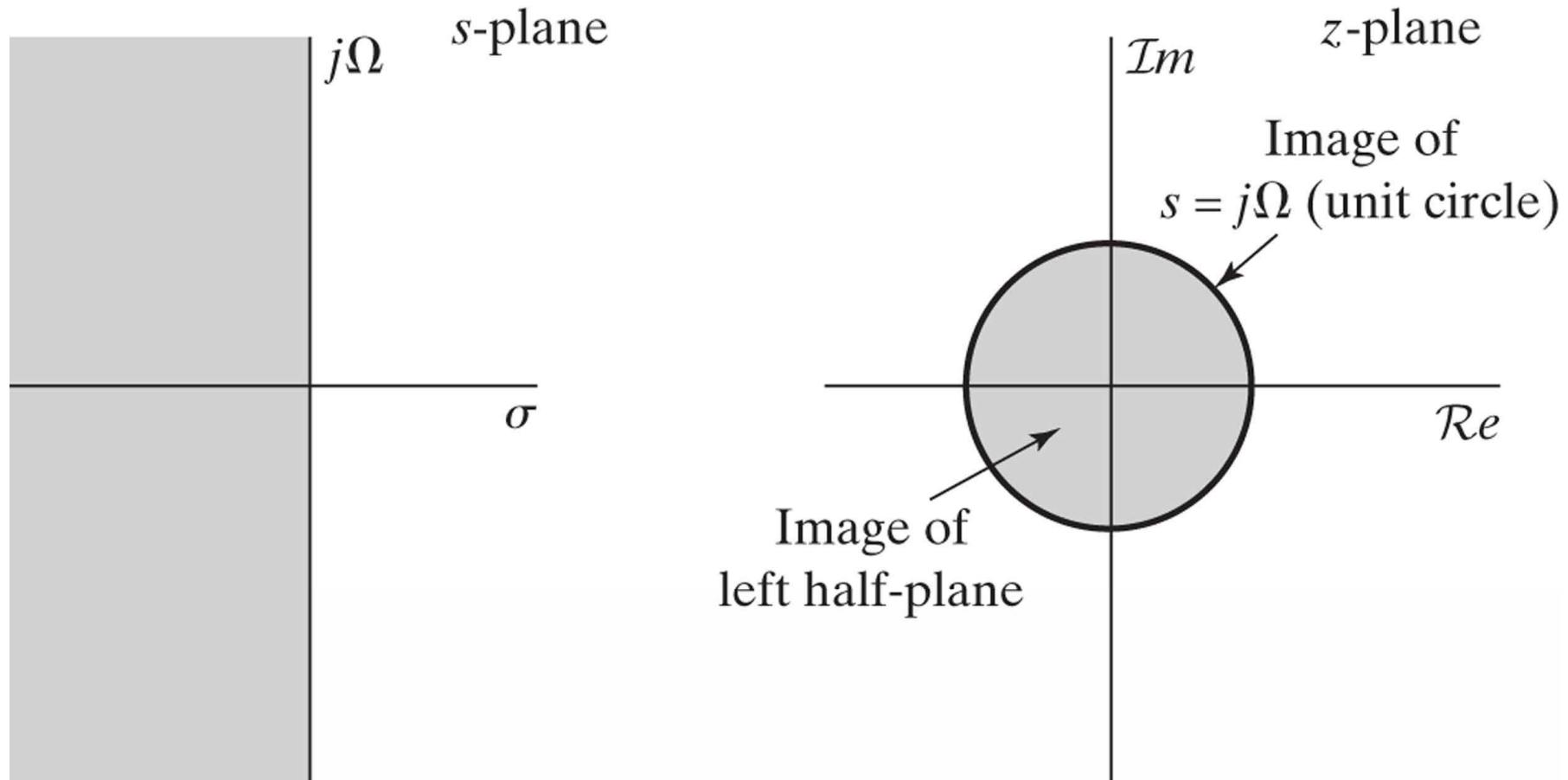


**Figure 7.7** Mapping of the continuous-time frequency axis onto the discrete-time frequency axis by bilinear transformation.

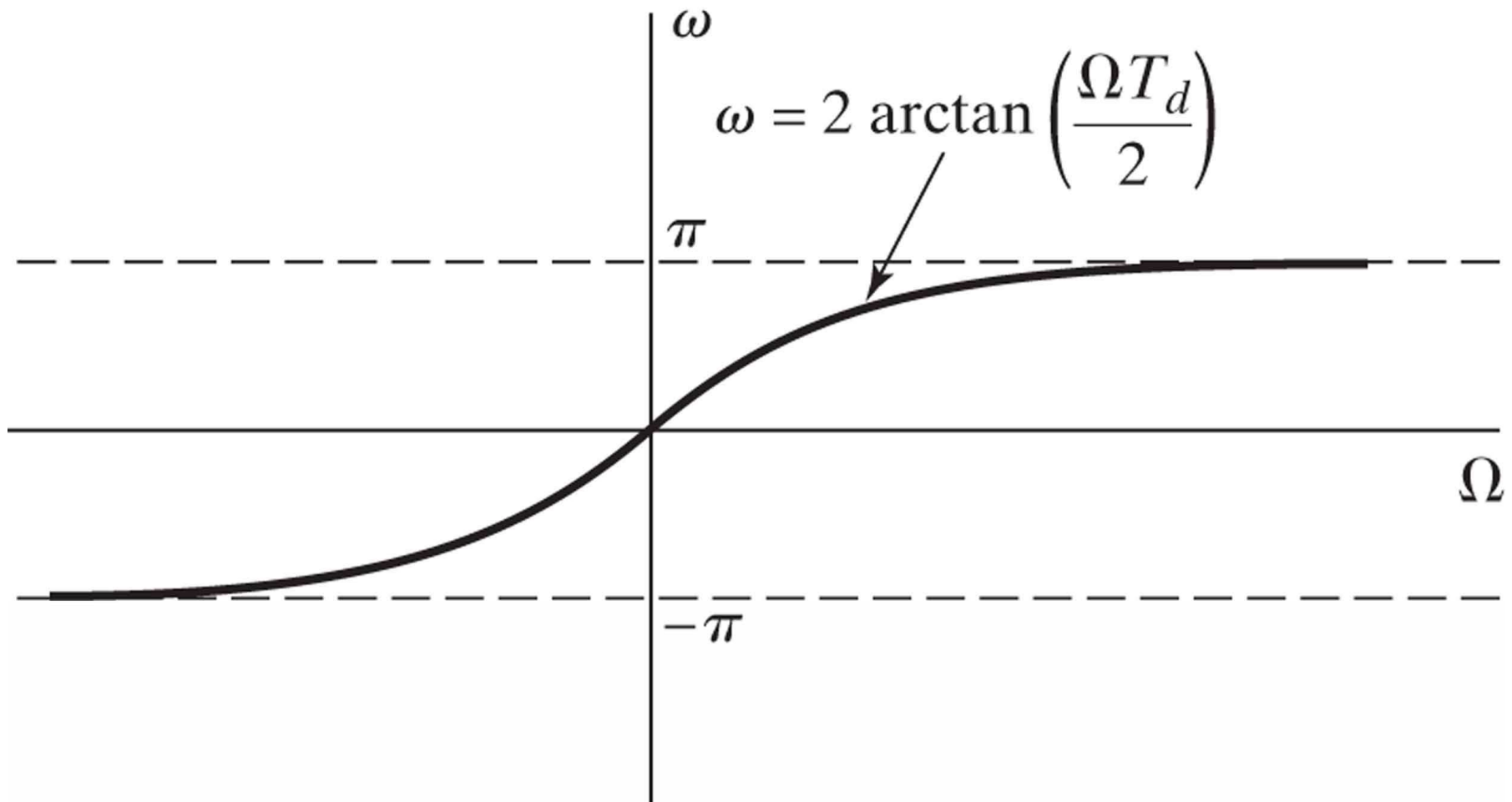


**Figure 7.8** Frequency warping inherent in the bilinear transformation of a continuous-time lowpass filter into a discrete-time lowpass filter. To achieve the desired discrete-time cutoff frequencies, the continuous-time cutoff frequencies must be prewarped as indicated.

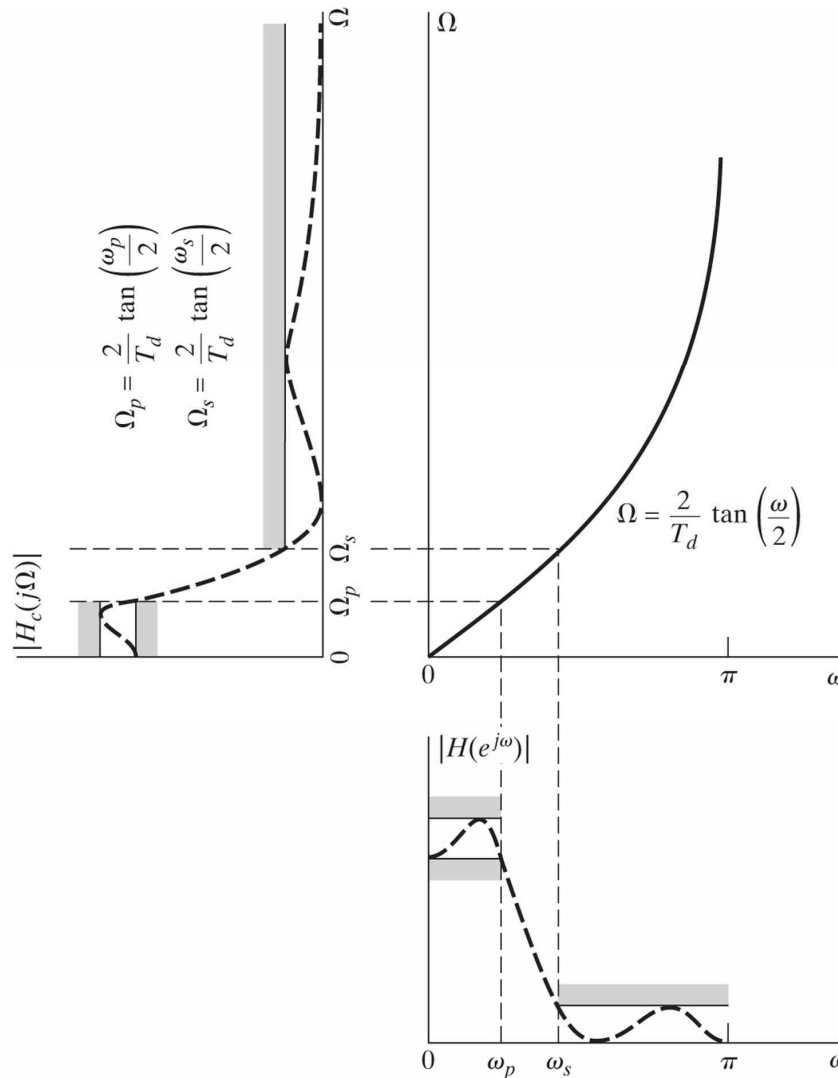


**Figure 7.9** Illustration of the effect of the bilinear transformation on a linearphase characteristic. (Dashed line is linear phase and solid line is phase resulting from bilinear transformation.)

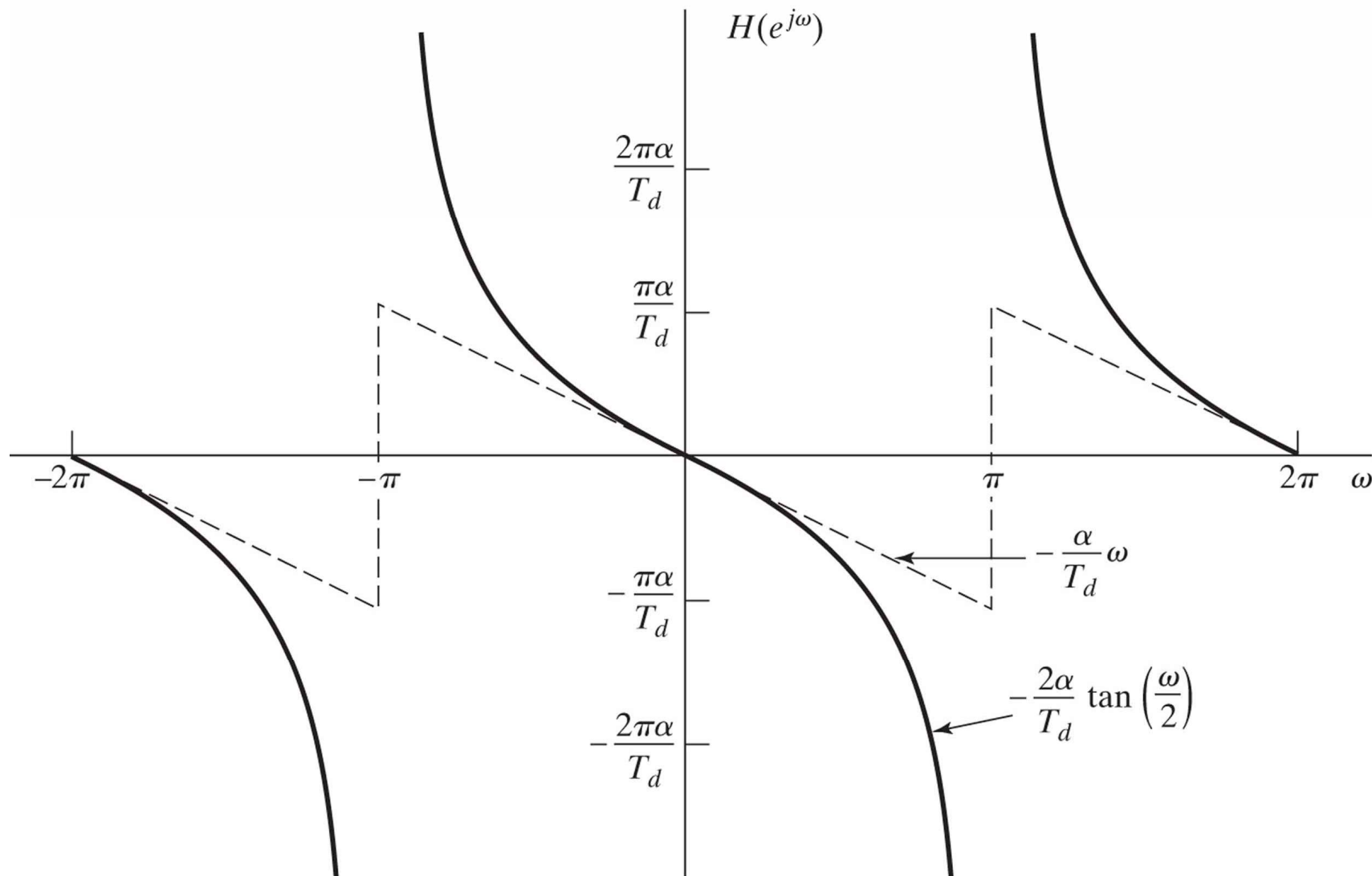


**Figure 7.10**  $s$ -plane locations for poles of  $H_c(s)H_c(-s)$  for 6<sup>th</sup>-order Butterworth filter in Example 7.3.

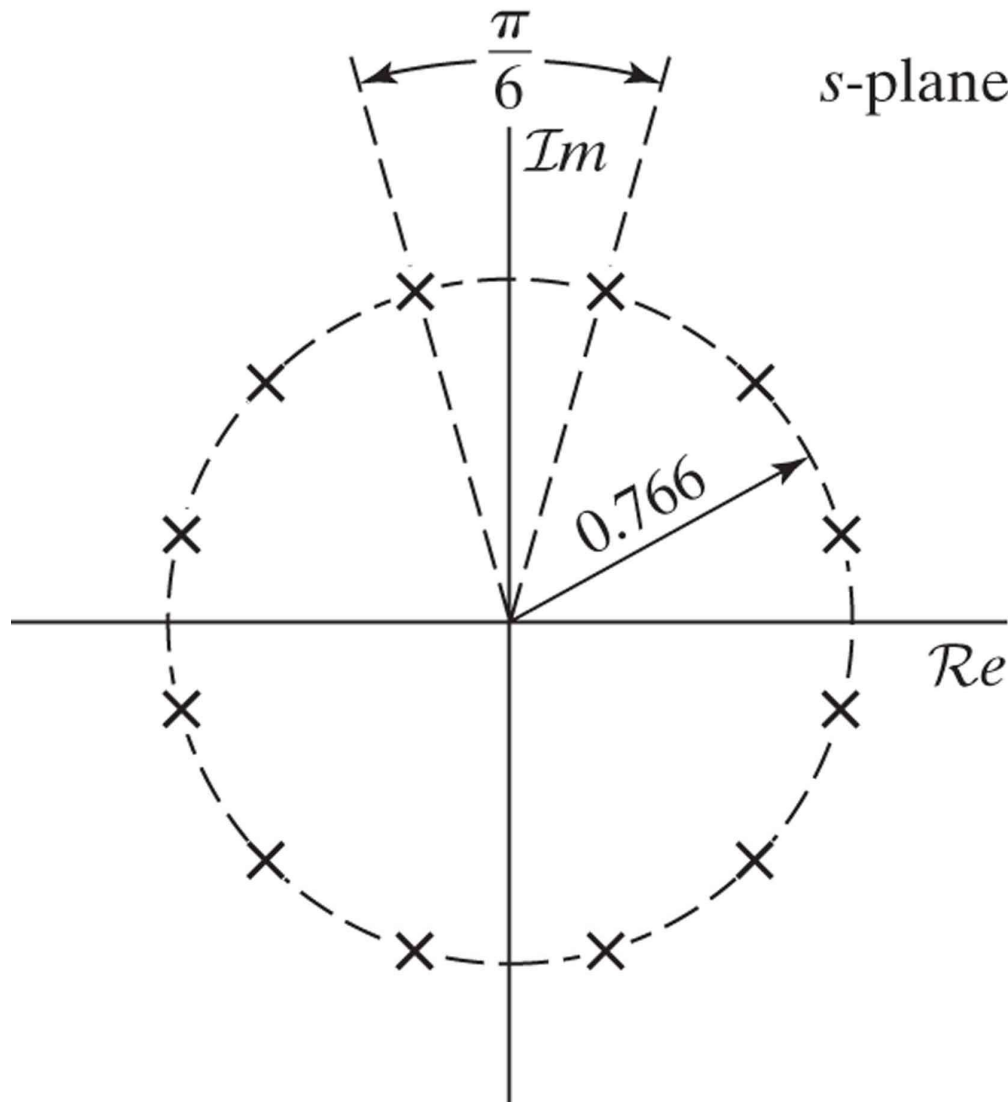


**Figure 7.11** Frequency response of 6<sup>th</sup>-order Butterworth filter transformed by bilinear transform. (a) Log magnitude in dB. (b) Magnitude. (c) Group delay.

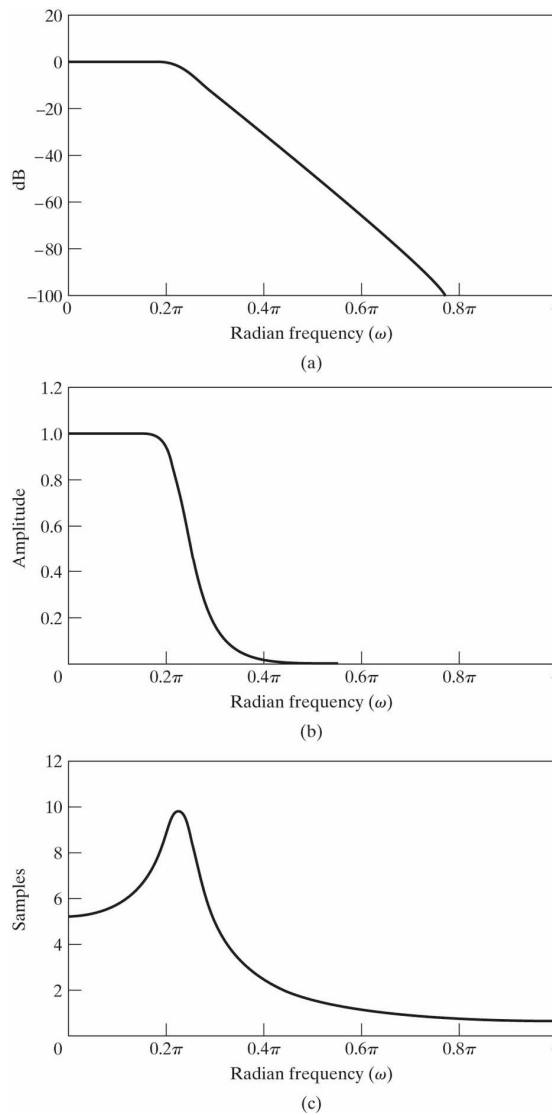


**Figure 7.12** Butterworth filter, 15<sup>th</sup>-order.

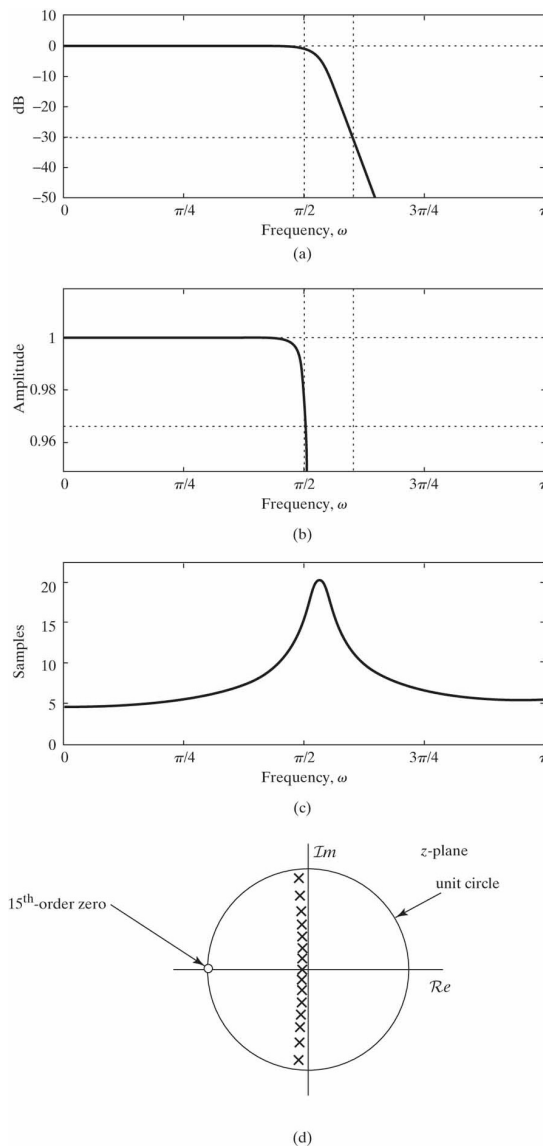


**Figure 7.13** Chebyshev Type I filter, 7<sup>th</sup>-order.

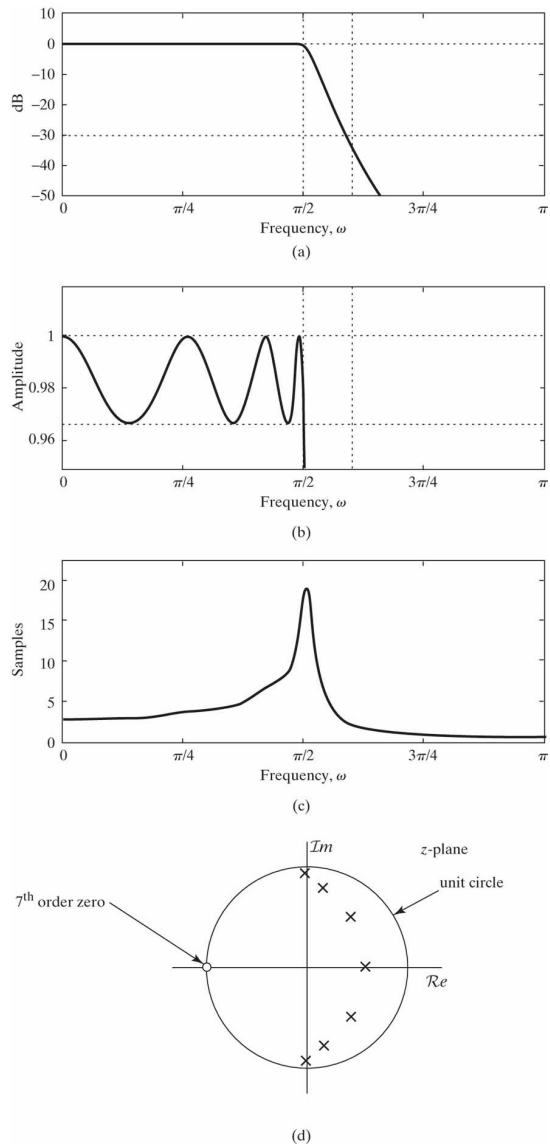


**Figure 7.14** Chebyshev Type II filter, 7<sup>th</sup>-order.

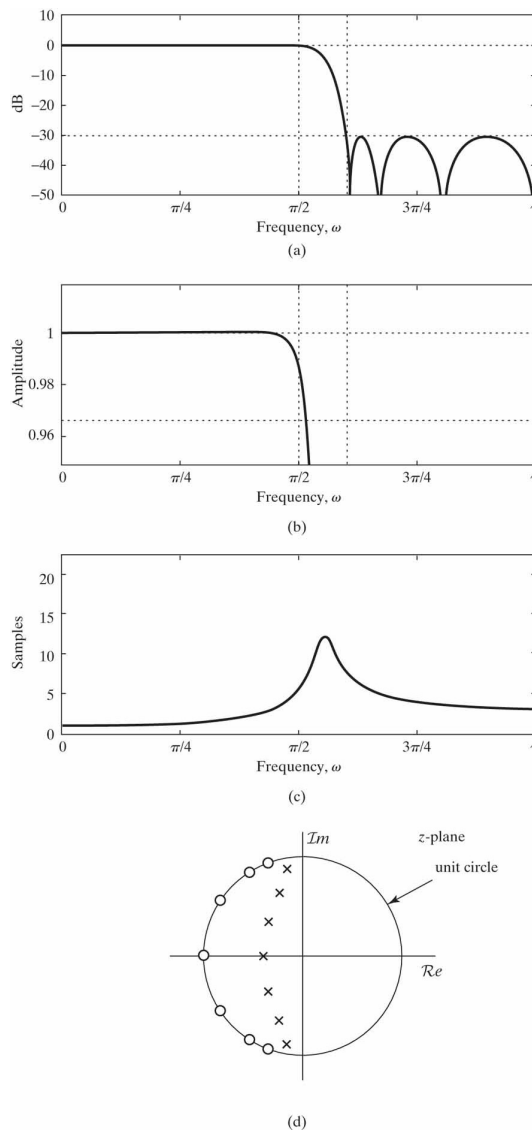


**Figure 7.15** Elliptic filter, 5<sup>th</sup>-order, exceeds design specifications.

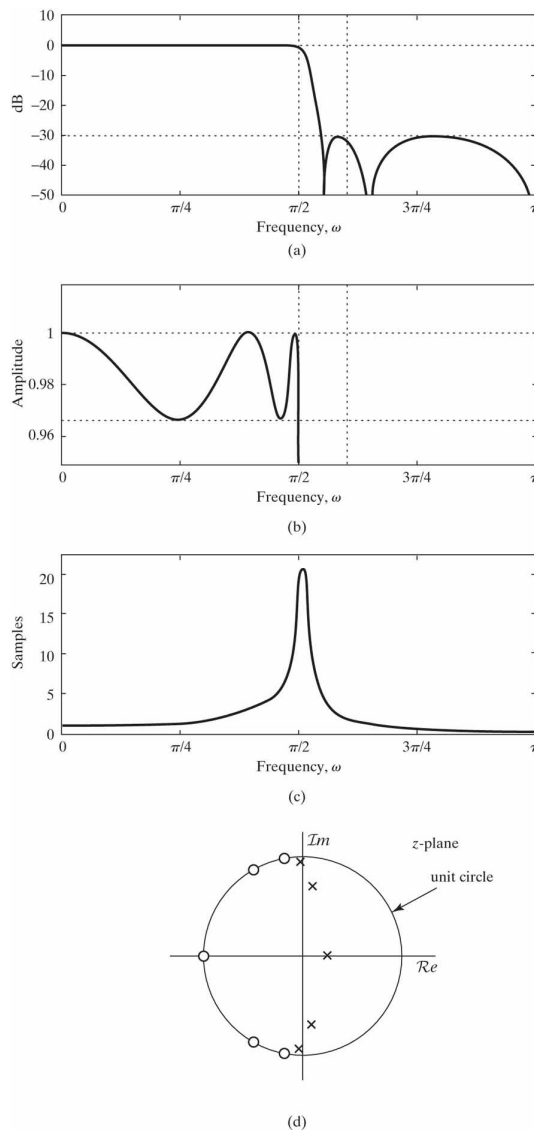


**Figure 7.16** Elliptic filter, 5<sup>th</sup>-order, minimizing the passband ripple.

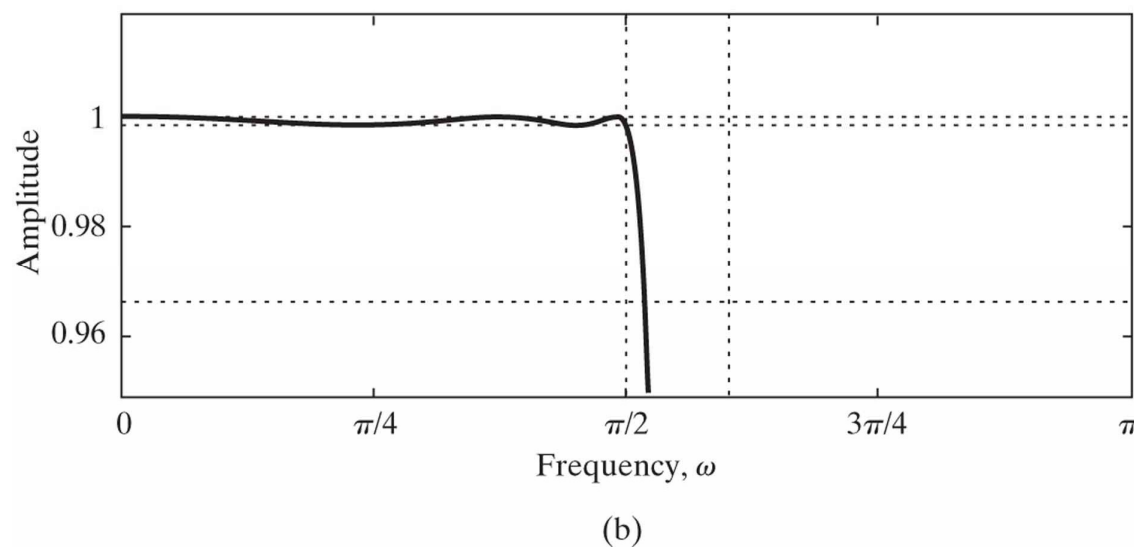
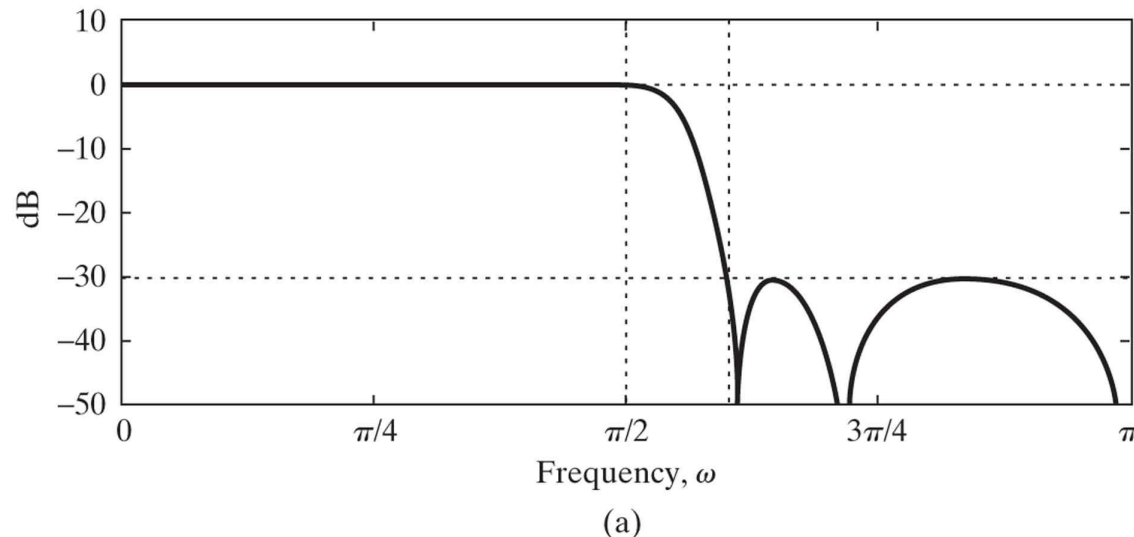


**Figure 7.17** Frequency response of 14<sup>th</sup>-order Butterworth filter in Example 7.5. (a) Log magnitude in dB. (b) Detailed plot of magnitude in passband. (c) Group delay.

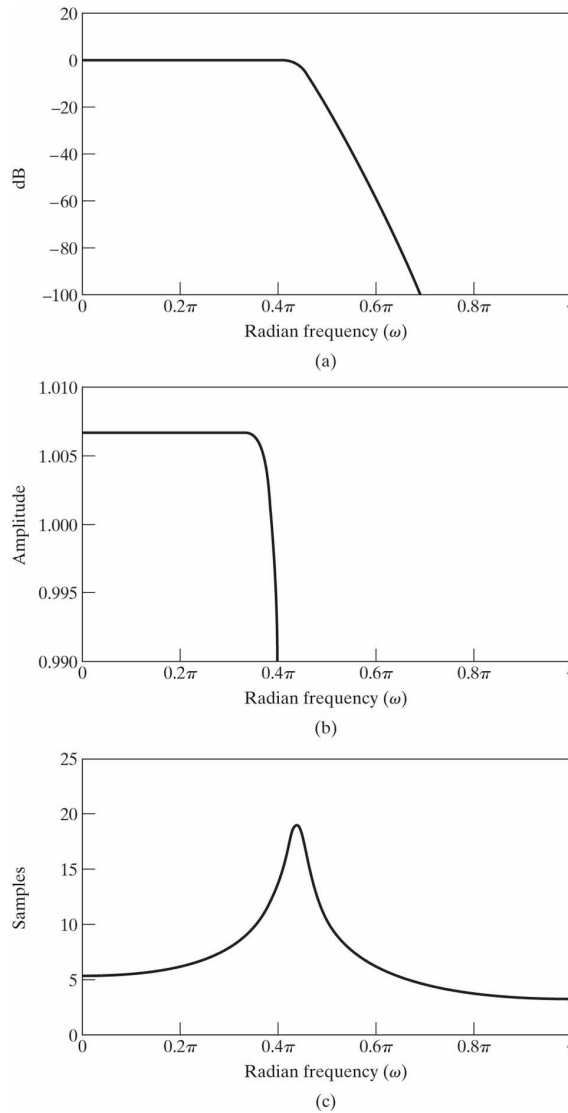


**Figure 7.17 (continued) (d)** Pole–zero plot of 14<sup>th</sup>-order Butterworth filter in Example 7.5.

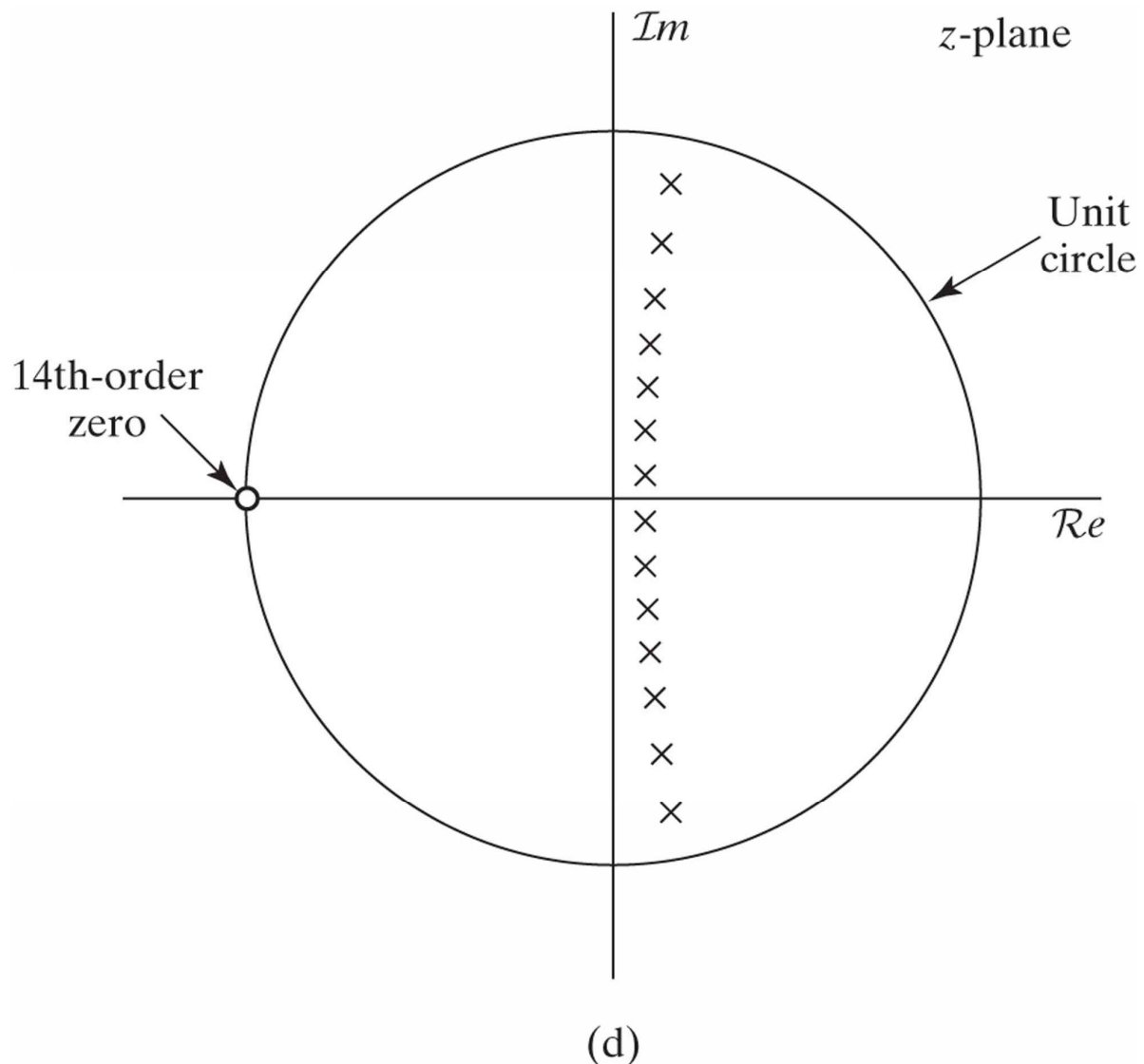


**Figure 7.18** Frequency response of 8<sup>th</sup>-order Chebyshev type I filter in Example 7.5. (a) Log magnitude in dB. (b) Detailed plot of magnitude in passband. (c) Group delay.

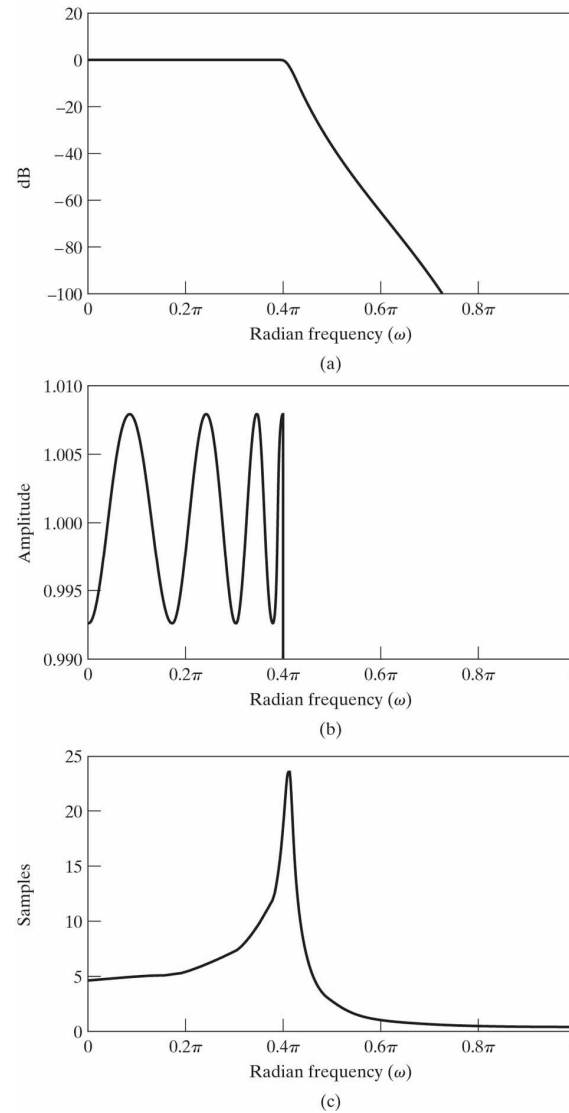


**Figure 7.19** Frequency response of 8<sup>th</sup>-order Chebyshev type II filter in Example 7.5. (a) Log magnitude in dB. (b) Detailed plot of magnitude in passband. (c) Group delay.

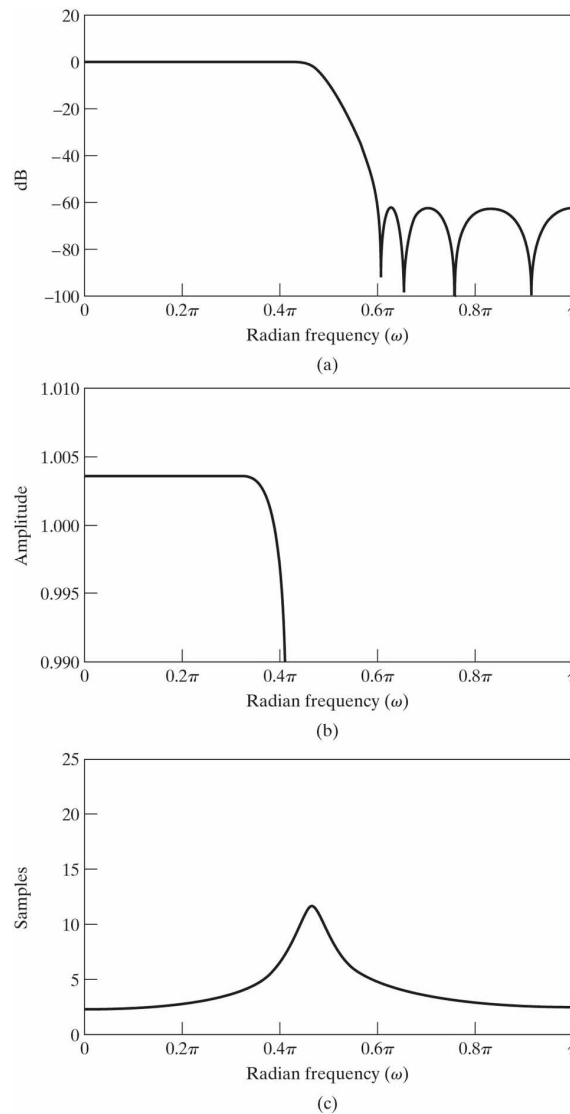


**Figure 7.20** Pole–zero plot of 8<sup>th</sup>-order Chebyshev filters in Example 7.5. (a) Type I. (b) Type II.

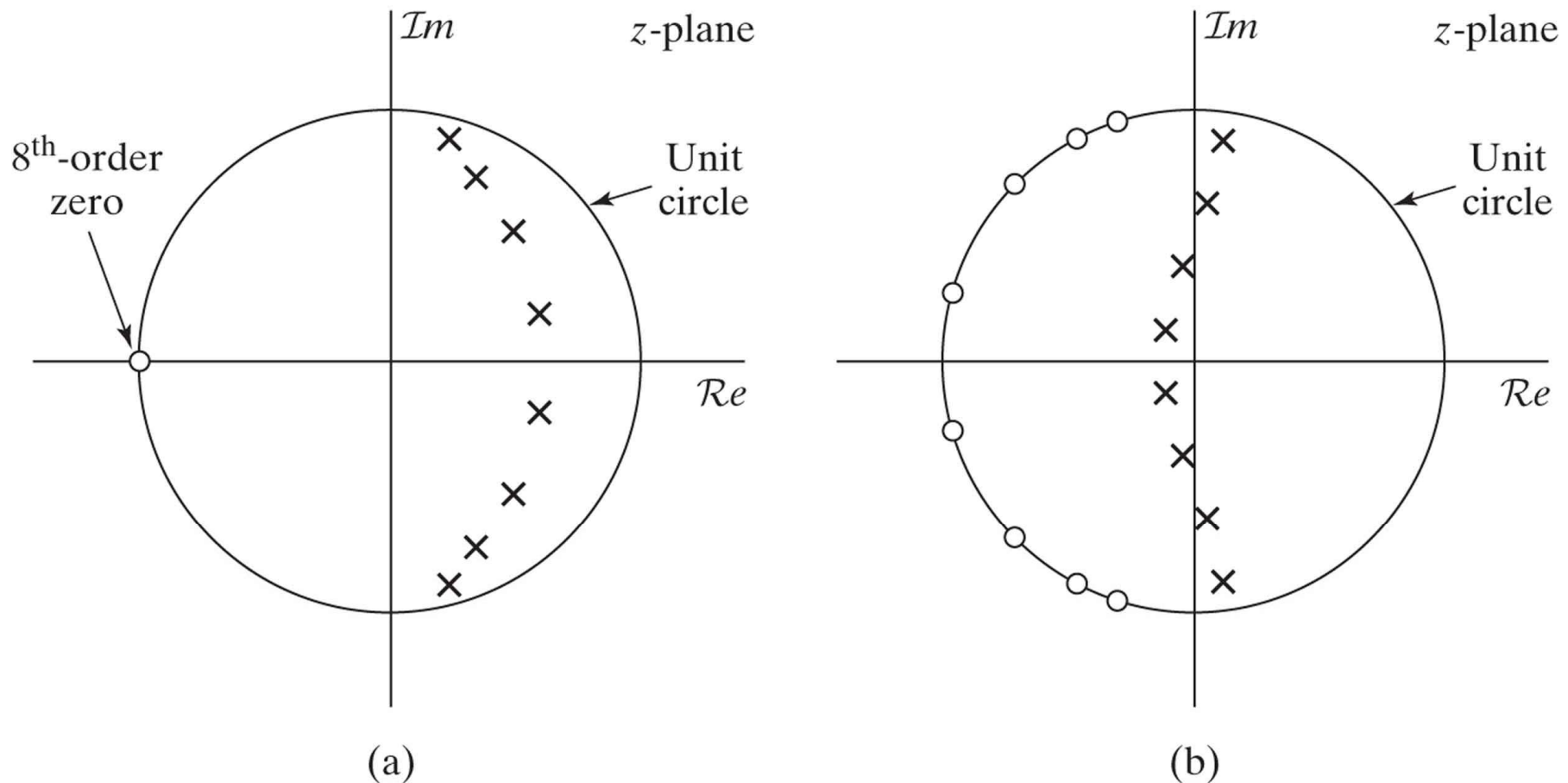


**Figure 7.21** Frequency response of 6<sup>th</sup>-order elliptic filter in Example 7.5. (a) Log magnitude in dB. (b) Detailed plot of magnitude in passband. (c) Group delay.

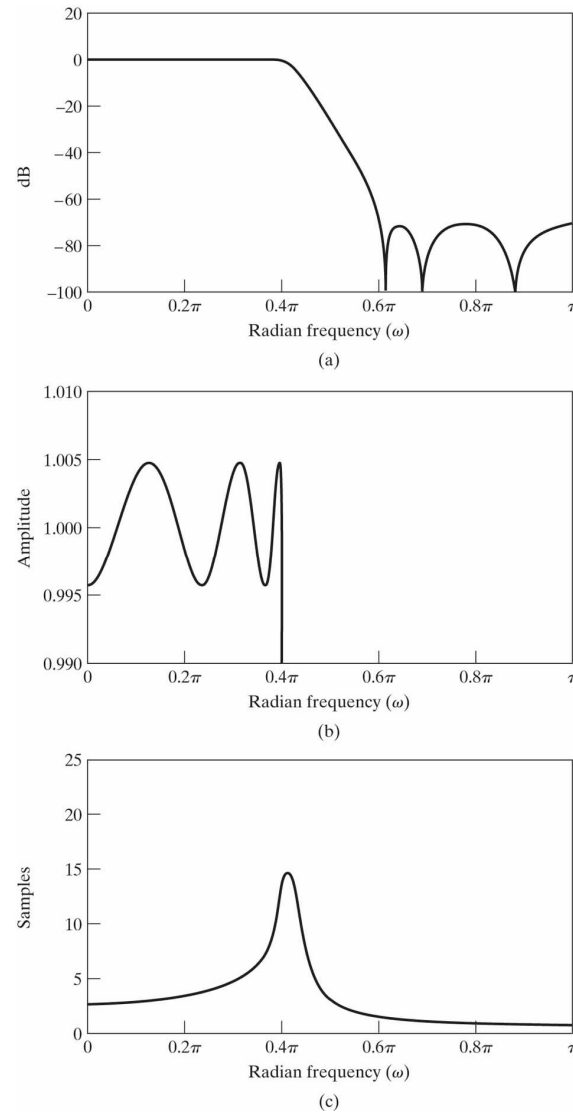


**Figure 7.22** Pole–zero plot of 6<sup>th</sup>-order elliptic filter in Example 7.5.

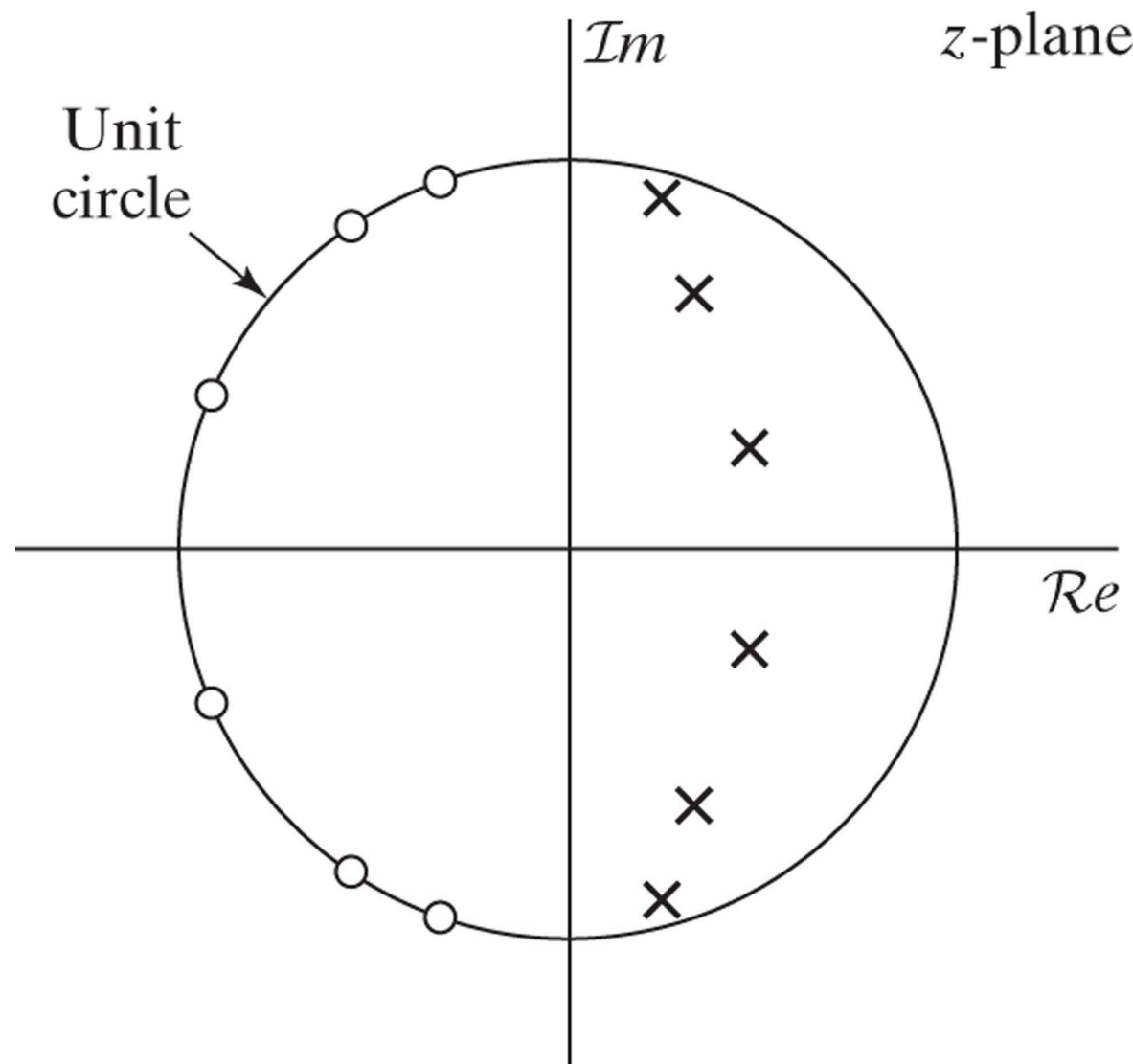


**Figure 7.23** Tolerance scheme for a multiband filter.

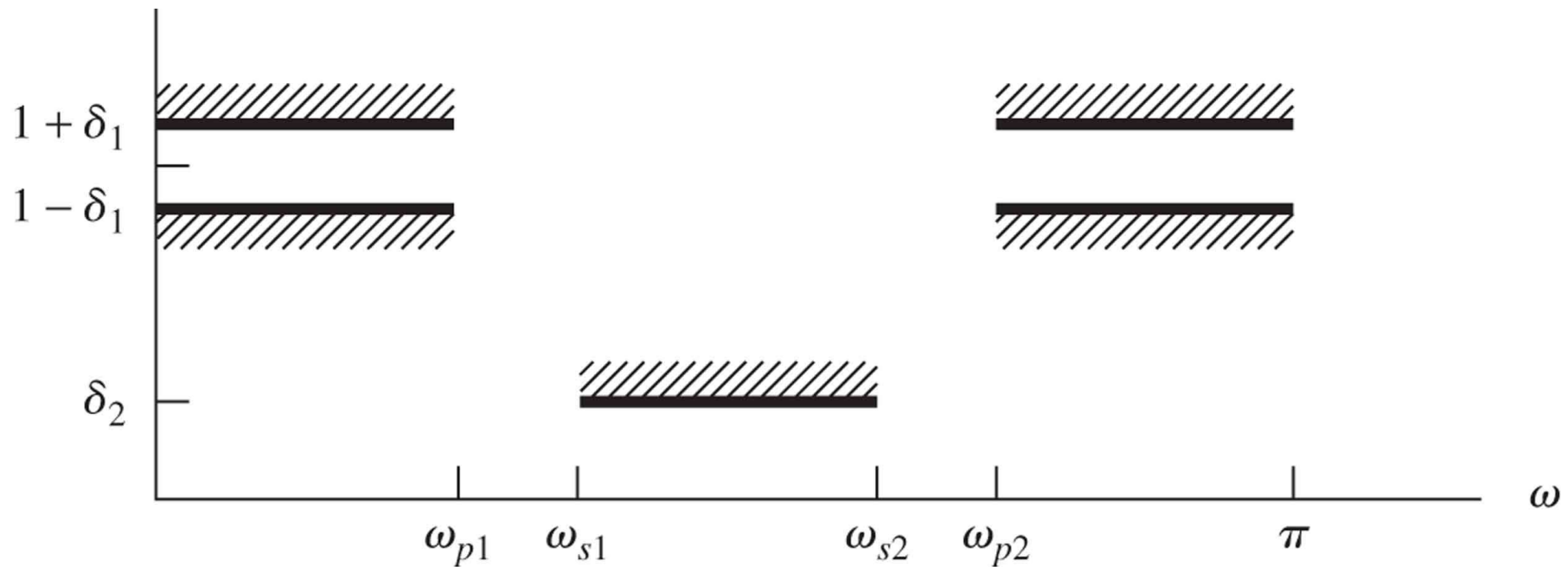


**Figure 7.24** Warping of the frequency scale in lowpass-to-lowpass transformation.

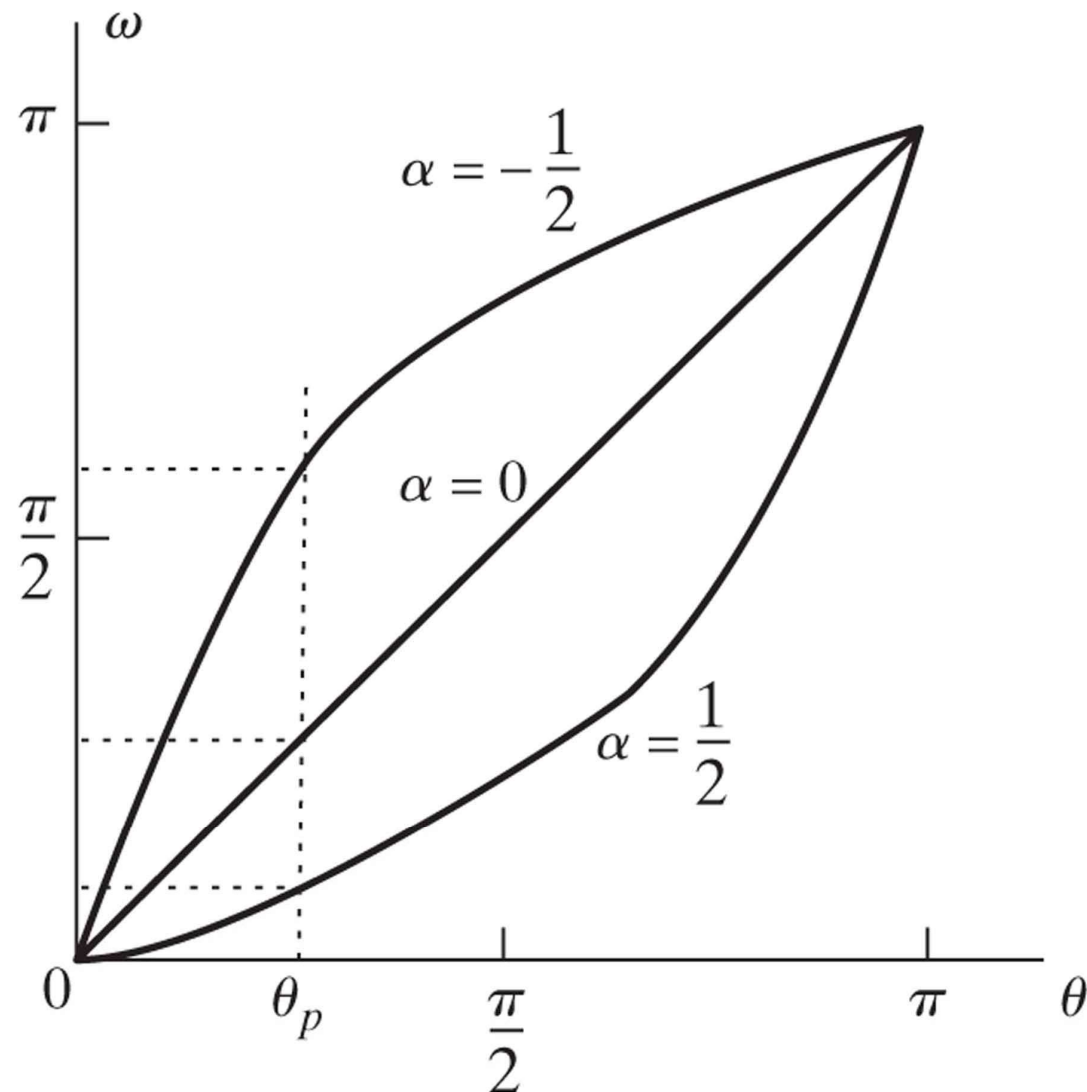


**Table 7.1** TRANSFORMATIONS FROM A LOWPASS DIGITAL FILTER PROTOTYPE OF CUTOFF FREQUENCY  $\theta_p$  TO HIGHPASS, BANDPASS, AND BANDSTOP FILTERS

**TABLE 7.1** TRANSFORMATIONS FROM A LOWPASS DIGITAL FILTER PROTOTYPE OF CUTOFF FREQUENCY  $\theta_p$  TO HIGHPASS, BANDPASS, AND BANDSTOP FILTERS

Filter Type	Transformations	Associated Design Formulas
Lowpass	$Z^{-1} = \frac{z^{-1} - \alpha}{1 - az^{-1}}$	$\alpha = \frac{\sin\left(\frac{\theta_p - \omega_p}{2}\right)}{\sin\left(\frac{\theta_p + \omega_p}{2}\right)}$ $\omega_p = \text{desired cutoff frequency}$
Highpass	$Z^{-1} = -\frac{z^{-1} + \alpha}{1 + \alpha z^{-1}}$	$\alpha = -\frac{\cos\left(\frac{\theta_p + \omega_p}{2}\right)}{\cos\left(\frac{\theta_p - \omega_p}{2}\right)}$ $\omega_p = \text{desired cutoff frequency}$
Bandpass	$Z^{-1} = -\frac{z^{-2} - \frac{2\alpha k}{k+1}z^{-1} + \frac{k-1}{k+1}}{\frac{k-1}{k+1}z^{-2} - \frac{2\alpha k}{k+1}z^{-1} + 1}$	$\alpha = \frac{\cos\left(\frac{\omega_{p2} + \omega_{p1}}{2}\right)}{\cos\left(\frac{\omega_{p2} - \omega_{p1}}{2}\right)}$ $k = \cot\left(\frac{\omega_{p2} - \omega_{p1}}{2}\right) \tan\left(\frac{\theta_p}{2}\right)$ $\omega_{p1} = \text{desired lower cutoff frequency}$ $\omega_{p2} = \text{desired upper cutoff frequency}$
Bandstop	$Z^{-1} = \frac{z^{-2} - \frac{2\alpha}{1+k}z^{-1} + \frac{1-k}{1+k}}{\frac{1-k}{1+k}z^{-2} - \frac{2\alpha}{1+k}z^{-1} + 1}$	$\alpha = \frac{\cos\left(\frac{\omega_{p2} + \omega_{p1}}{2}\right)}{\cos\left(\frac{\omega_{p2} - \omega_{p1}}{2}\right)}$ $k = \tan\left(\frac{\omega_{p2} - \omega_{p1}}{2}\right) \tan\left(\frac{\theta_p}{2}\right)$ $\omega_{p1} = \text{desired lower cutoff frequency}$ $\omega_{p2} = \text{desired upper cutoff frequency}$

**Figure 7.25** Frequency response of 4<sup>th</sup>-order Chebyshev lowpass filter. (a) Log magnitude in dB. (b) Magnitude. (c) Group delay.

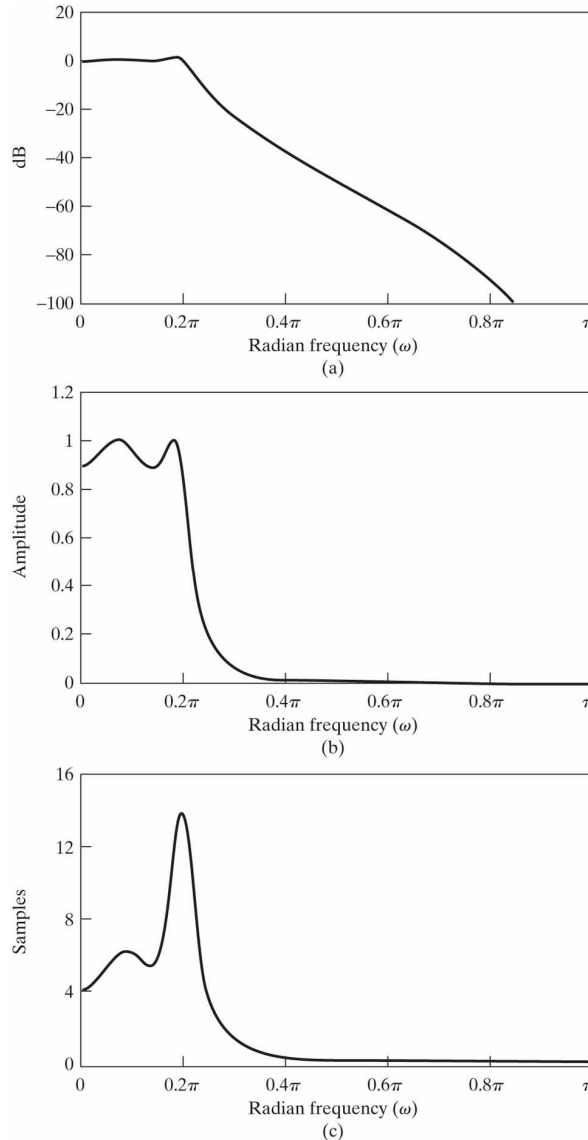


**Figure 7.26** Frequency response of 4<sup>th</sup>-order Chebyshev highpass filter obtained by frequency transformation. (a) Log magnitude in dB. (b) Magnitude. (c) Group delay.

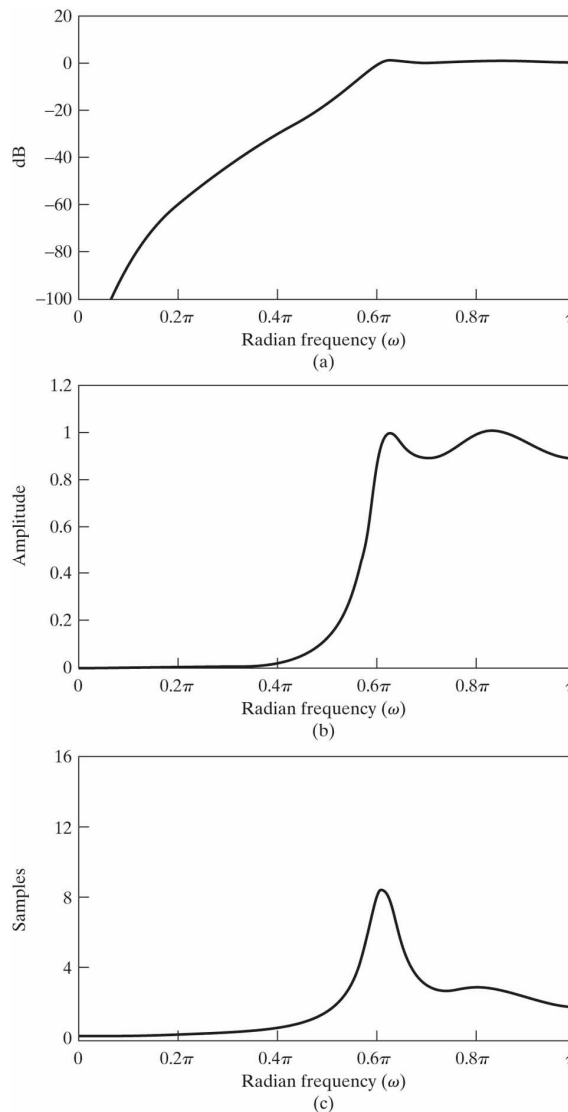
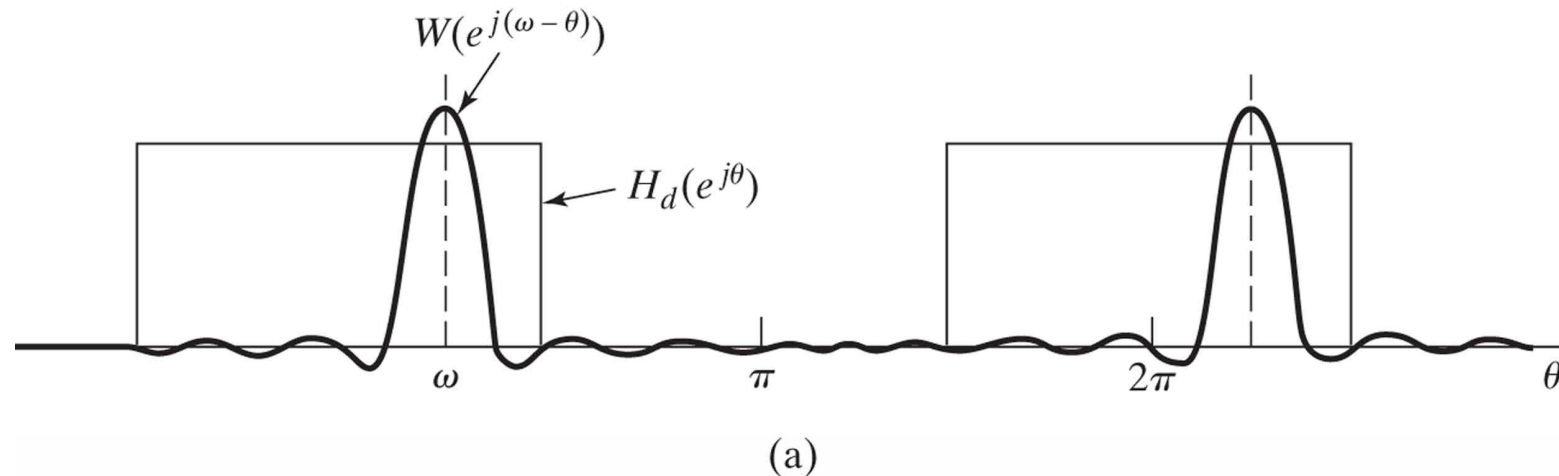
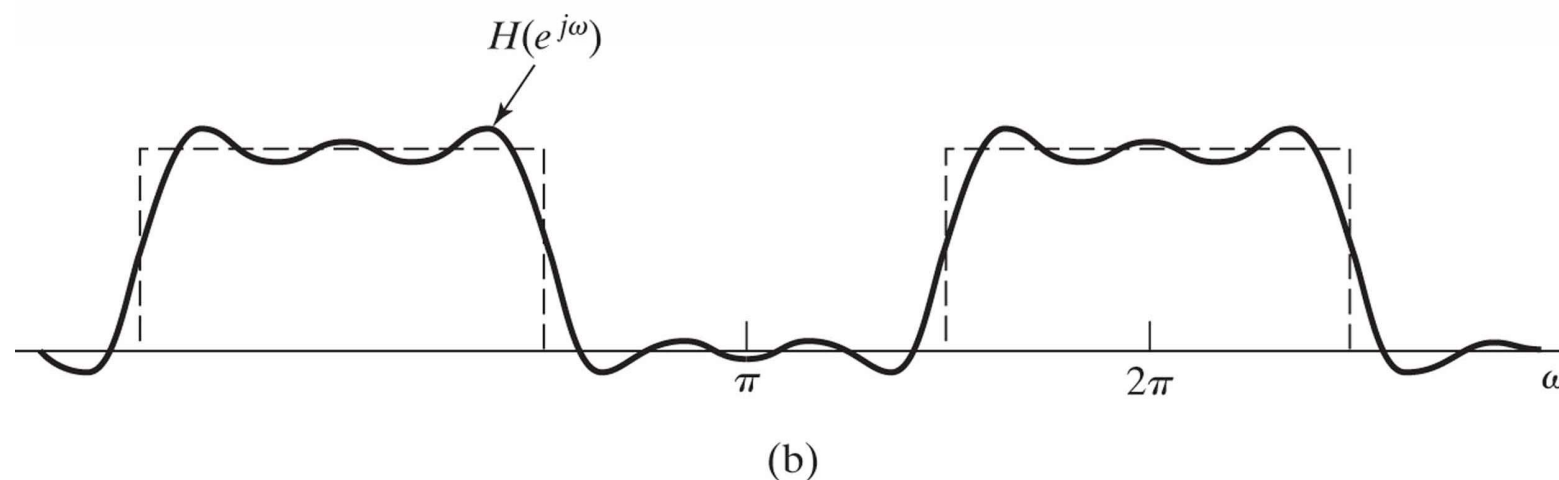


**Figure 7.27** (a) Convolution process implied by truncation of the ideal impulse response. (b) Typical approximation resulting from windowing the ideal impulse response.



(a)



(b)

**Figure 7.28** Magnitude of the Fourier transform of a rectangular window ( $M = 7$ ).

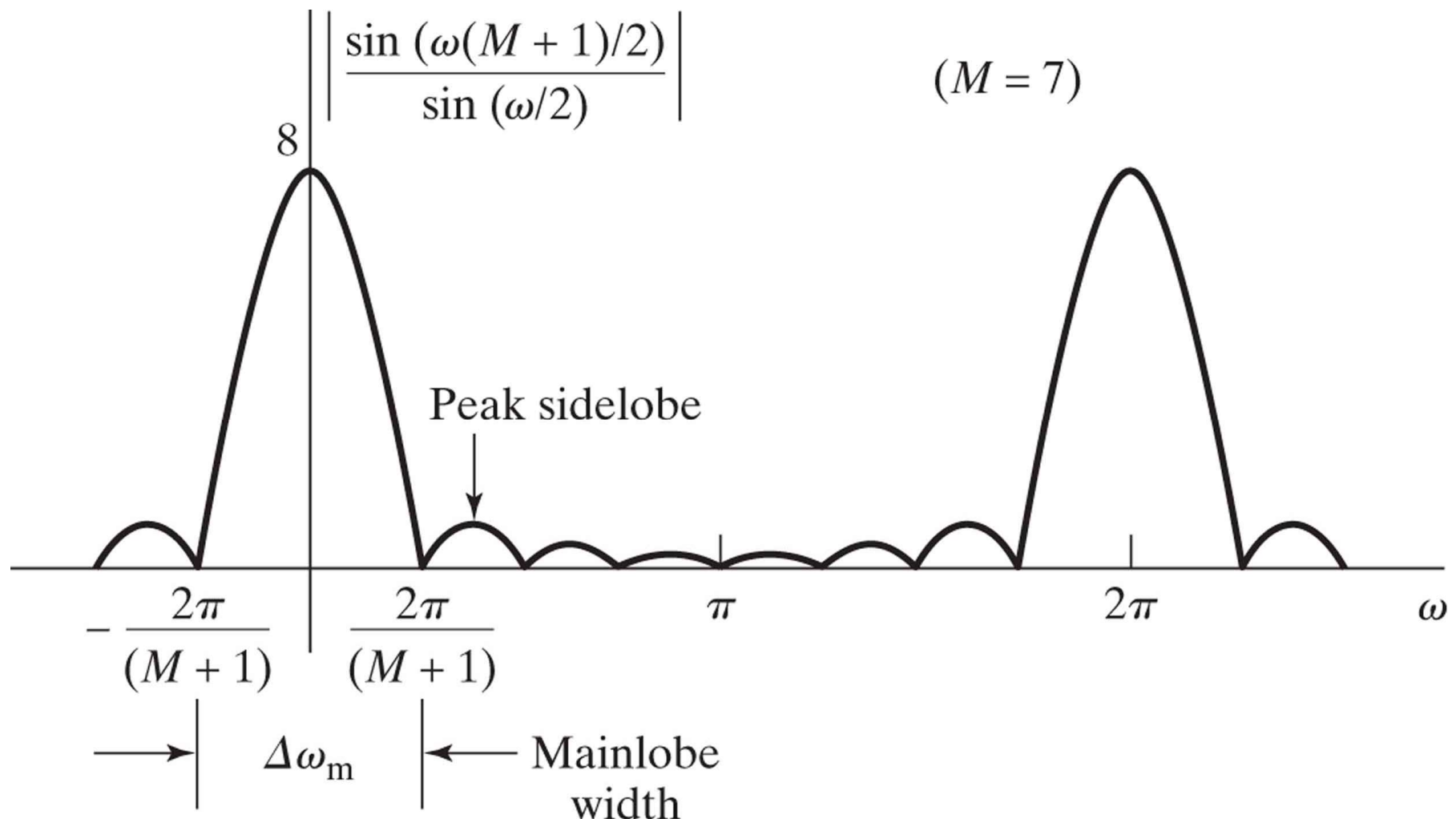


**Figure 7.29** Commonly used windows.

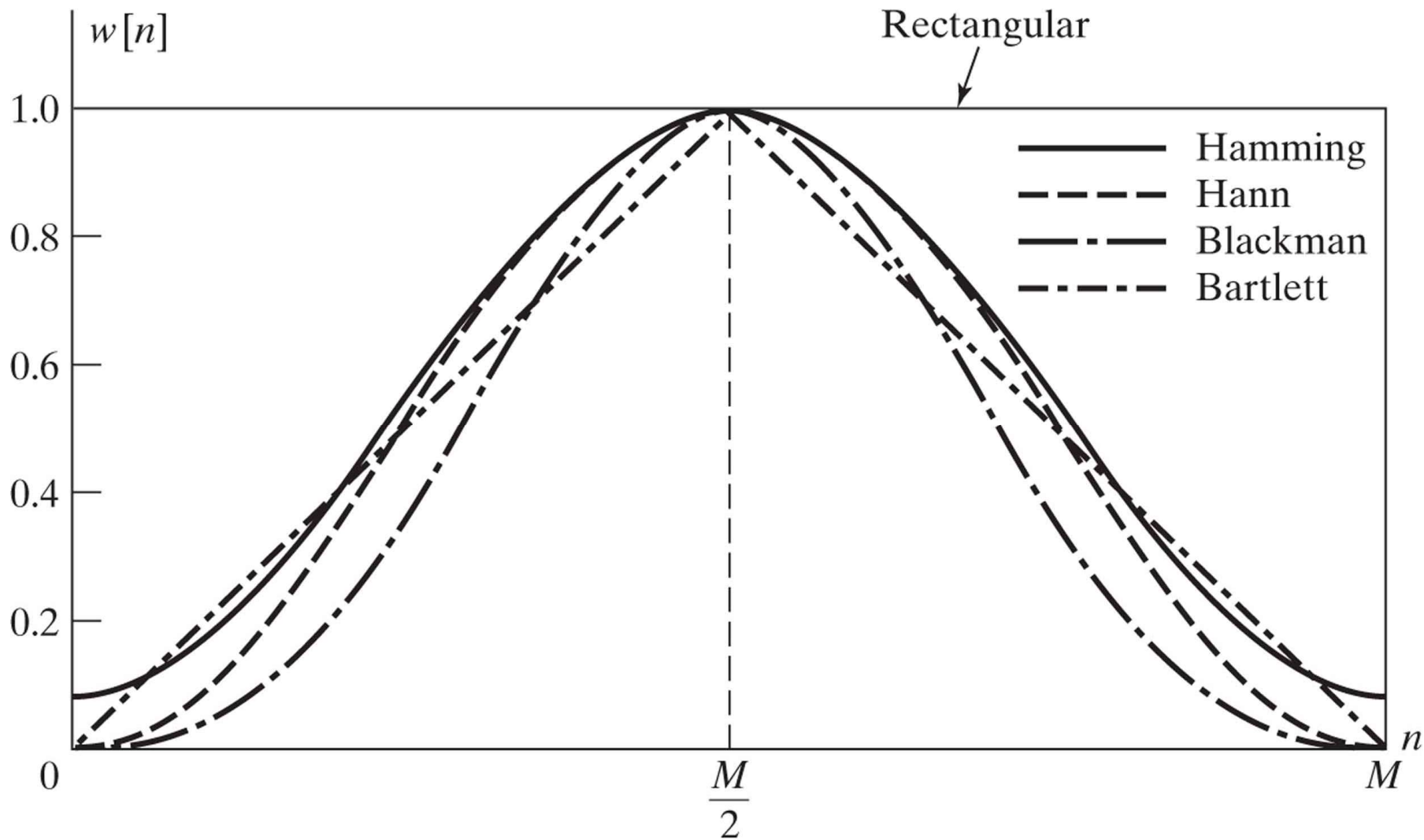


**Figure 7.30** Fourier transforms (log magnitude) of windows of Figure 7.29 with  $M = 50$ . (a) Rectangular. (b) Bartlett.

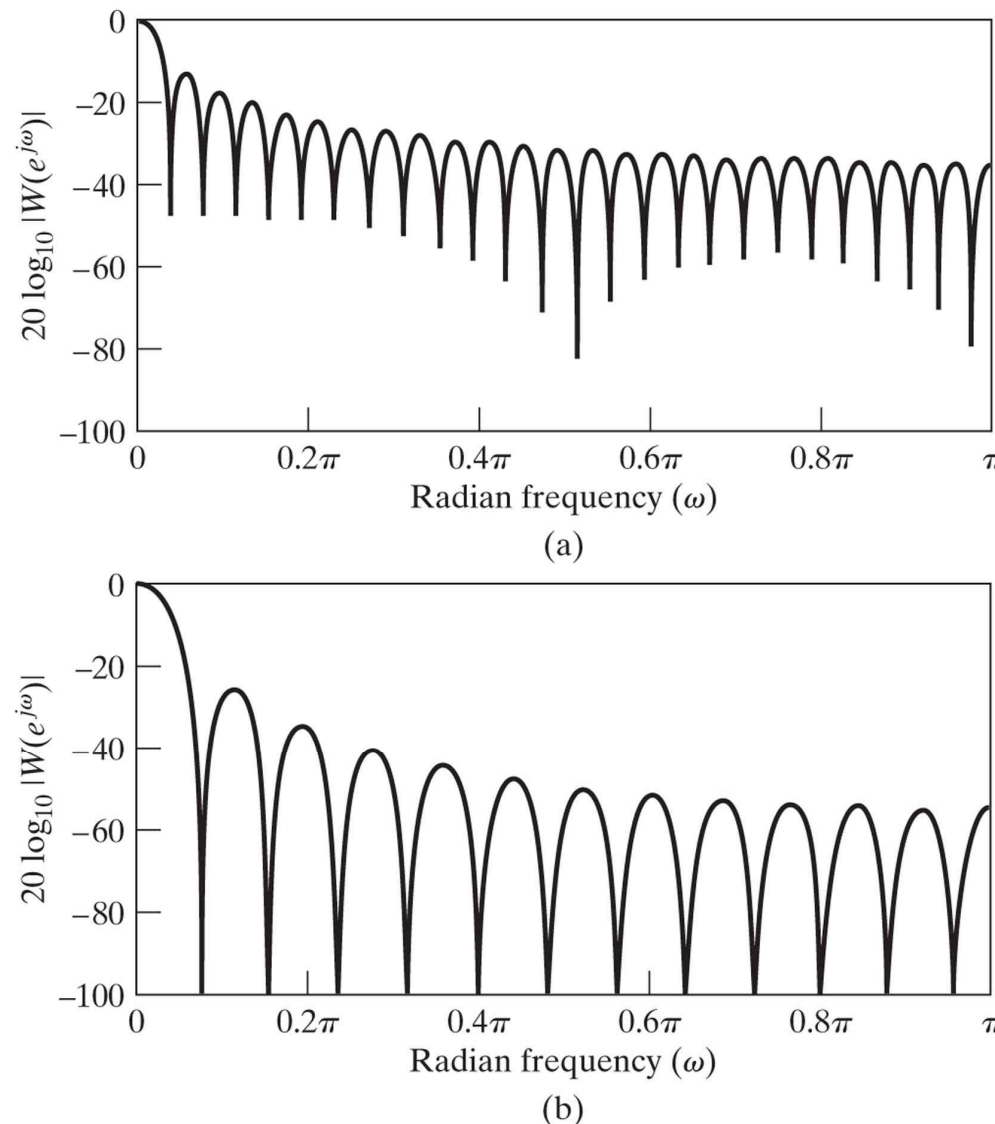
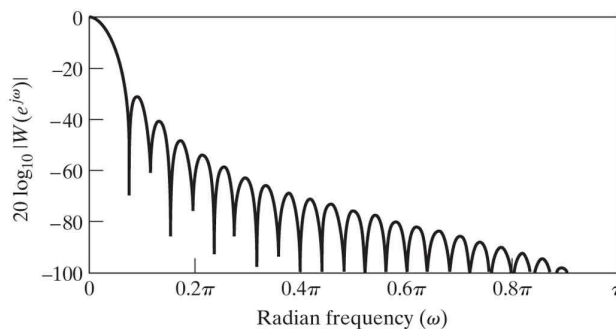
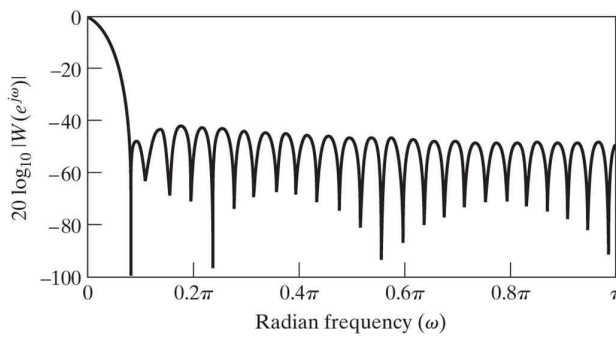


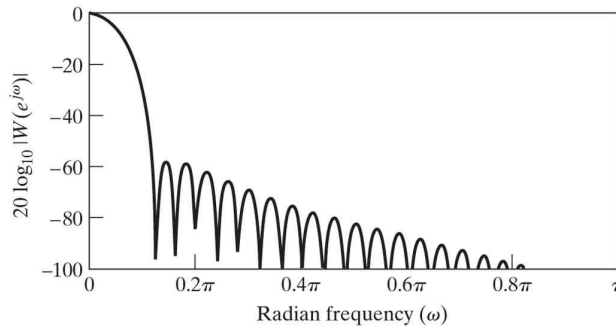
**Figure 7.30 (continued)** (c) Hann. (d) Hamming. (e) Blackman.



(c)



(d)



(e)

**Table 7.2** COMPARISON OF COMMONLY USED WINDOWS

**TABLE 7.2** COMPARISON OF COMMONLY USED WINDOWS

Type of Window	Peak Side-Lobe Amplitude (Relative)	Approximate Width of Main Lobe	Peak Approximation Error, $20 \log_{10} \delta$ (dB)	Equivalent Kaiser Window, $\beta$	Transition Width of Equivalent Kaiser Window
Rectangular	-13	$4\pi/(M + 1)$	-21	0	$1.81\pi/M$
Bartlett	-25	$8\pi/M$	-25	1.33	$2.37\pi/M$
Hann	-31	$8\pi/M$	-44	3.86	$5.01\pi/M$
Hamming	-41	$8\pi/M$	-53	4.86	$6.27\pi/M$
Blackman	-57	$12\pi/M$	-74	7.04	$9.19\pi/M$

**Figure 7.31** Illustration of type of approximation obtained at a discontinuity of the ideal frequency response.

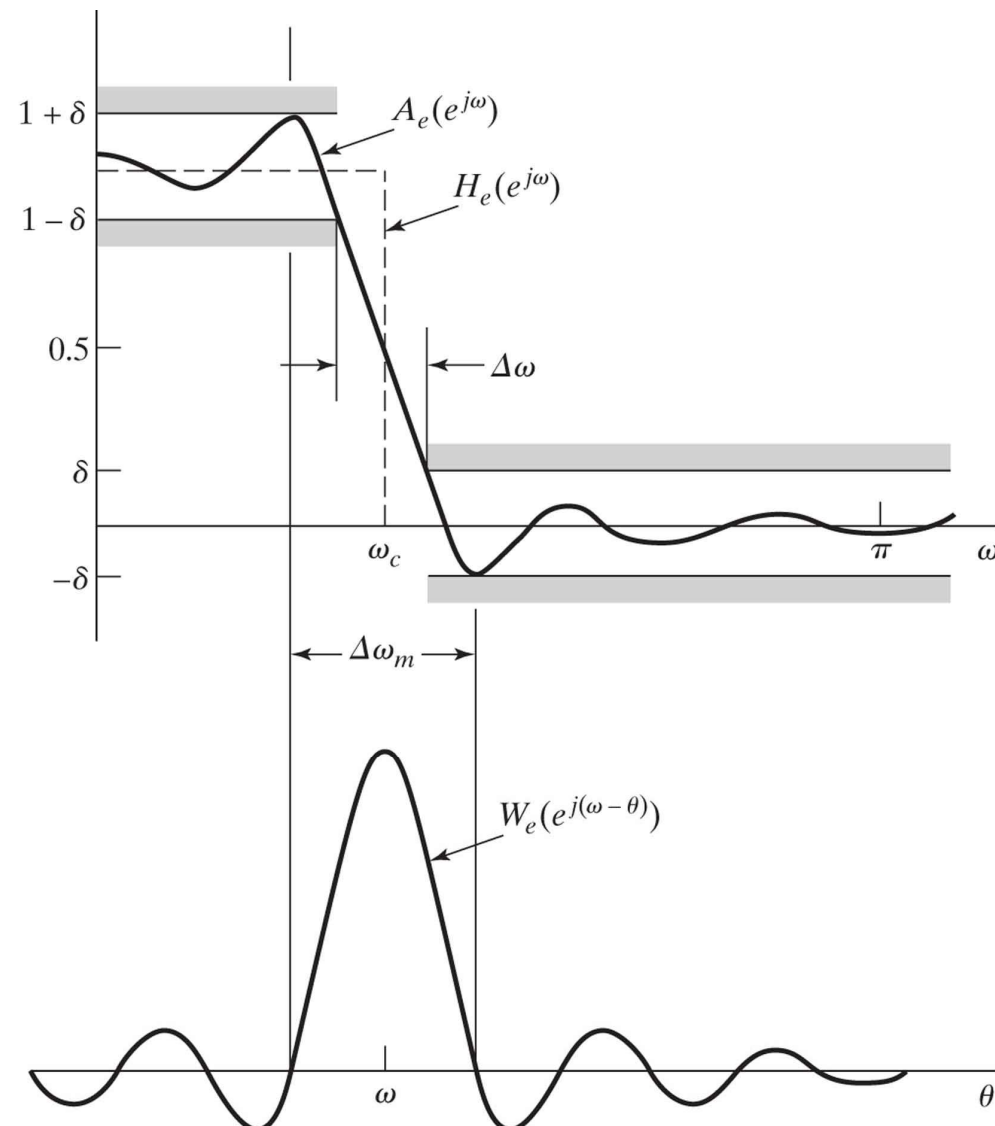


**Figure 7.32** (a) Kaiser windows for  $\beta = 0$ , 3, and 6 and  $M = 20$ . (b) Fourier transforms corresponding to windows in (a). (c) Fourier transforms of Kaiser windows with  $\beta = 6$  and  $M = 10$ , 20, and 40.

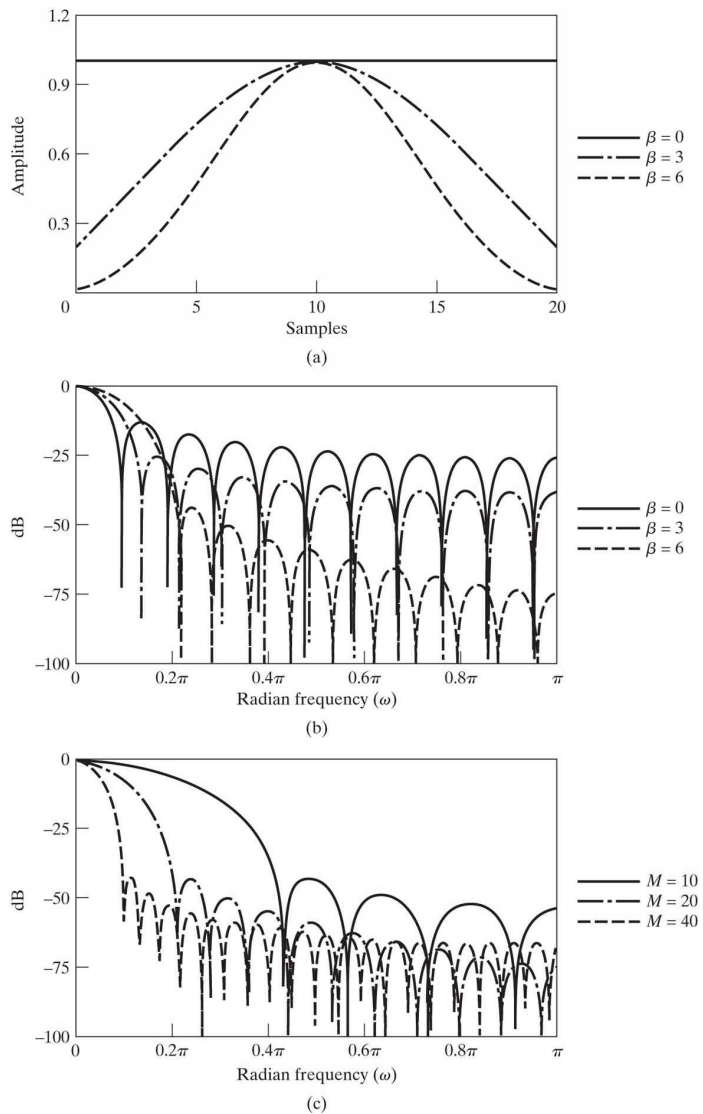


**Figure 7.33** Comparison of fixed windows with Kaiser windows in a lowpass filter design application ( $M = 32$  and  $\omega_c = \pi/2$ ). (Note that the designation “Kaiser 6” means Kaiser window with  $\beta = 6$ , etc.)

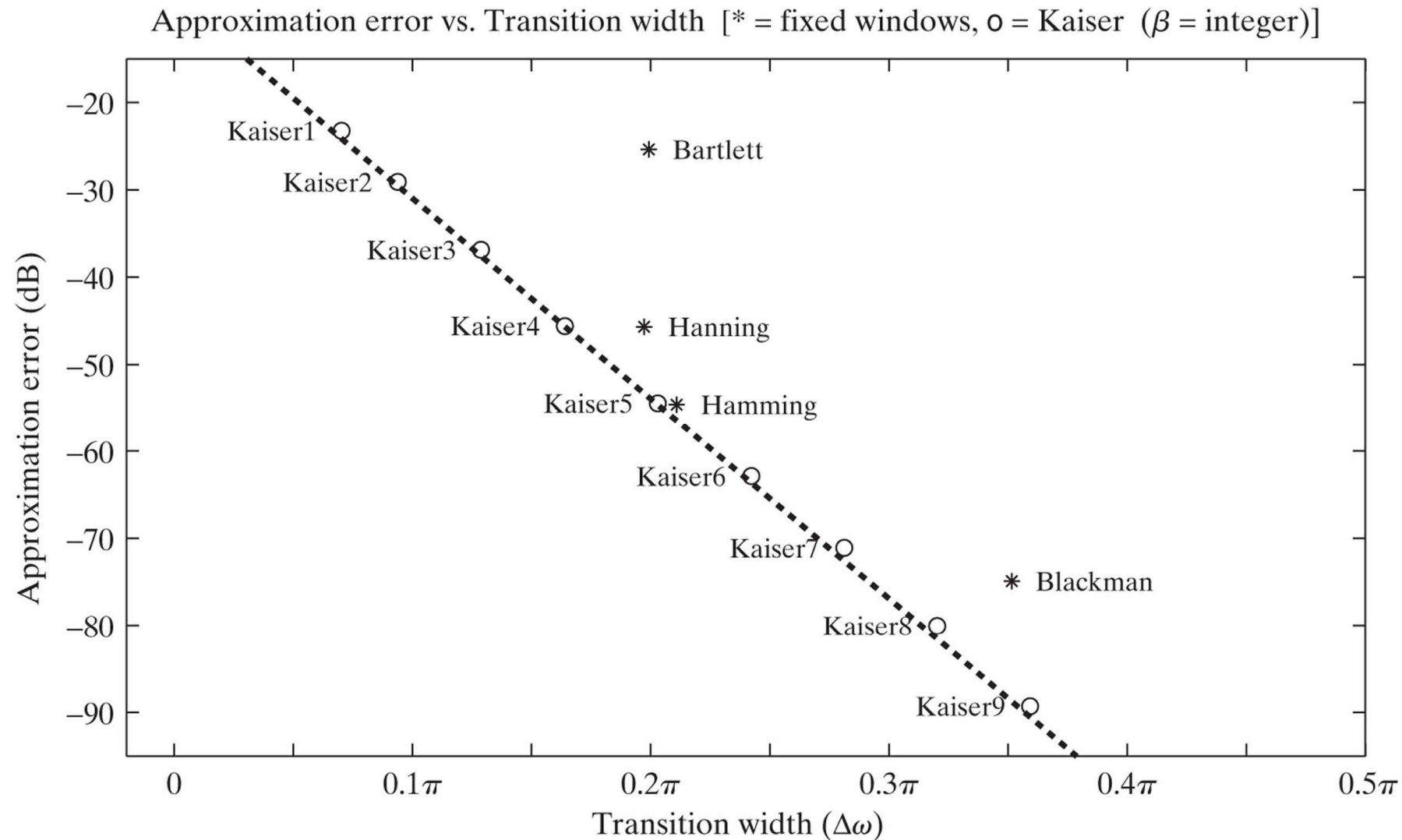


**Figure 7.34** Response functions for the lowpass filter designed with a Kaiser window. (a) Impulse response ( $M = 37$ ). (b) Log magnitude. (c) Approximation error for  $A_e (e^{j\omega})$ .

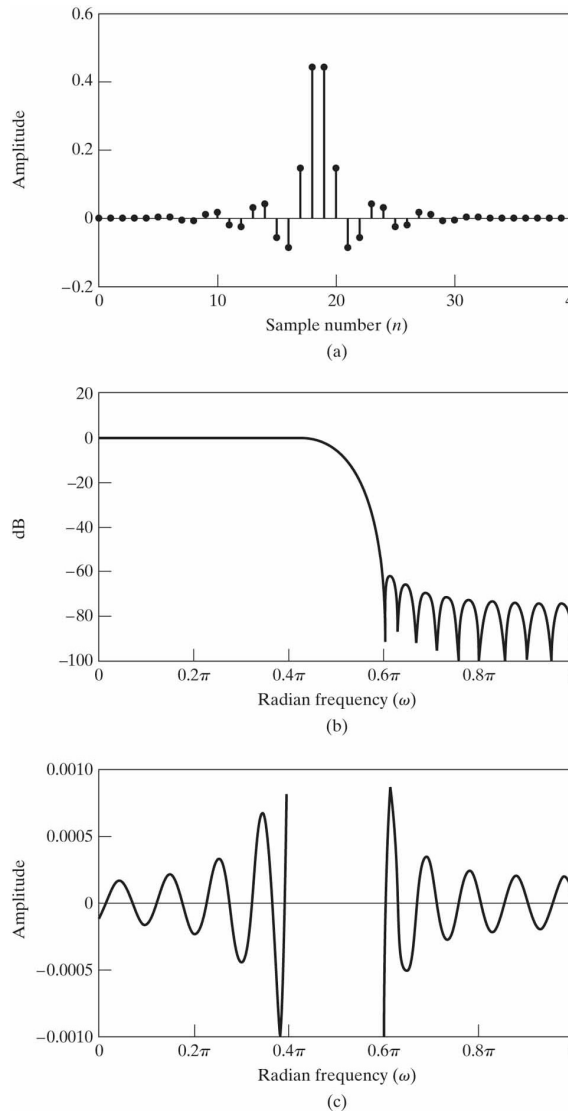


**Figure 7.35** Response functions for type I FIR highpass filter. (a) Impulse response ( $M = 24$ ). (b) Log magnitude. (c) Approximation error for  $A_e (e^{j\omega})$ .

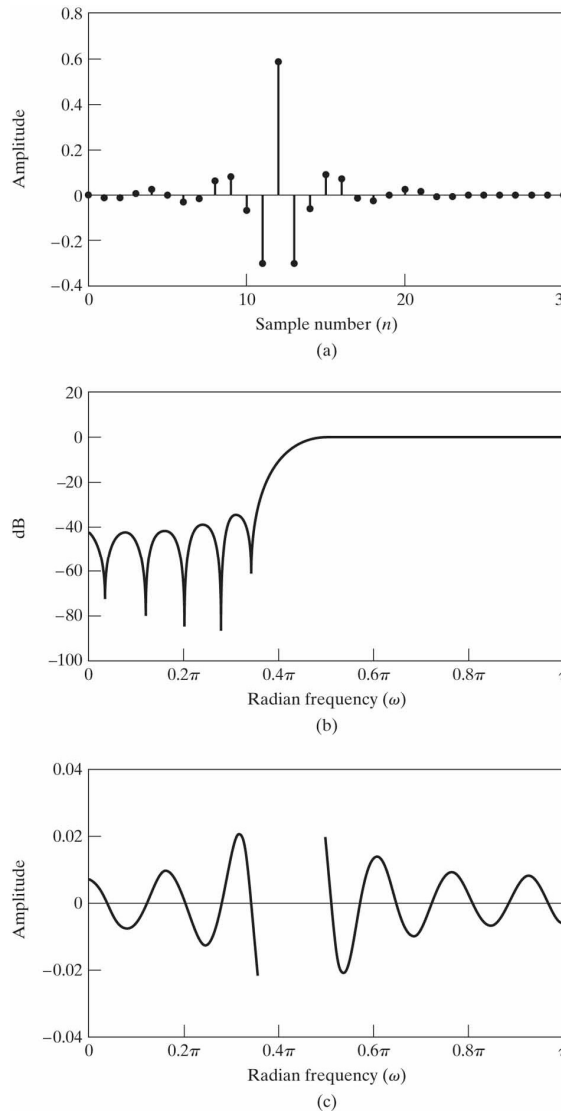
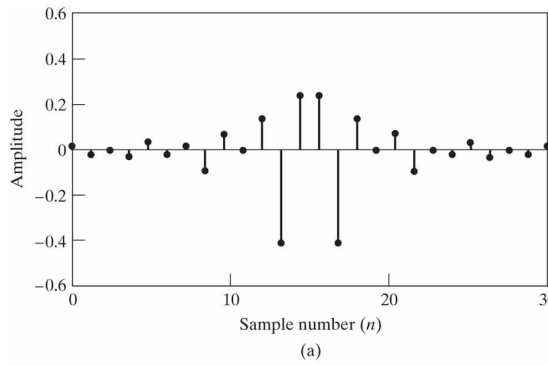
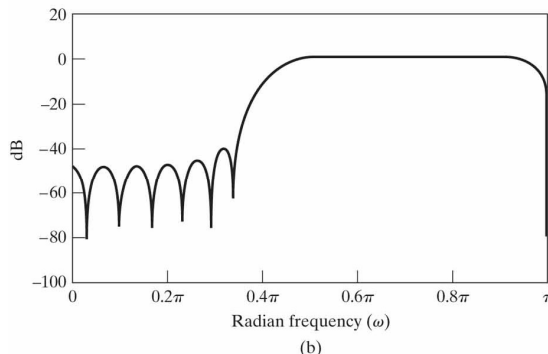


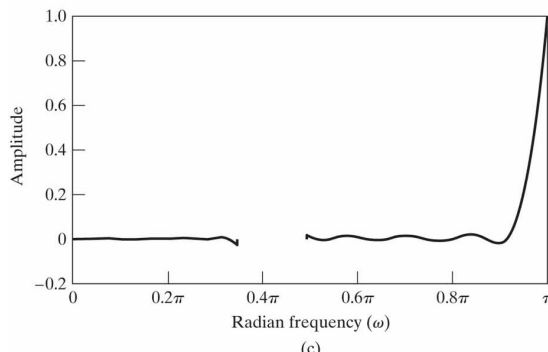
**Figure 7.36** Response functions for type II FIR highpass filter. (a) Impulse response ( $M = 25$ ). (b) Log magnitude of Fourier transform. (c) Approximation error for  $A_e(e^{j\omega})$ .



(a)



(b)



(c)

**Figure 7.37** Ideal frequency response for multiband filter.

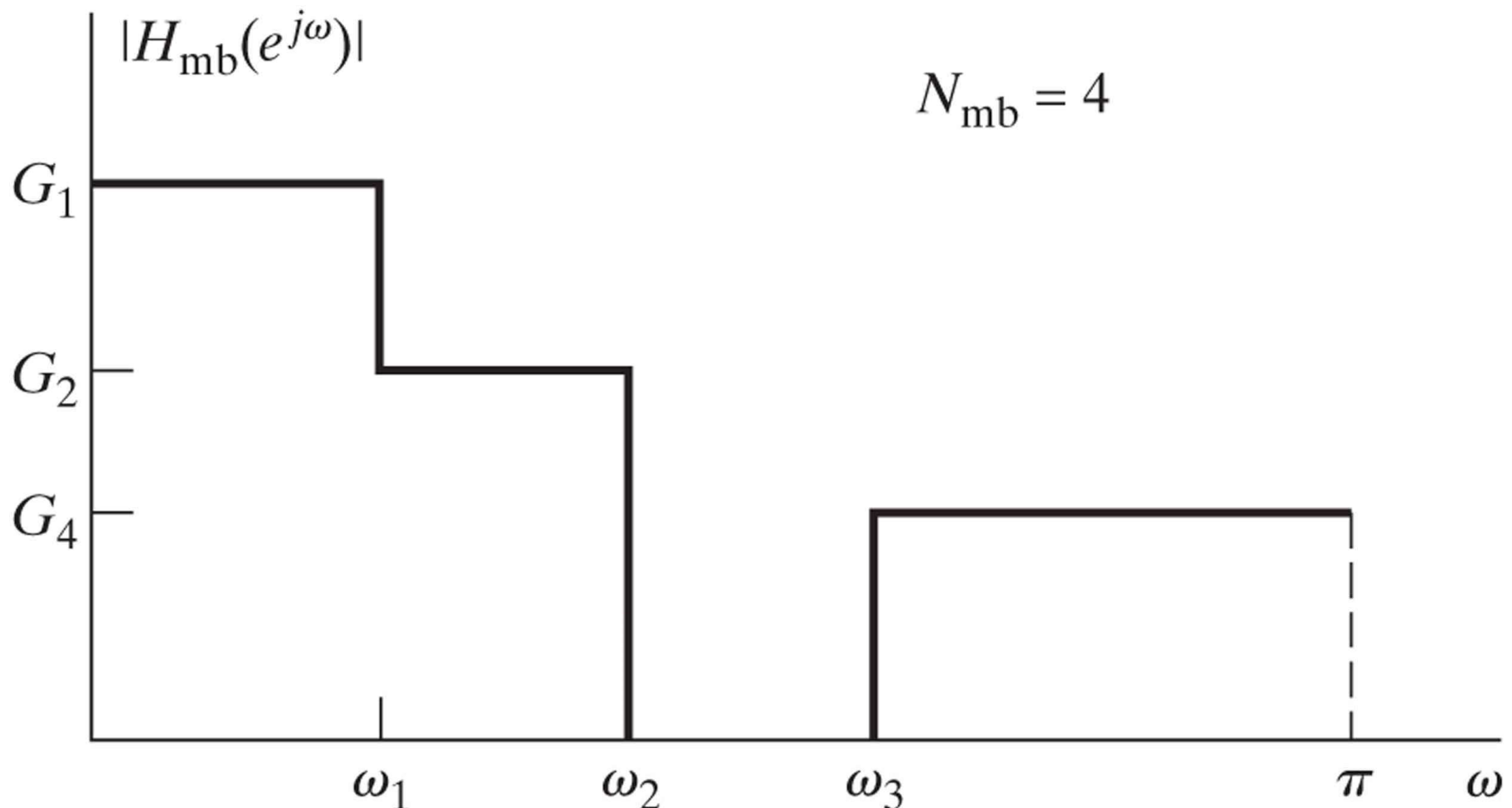
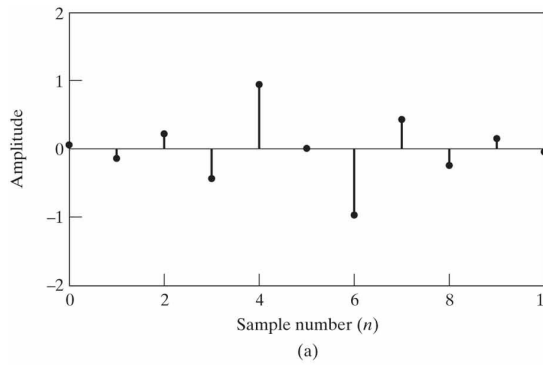
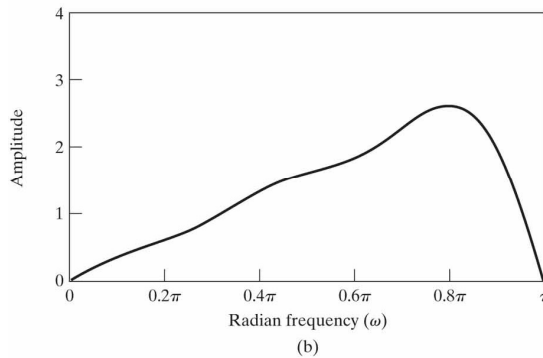


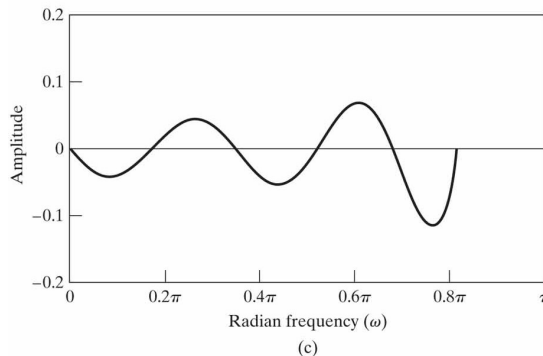
**Figure 7.38** Response functions for type III FIR discrete-time differentiator. (a) Impulse response ( $M = 10$ ). (b) Magnitude. (c) Approximation error for  $A_0(e^{j\omega})$ .



(a)

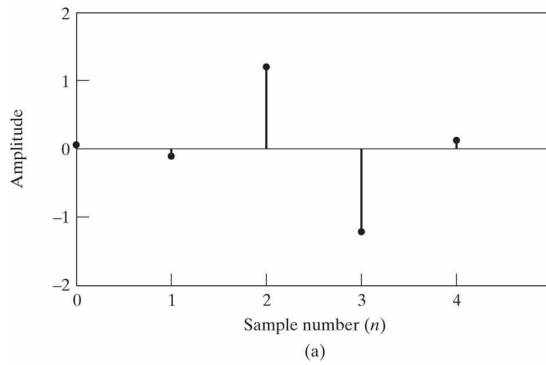


(b)

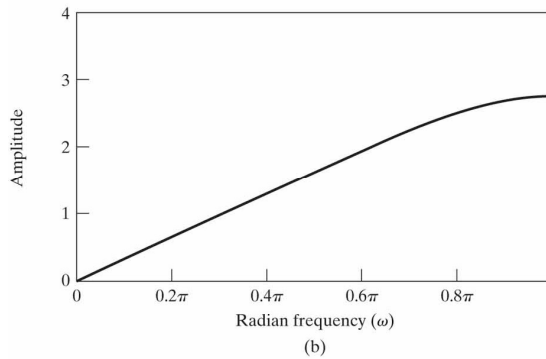


(c)

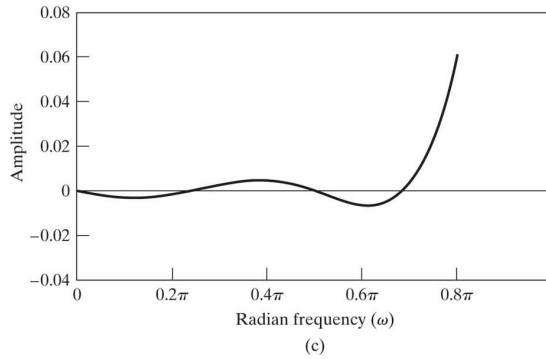
**Figure 7.39** Response functions for type IV FIR discrete-time differentiator. (a) Impulse response ( $M = 5$ ). (b) Magnitude. (c) Approximation error for  $A_0(e^{j\omega})$ .



(a)



(b)



(c)

**Figure 7.40** Tolerance scheme and ideal response for lowpass filter.

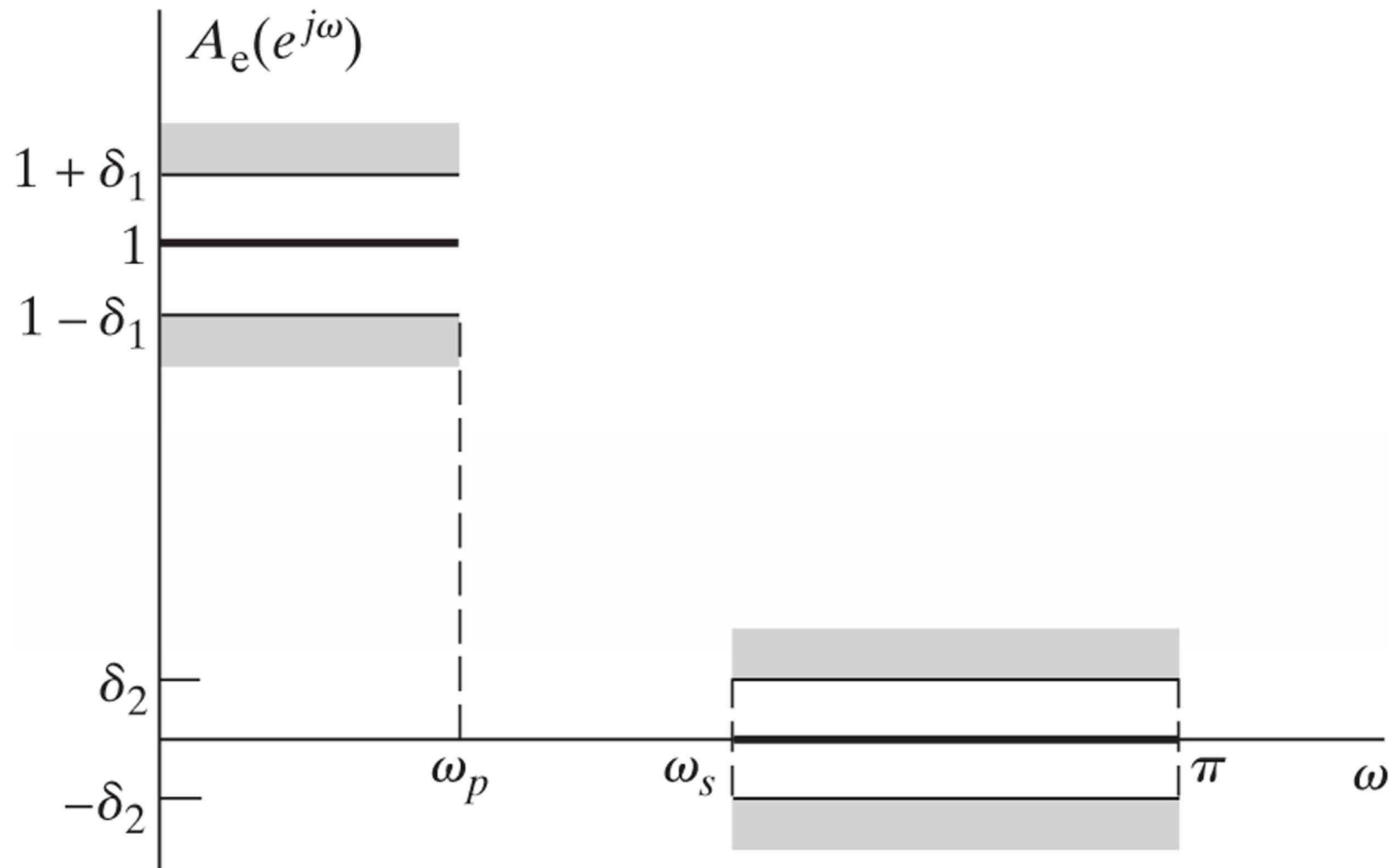


**Figure 7.41** Typical frequency response meeting the specifications of Figure 7.40.

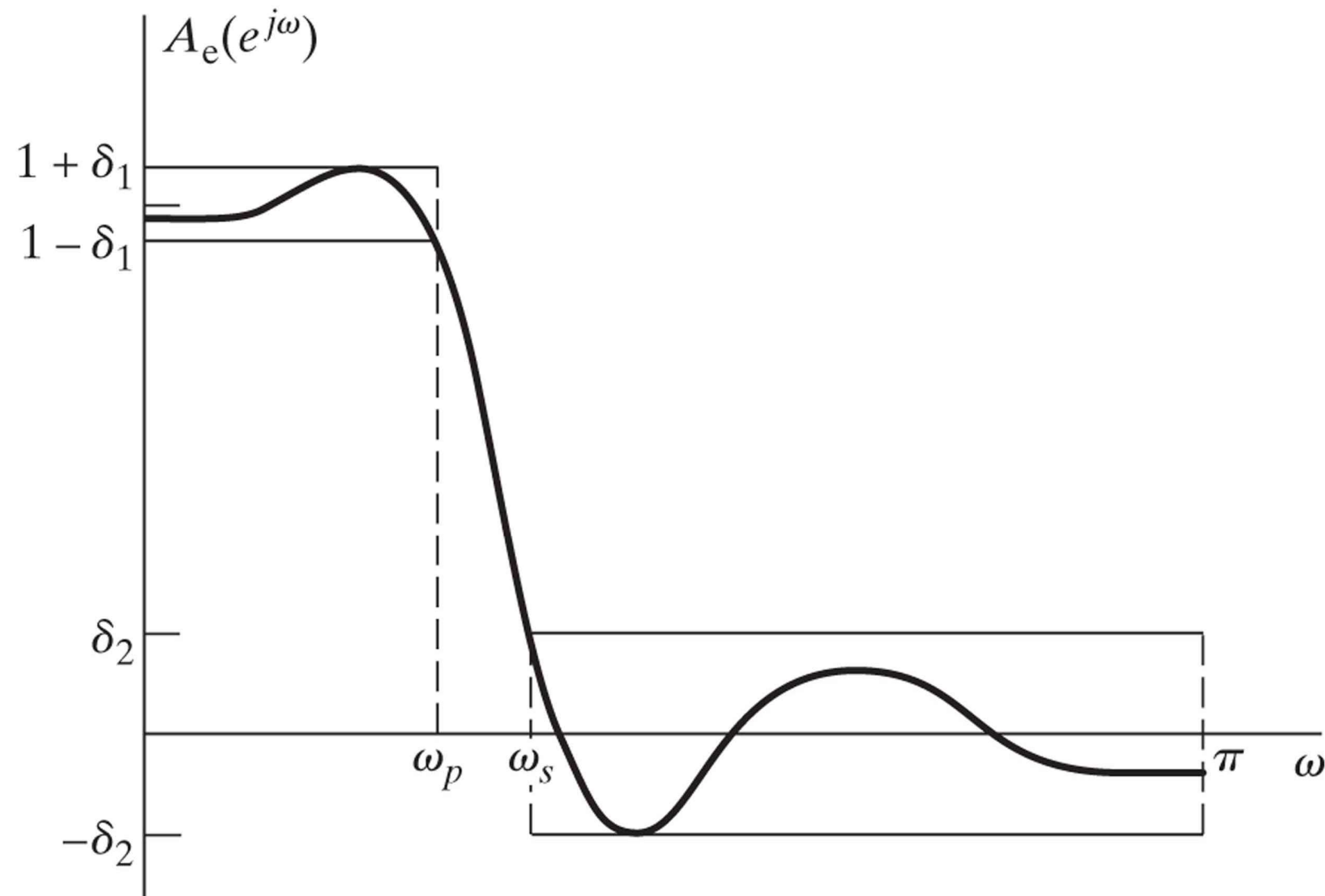


**Figure 7.42** Weighted error for the approximation of Figure 7.41.

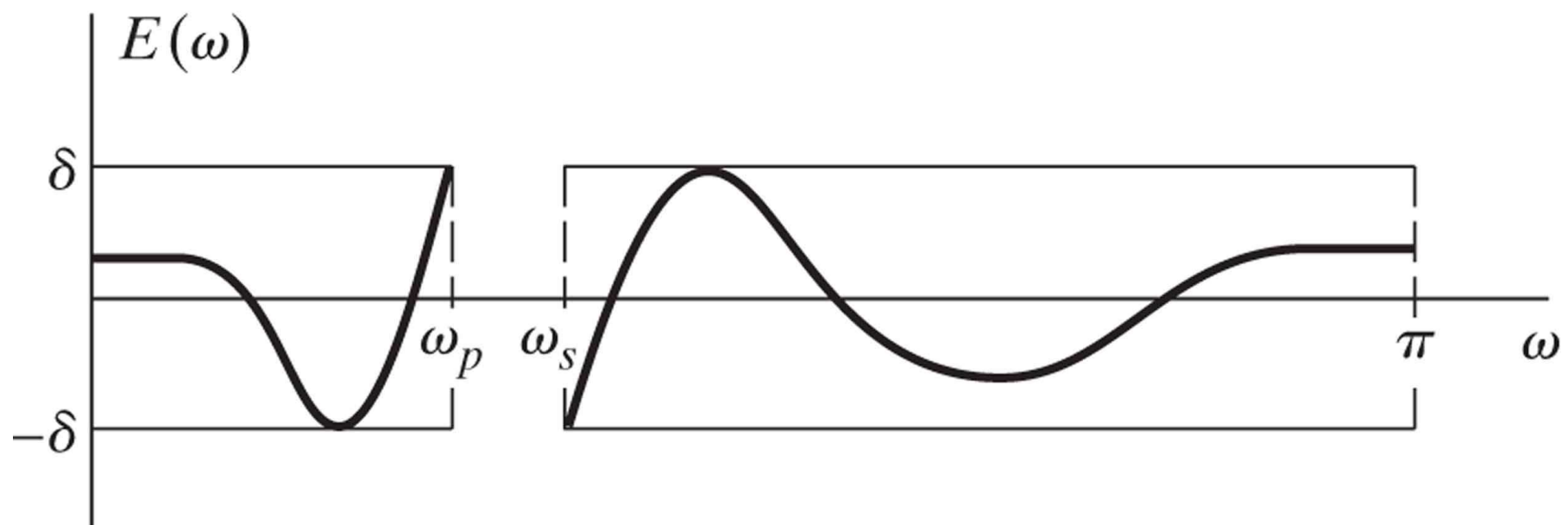


**Figure 7.43** 5<sup>th</sup>-order polynomials for Example 7.8. Alternation points are indicated by  $\circ$ .

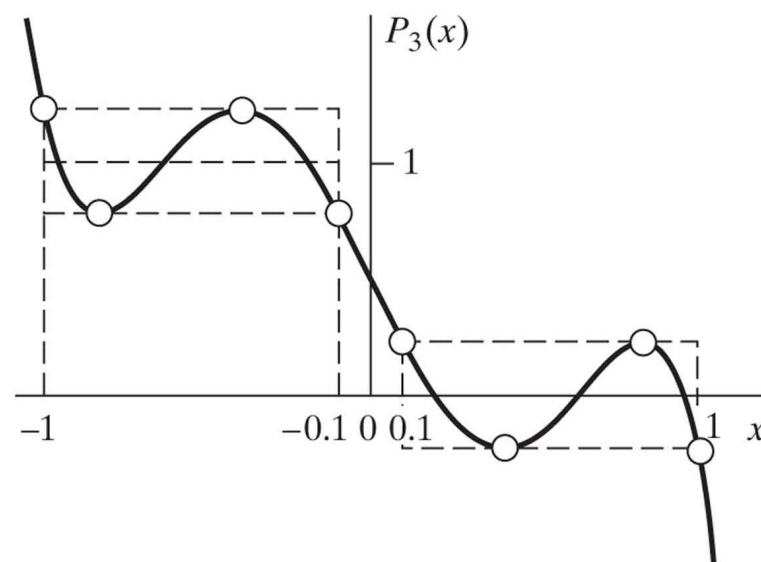
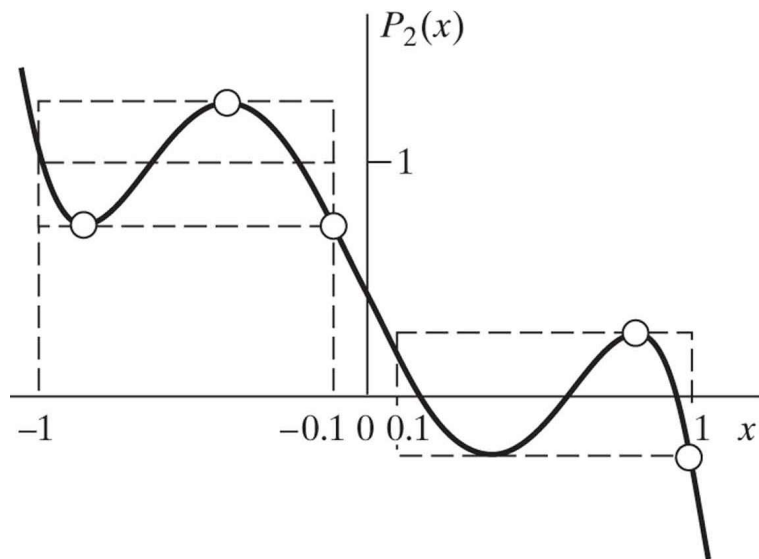
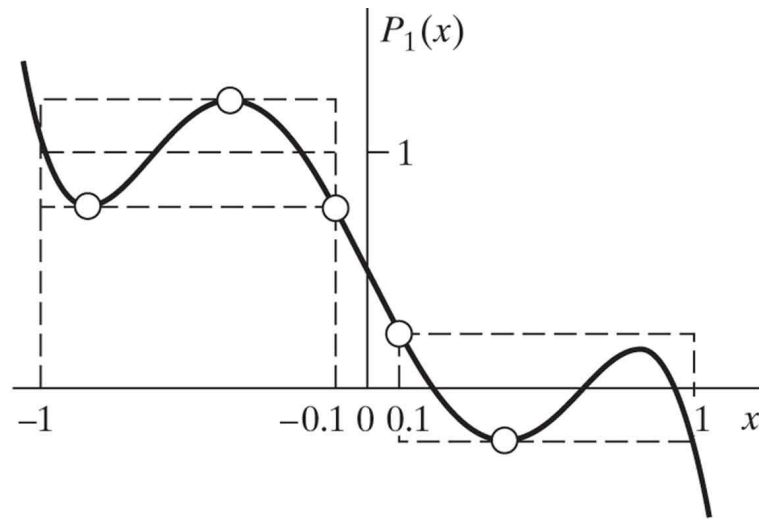


**Figure 7.44** Typical example of a lowpass filter approximation that is optimal according to the alternation theorem for  $L = 7$ .

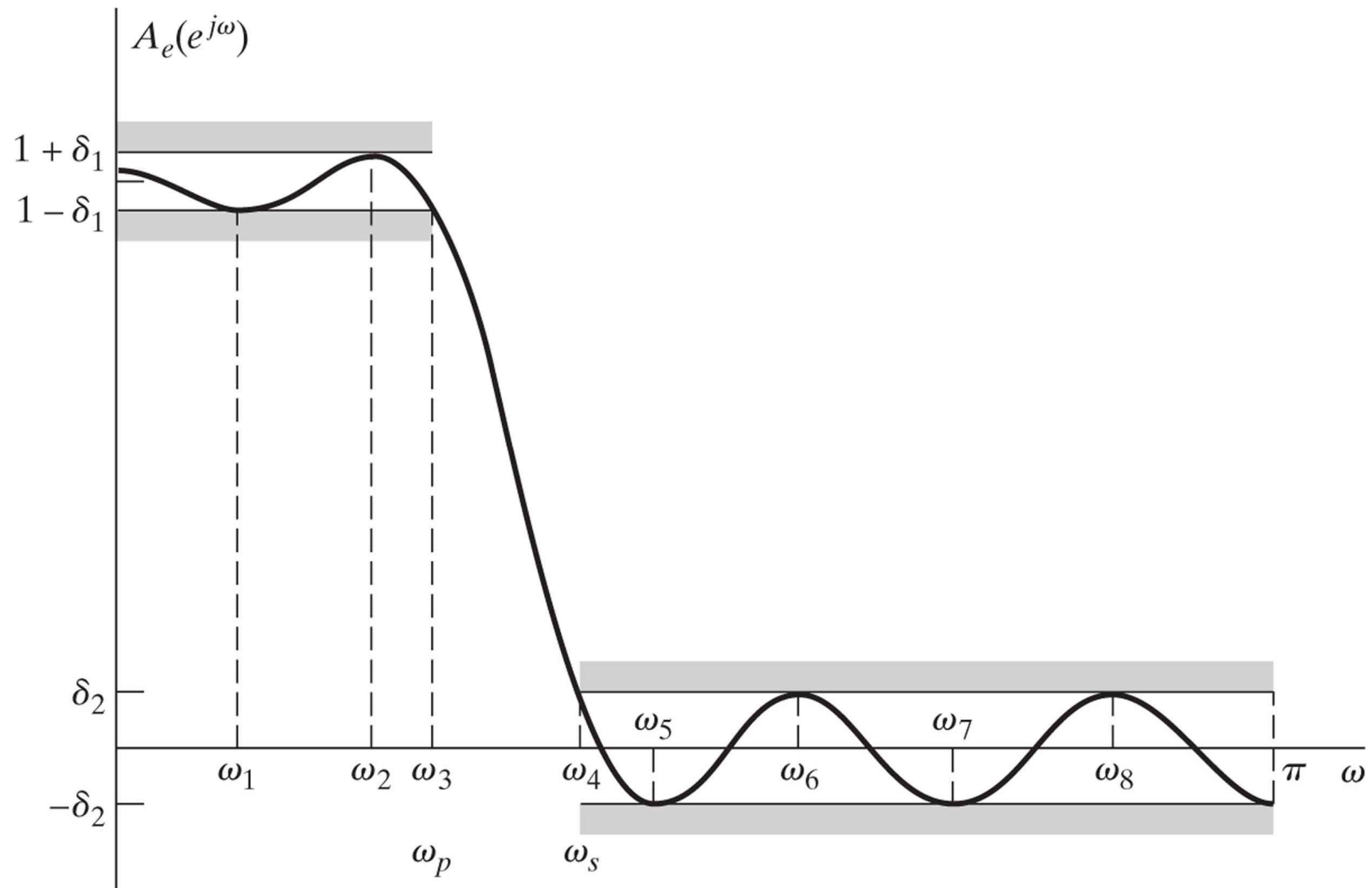
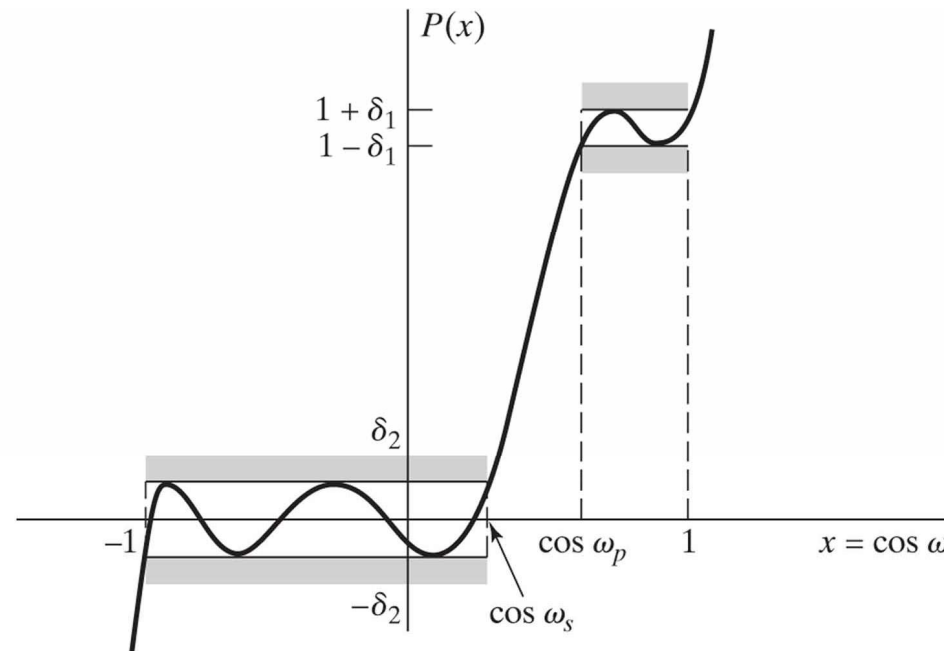
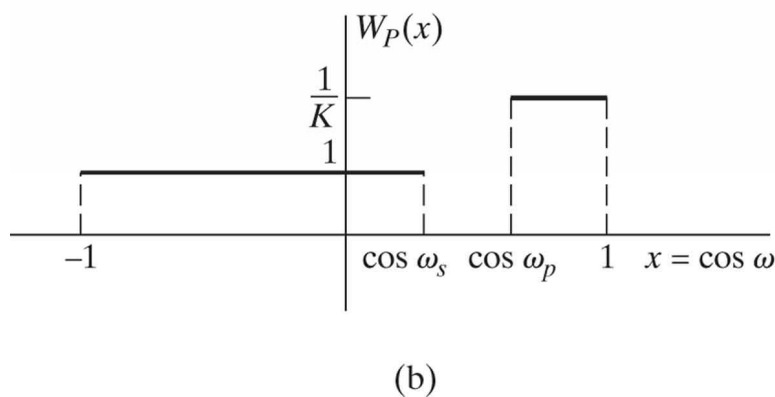


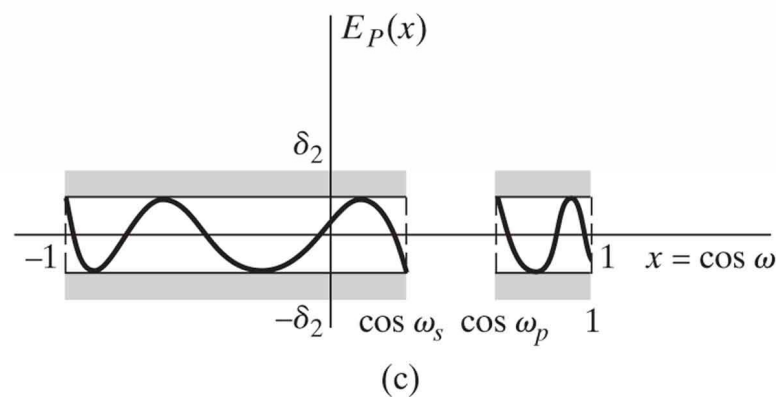
**Figure 7.45** Equivalent polynomial approximation functions as a function of  $x = \cos \omega$ . (a) Approximating polynomial. (b) Weighting function. (c) Approximation error.



(a)



(b)



(c)

**Figure 7.46** Possible optimum lowpass filter approximations for  $L = 7$ . (a)  $L + 3$  alternations (extraripple case). (b)  $L + 2$  alternations (extremum at  $\omega = \pi$ ). (c)  $L + 2$  alternations (extremum at  $\omega = 0$ ). (d)  $L + 2$  alternations (extremum at both  $\omega = 0$  and  $\omega = \pi$ ).

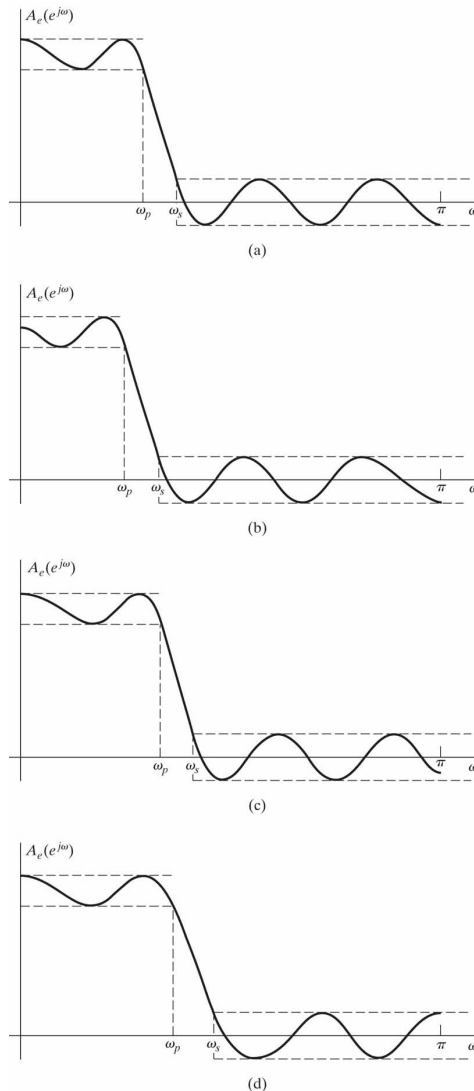


**Figure 7.47** Illustration that the passband edge  $\omega_p$  must be an alternation frequency.

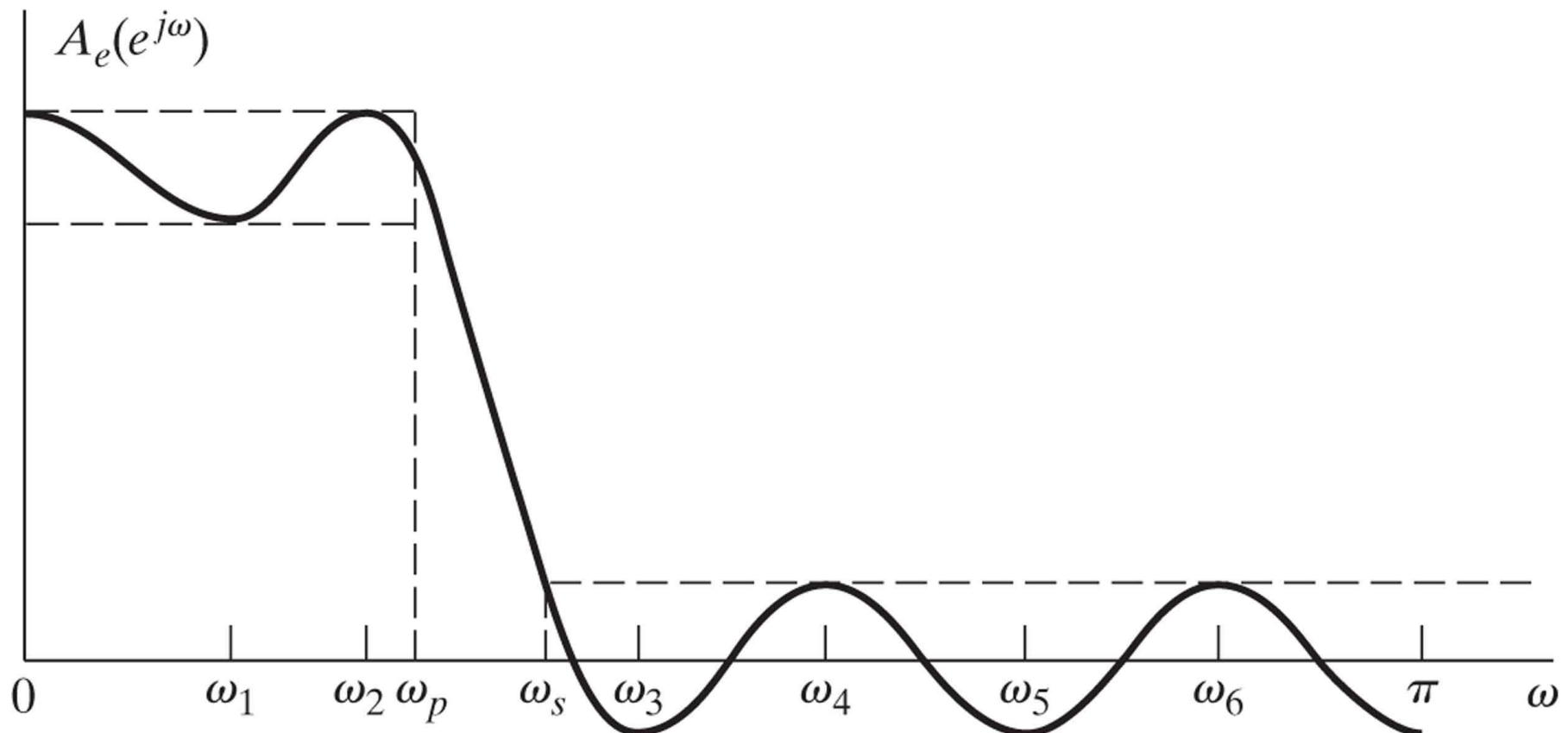


**Figure 7.48** Illustration that the frequency response must be equiripple in the approximation bands.

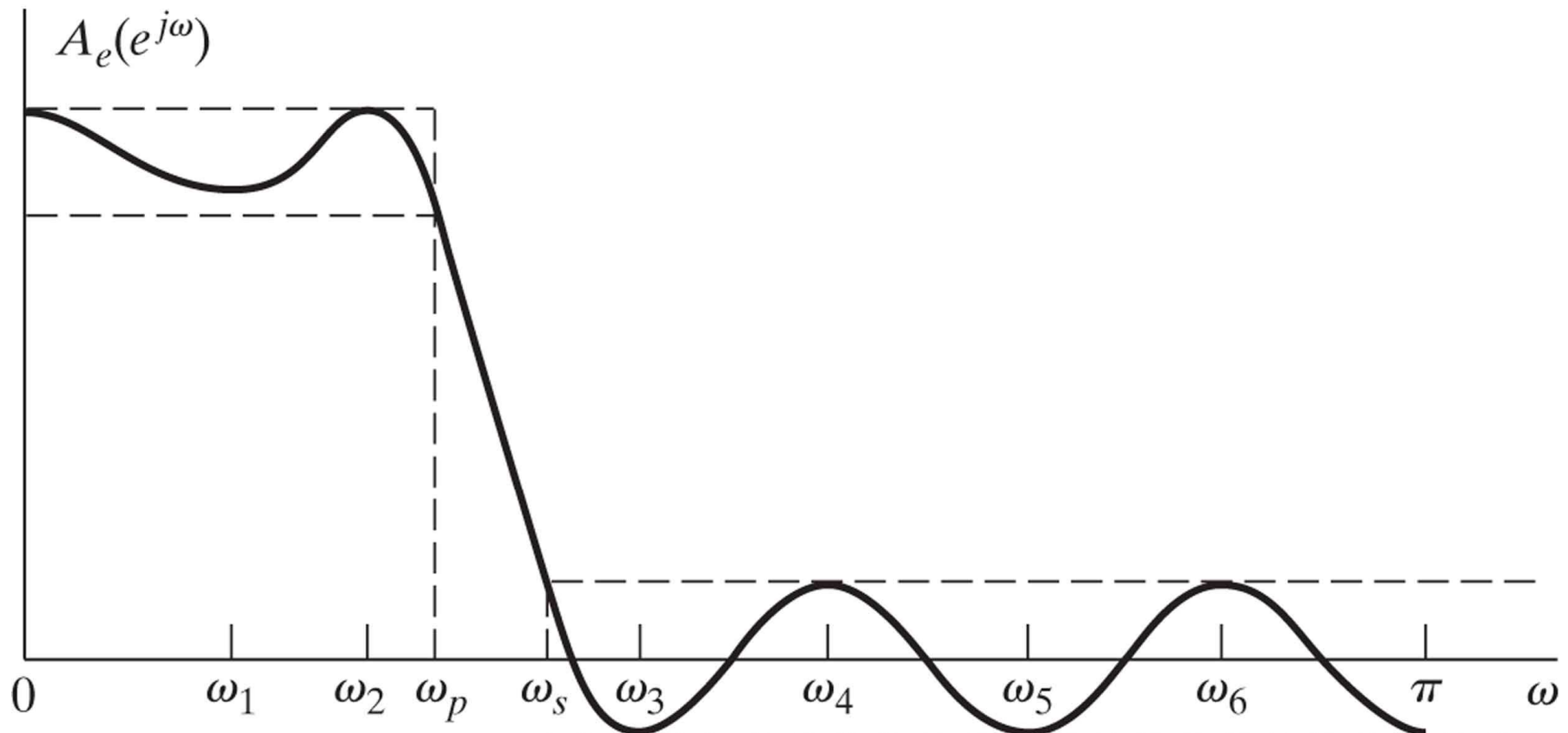


**Figure 7.49** Illustration of the Parks–McClellan algorithm for equiripple approximation.

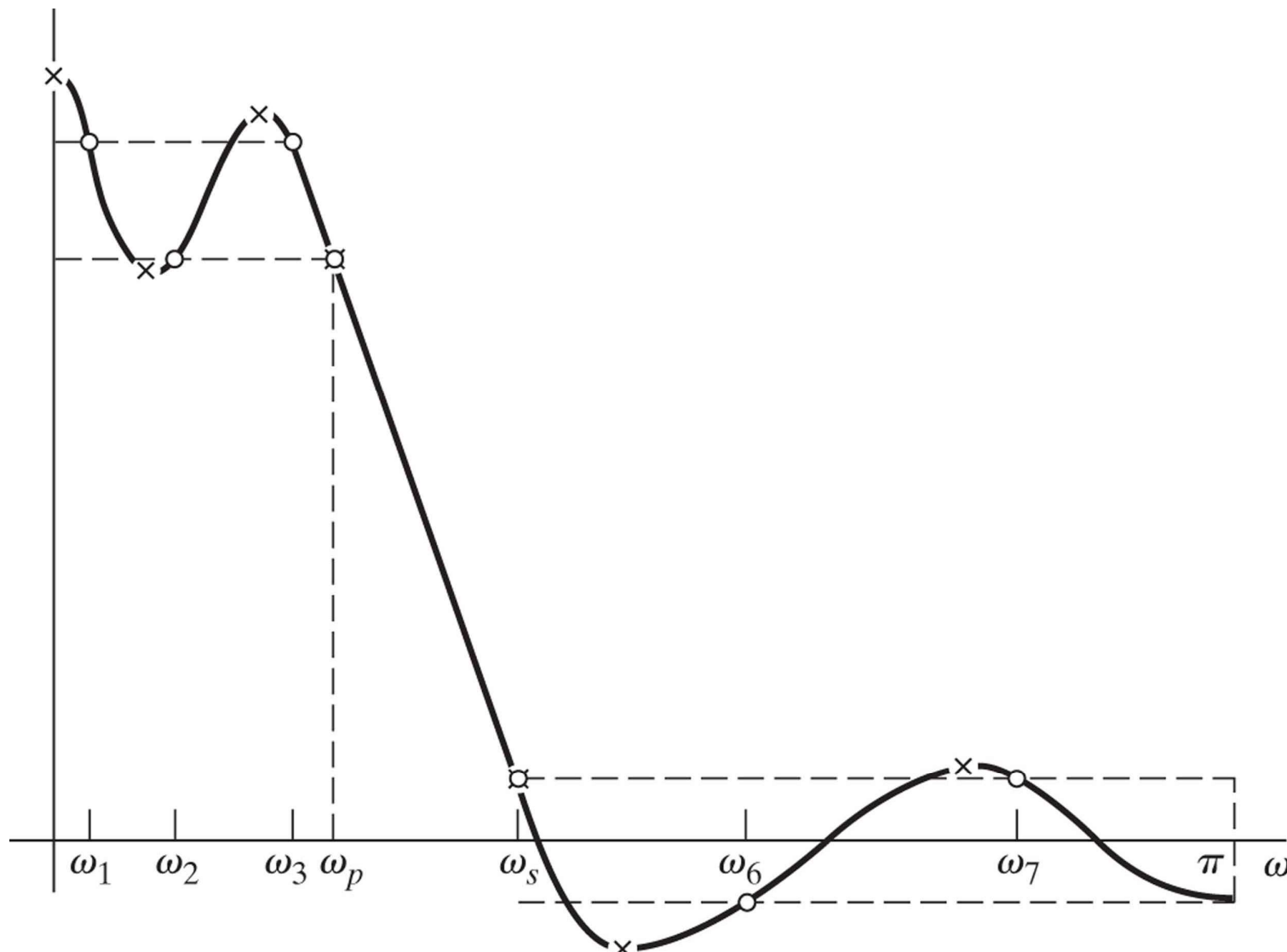


**Figure 7.50** Flowchart of Parks–McClellan algorithm.

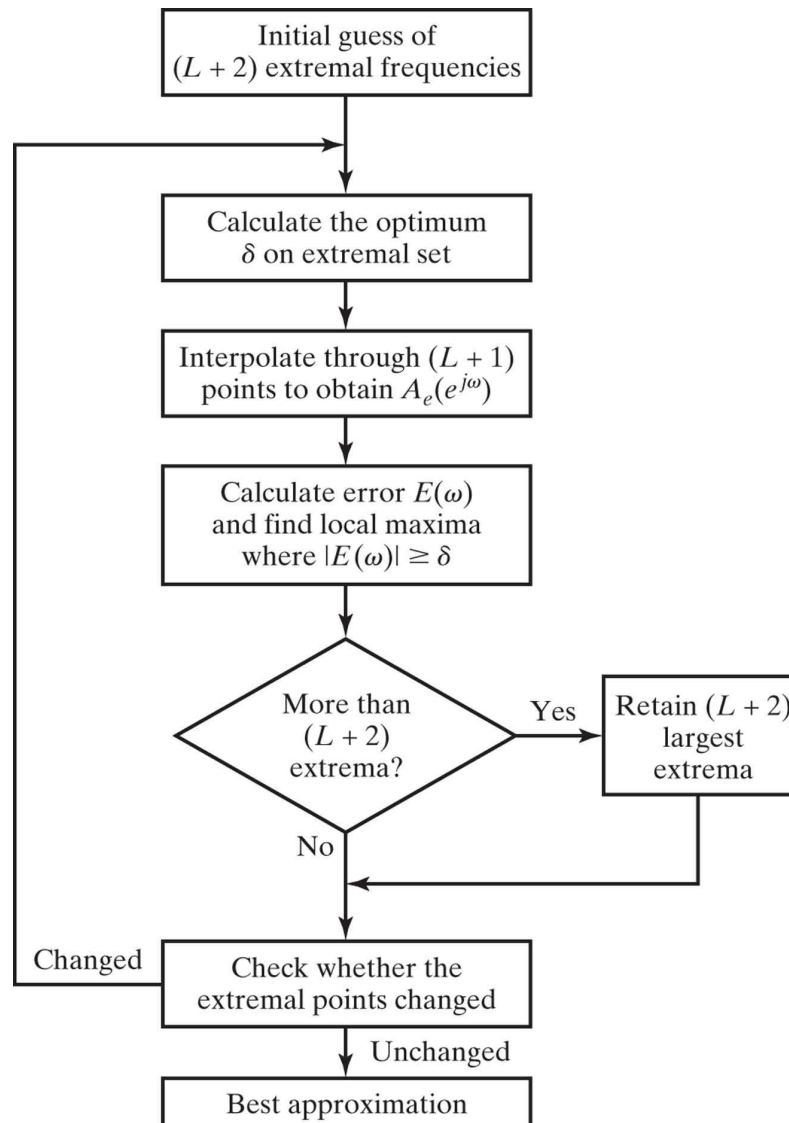


**Figure 7.51** Illustration of the dependence of passband and stopband error on cutoff frequency for optimal approximations of a lowpass filter. For this example,  $K = 1$  and  $(\omega_s - \omega_p) = 0.2\pi$ . (After Herrmann, Rabiner and Chan, 1973.)

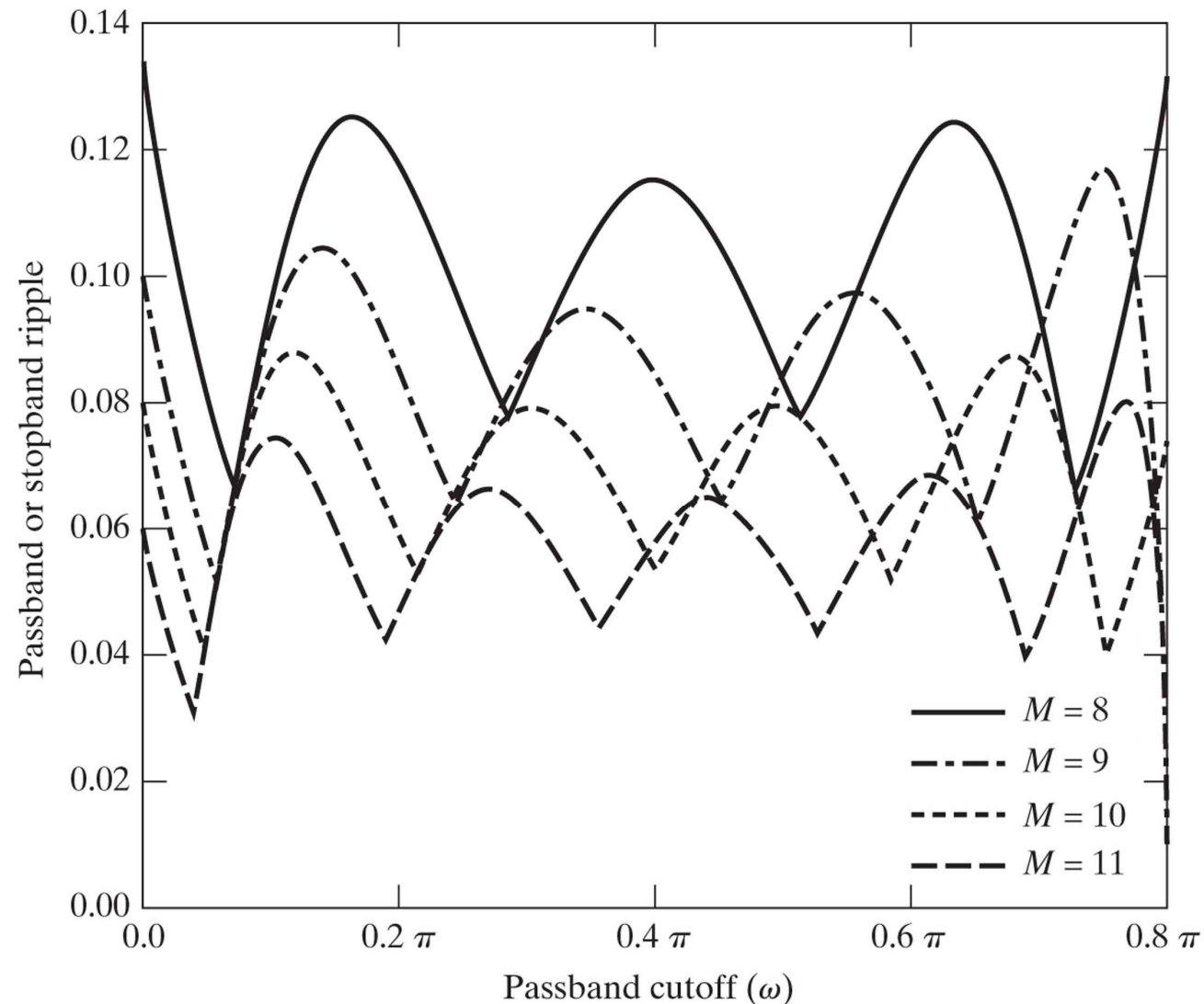


**Figure 7.52** Optimum type I FIR lowpass filter for  $\omega_p = 0.4\pi$ ,  $\omega_s = 0.6\pi$ ,  $K = 10$ , and  $M = 26$ . (a) Impulse response. (b) Log magnitude of the frequency response. (c) Approximation error (unweighted).

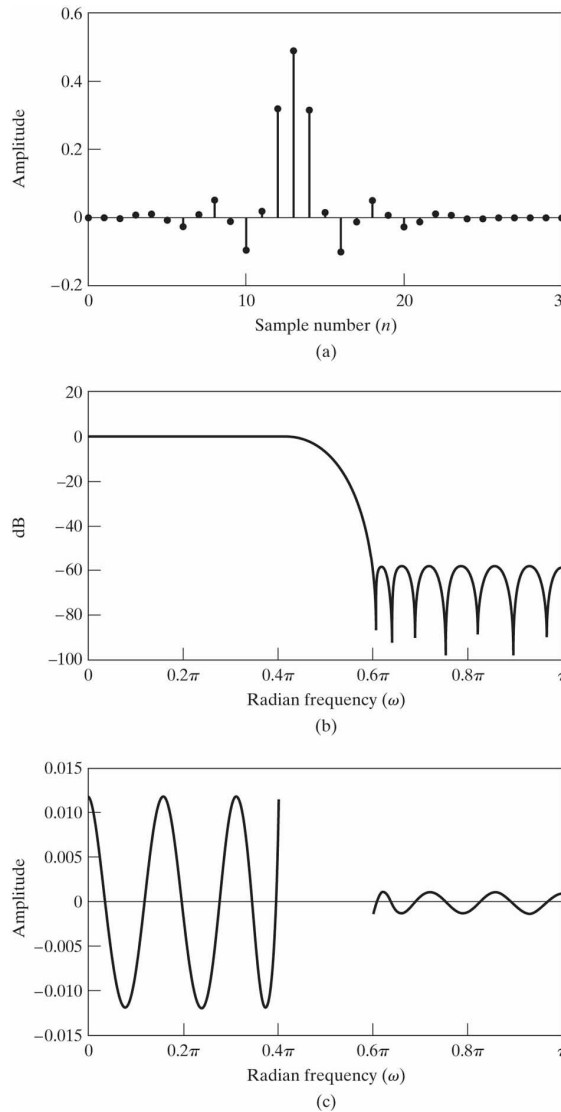


**Figure 7.53** Optimum type II FIR lowpass filter for  $\omega_p = 0.4\pi$ ,  $\omega_s = 0.6\pi$ ,  $K = 10$ , and  $M = 27$ . (a) Impulse response. (b) Log magnitude of frequency response. (c) Approximation error (unweighted).

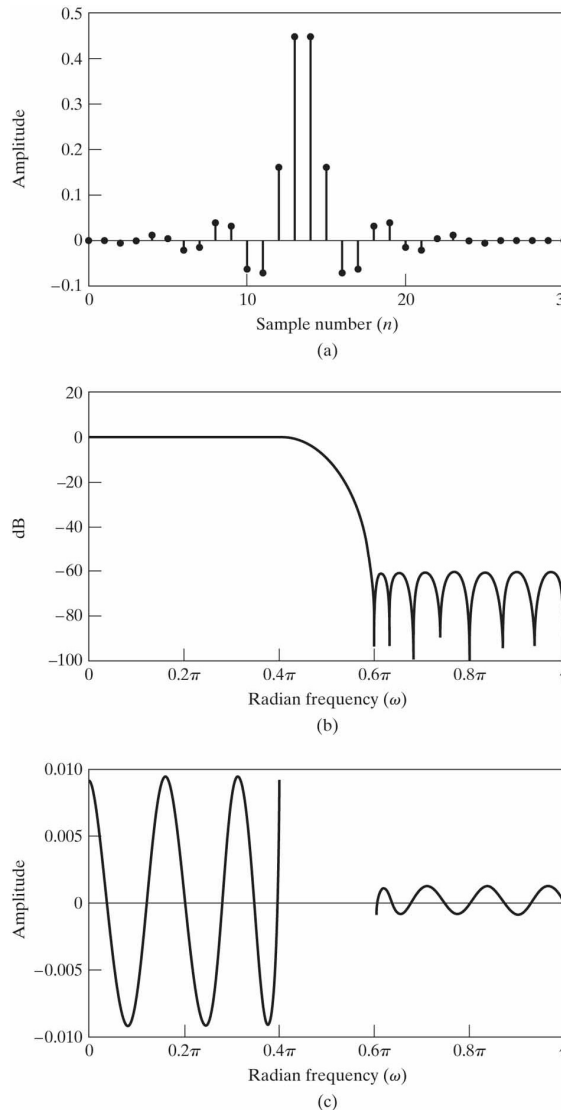


**Figure 7.54** Precompensation of a discrete-time filter for the effects of a D/A converter.

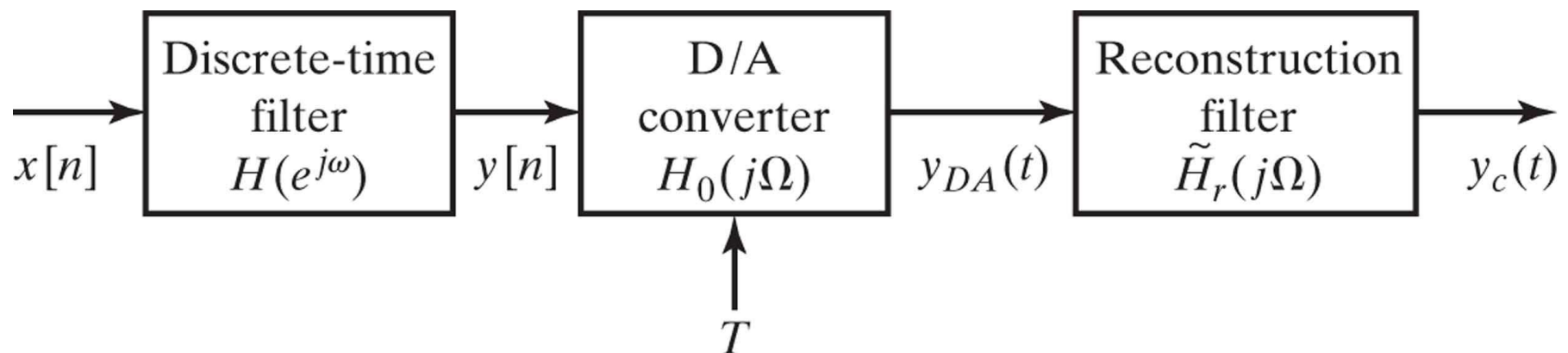


**Figure 7.55** Optimum D/A-compensated lowpass filter for  $\omega_p = 0.4\pi$ ,  $\omega_s = 0.6\pi$ ,  $K = 10$ , and  $M = 28$ . (a) Impulse response. (b) Log magnitude of the frequency response. (c) Magnitude response in passband.

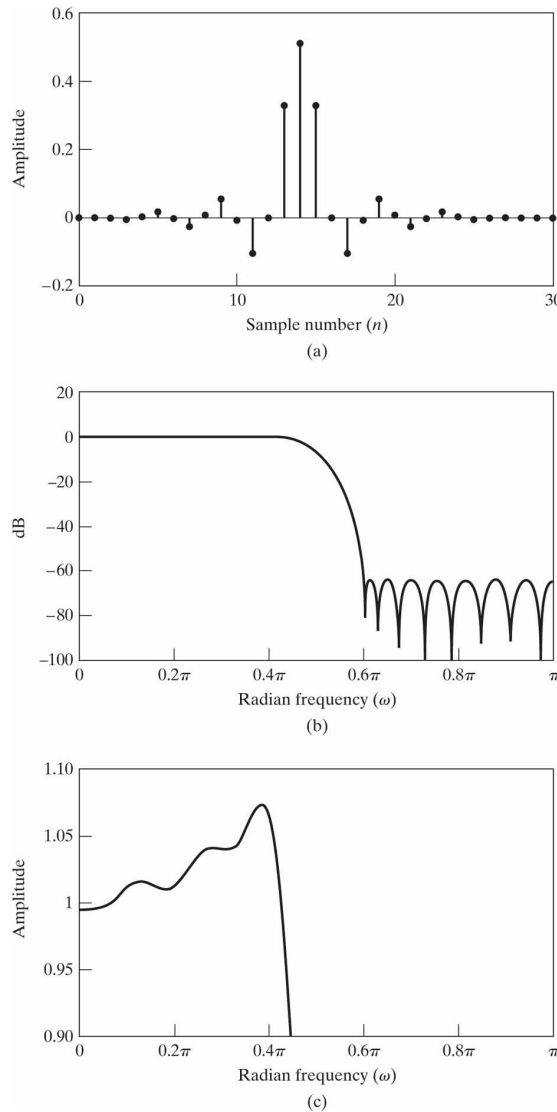
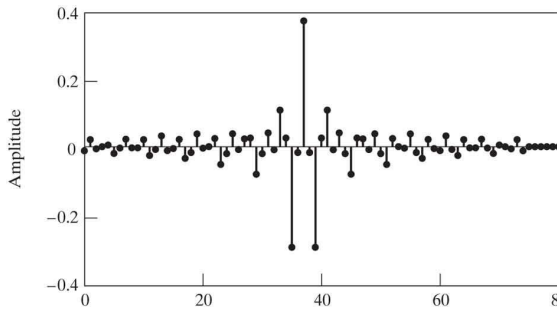
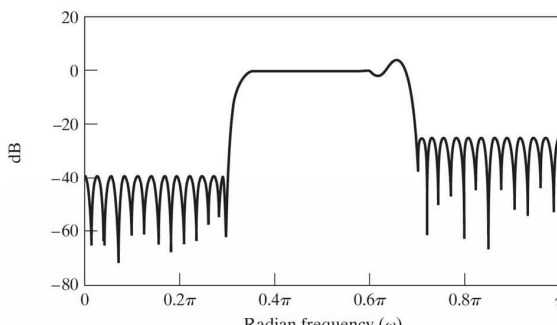


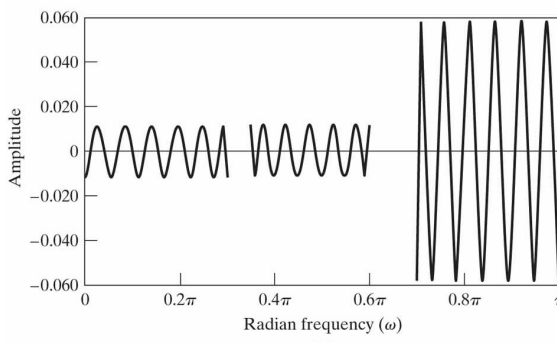
**Figure 7.56** Optimum FIR bandpass filter for  $M = 74$ . (a) Impulse response. (b) Log magnitude of the frequency response. (c) Approximation error (unweighted).



(a)



(b)



(c)

**Table 7.3** ORDERS OF DESIGNED FILTERS.

**TABLE 7.3** ORDERS  
OF DESIGNED FILTERS.

Filter design	Order
Butterworth	18
Chebyshev I	8
Chebyshev II	8
Elliptic	5
Kaiser	63
Parks–McClellan	44

**Figure 7.57** Pole–zero plots for the six designs. (a) Butterworth filter. (b) Chebyshev I filter. (c) Chebyshev II filter. (d) Elliptic filter. (e) Kaiser filter. (f) Parks–McClellan filter.

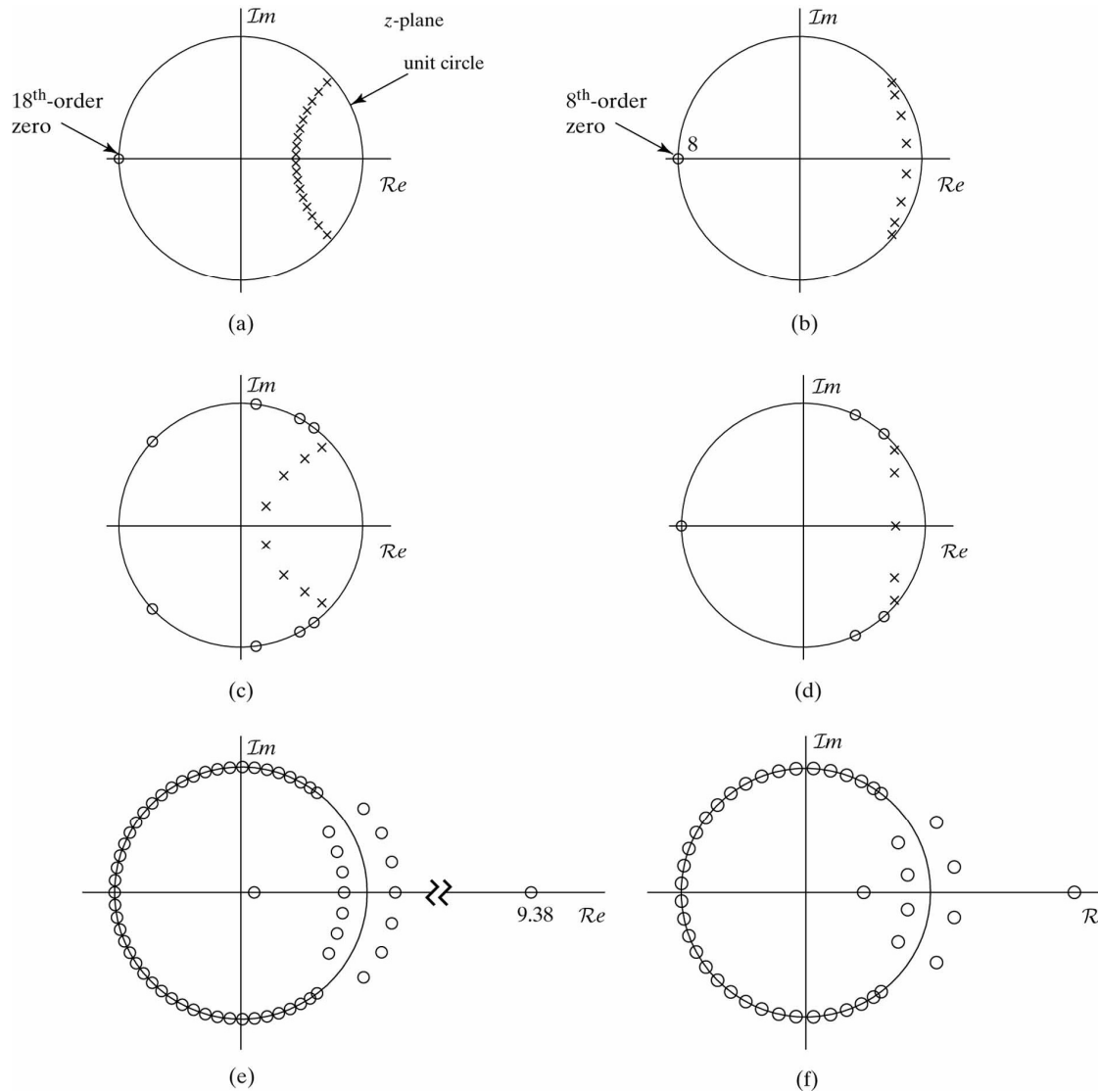


**Table 7.4** AVERAGE NUMBER OF REQUIRED MULTIPLICATIONS PER OUTPUT SAMPLE FOR EACH OF THE DESIGNED FILTERS.

**TABLE 7.4** AVERAGE NUMBER OF REQUIRED MULTIPLICATIONS PER OUTPUT SAMPLE FOR EACH OF THE DESIGNED FILTERS.

Filter design	Direct form	Symmetric	Polyphase
Butterworth	37	18	18
Chebyshev I	17	8	8
Chebyshev II	17	13	10.25
Elliptic	11	8	6.5
Kaiser	64	32	16
Parks–McClellan	45	23	11.25

**Figure P7.8**

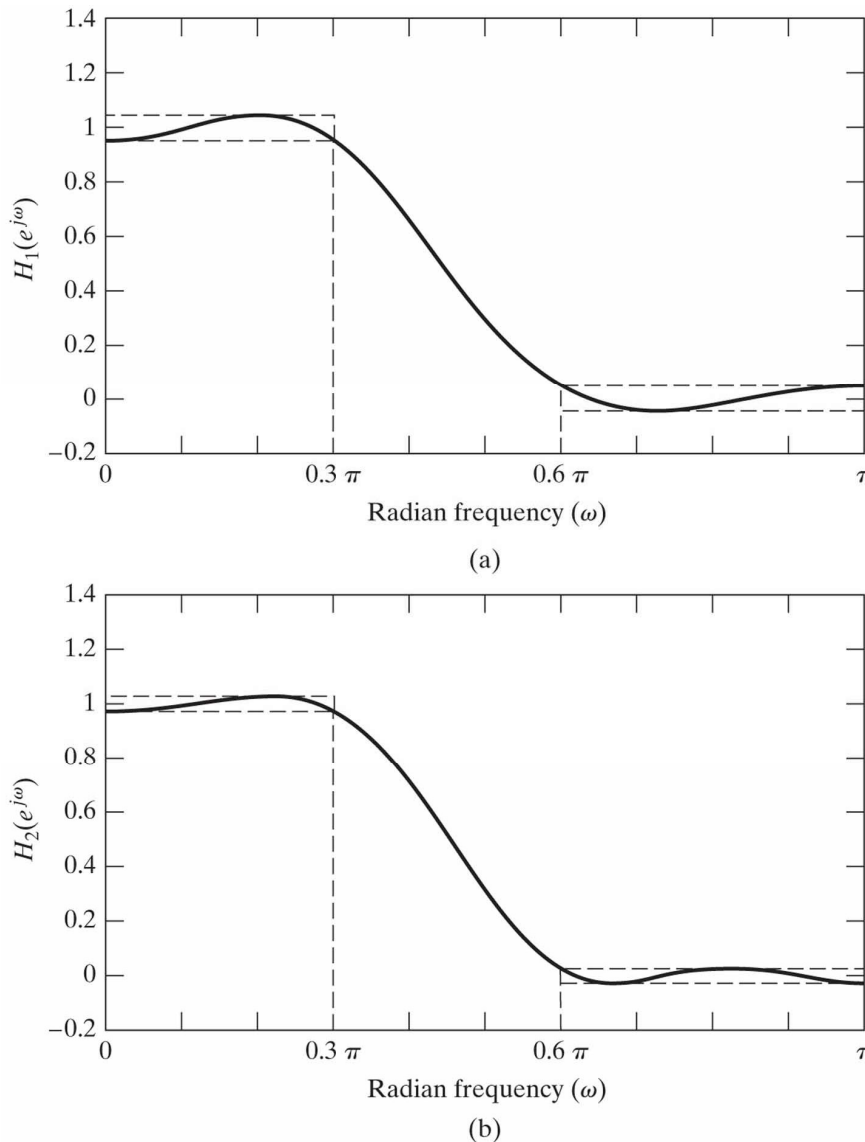


**Figure P7.21-1**

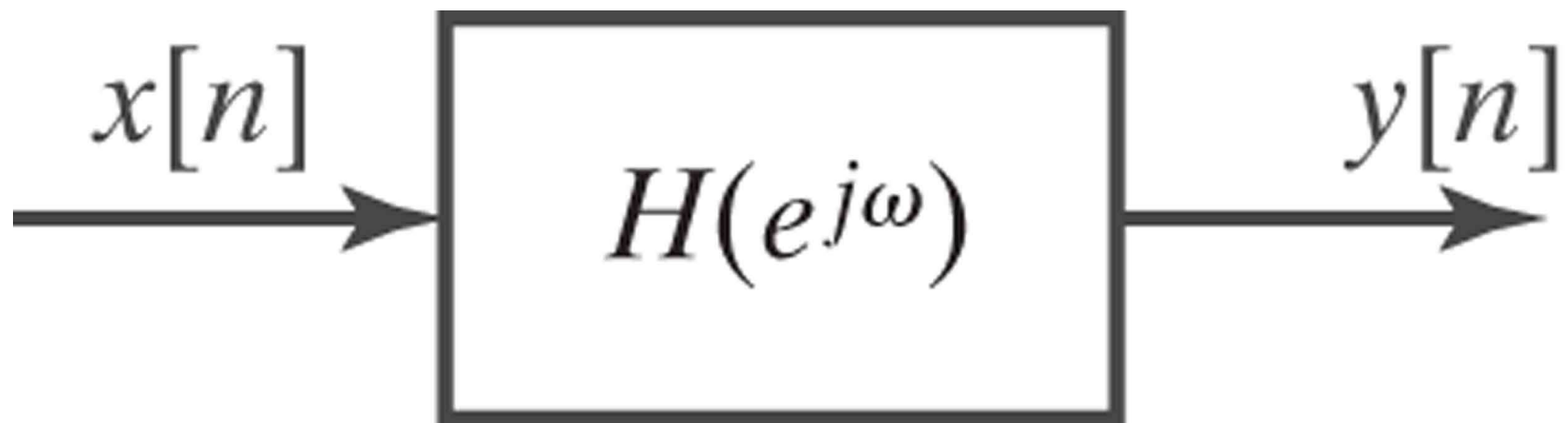


**Figure P7.21-2**

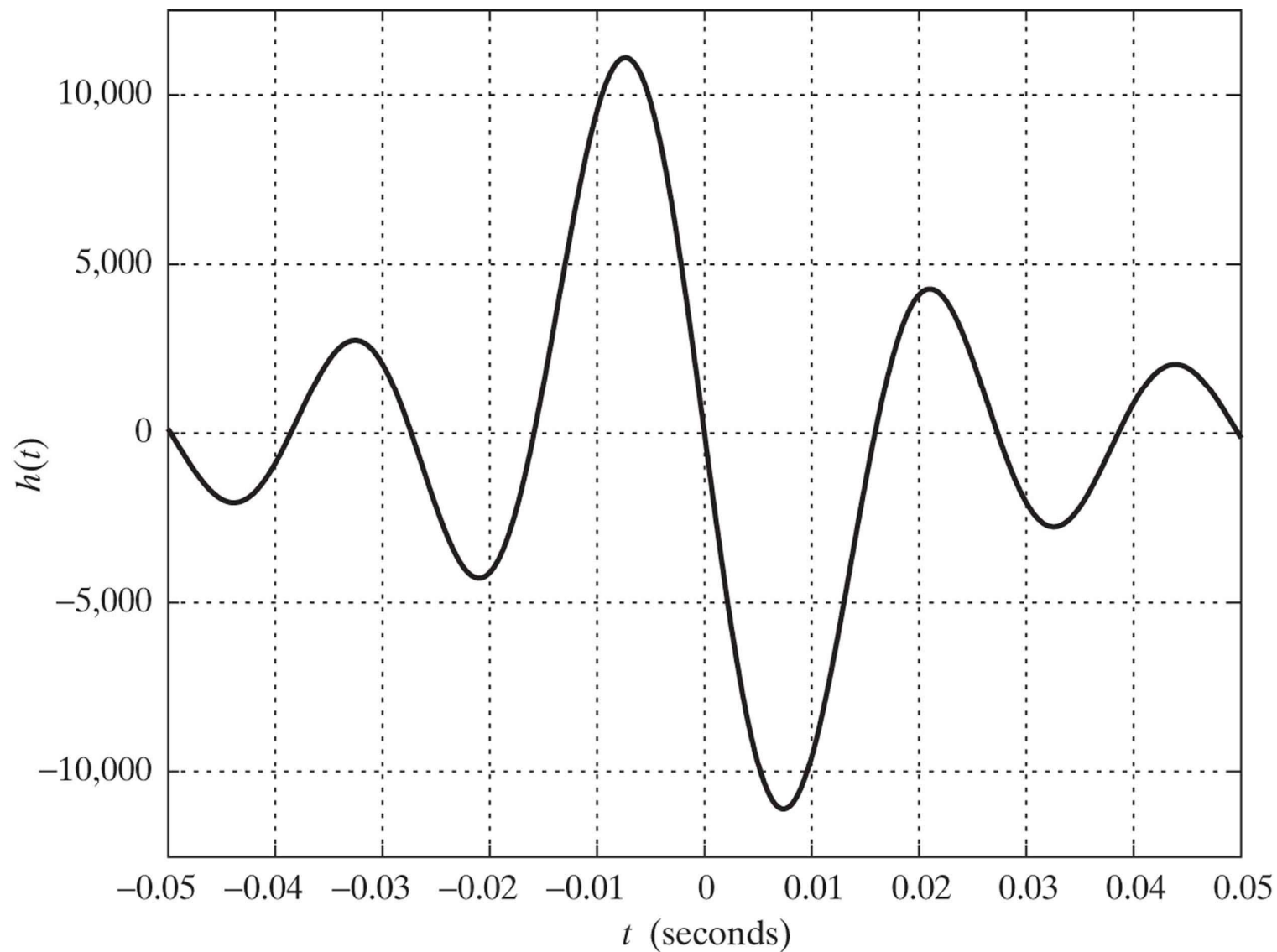


**Figure P7.22**

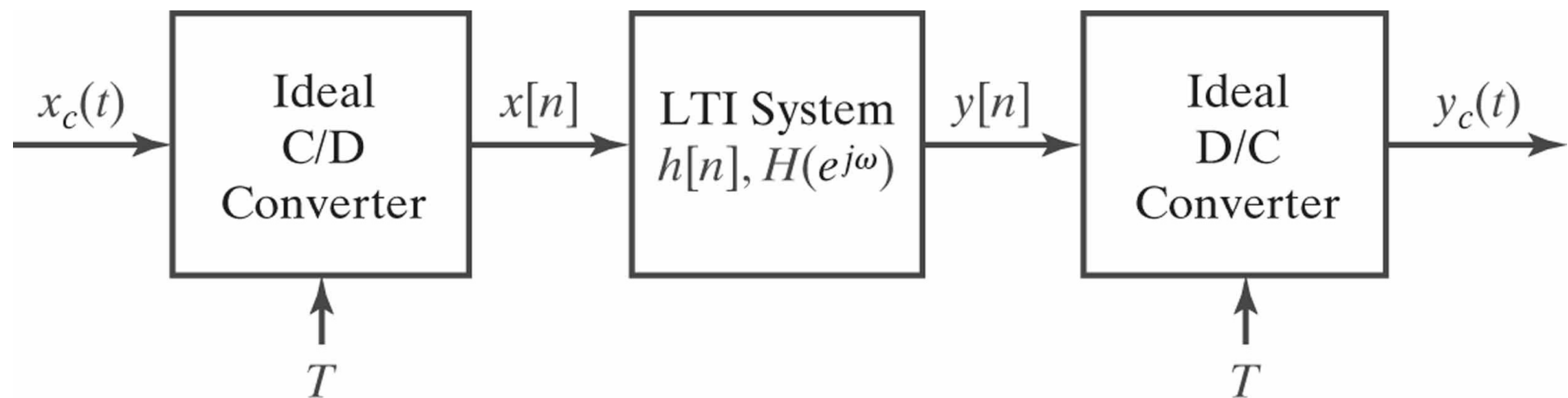


**Figure P7.24**

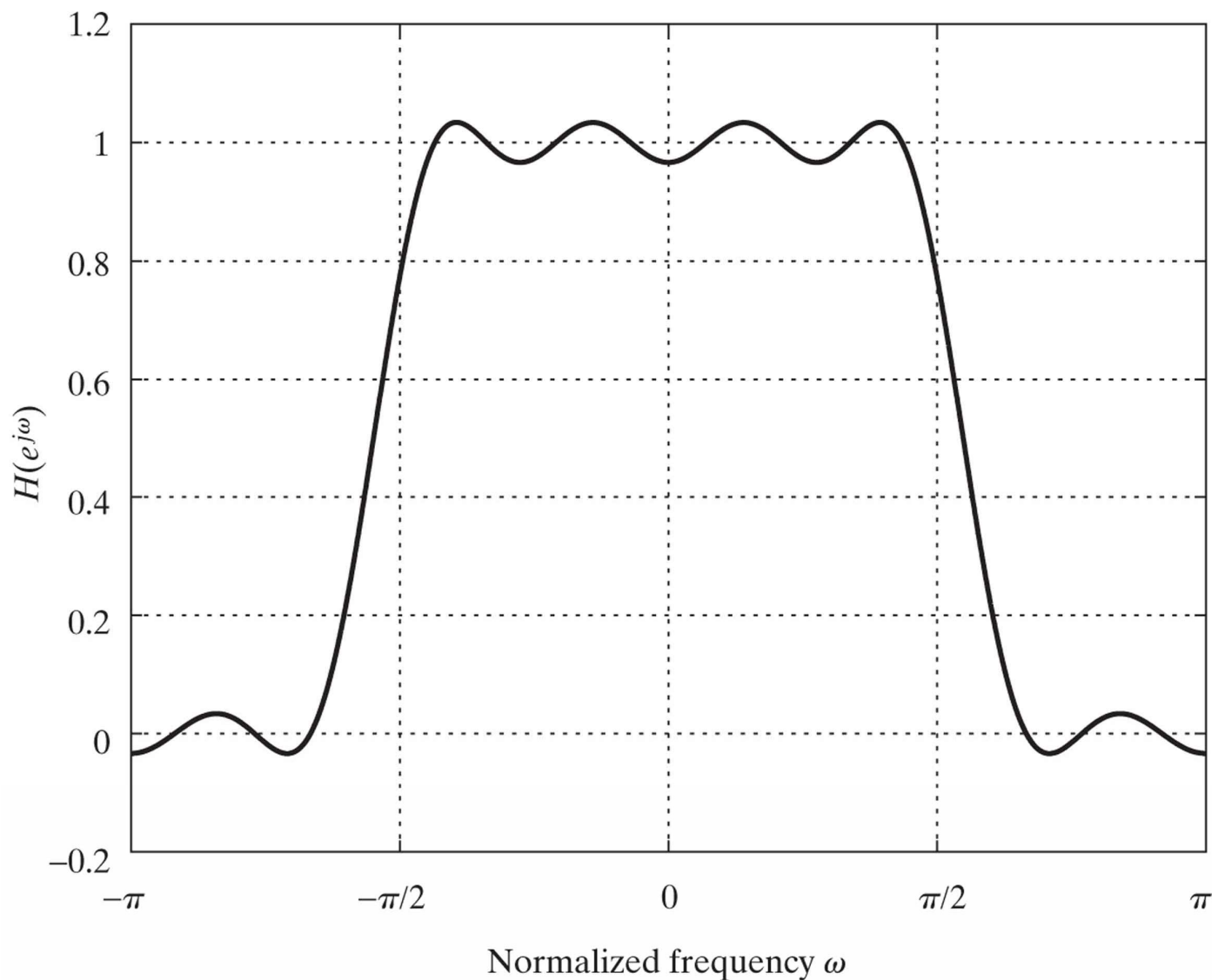


**Figure P7.28**

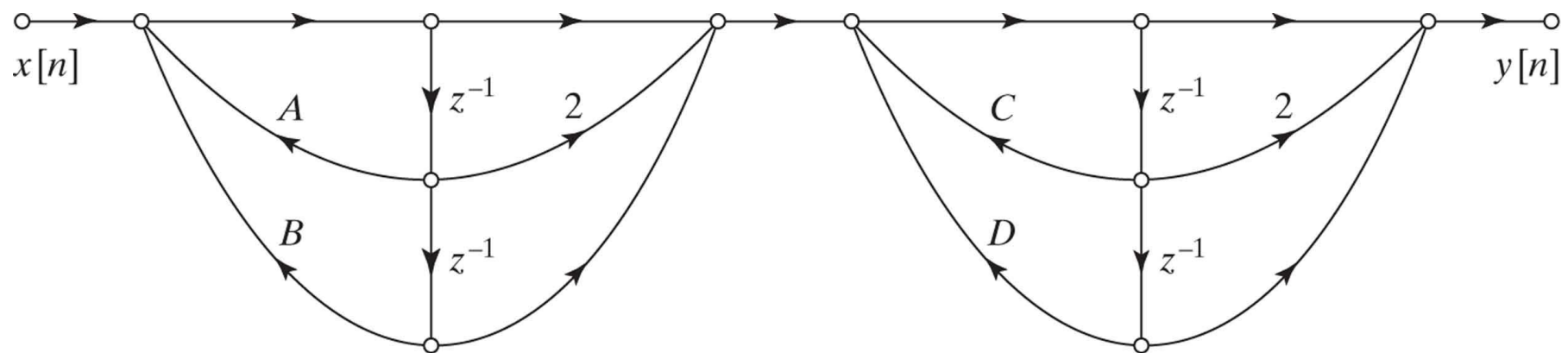


**Figure P7.33**

$$|H_a(j\Omega)|$$

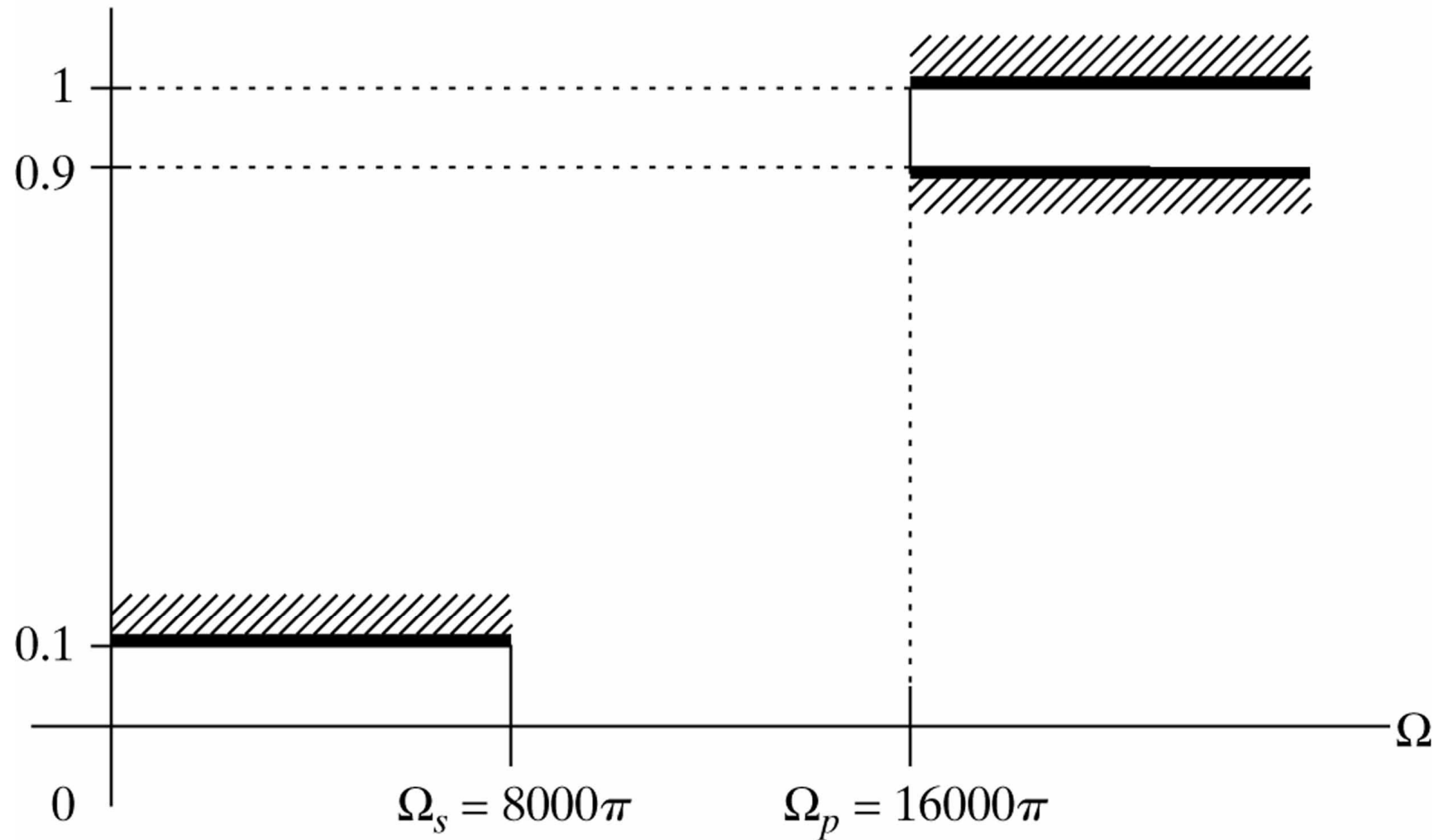


**Figure P7.34**

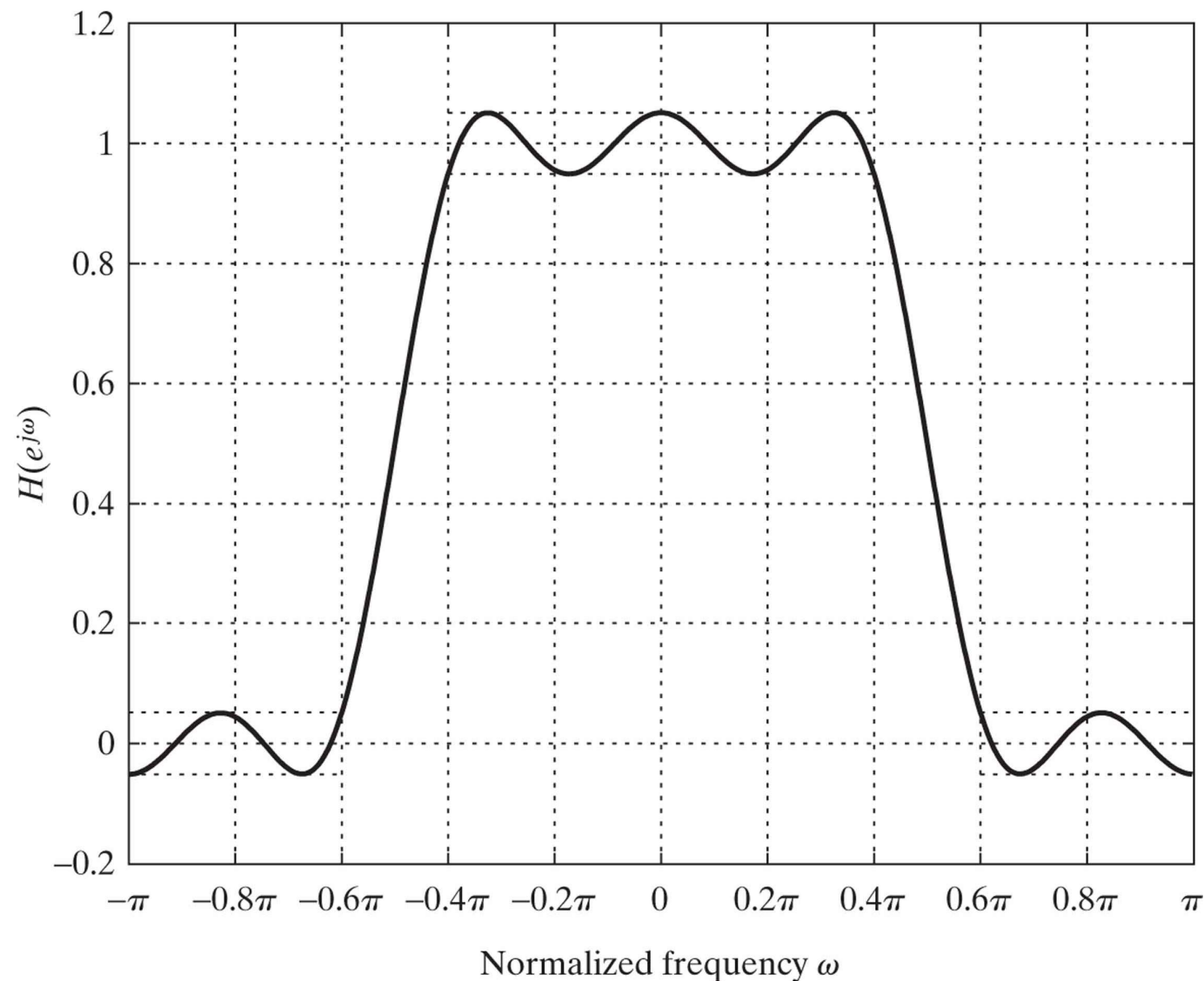


**Figure P7.35**

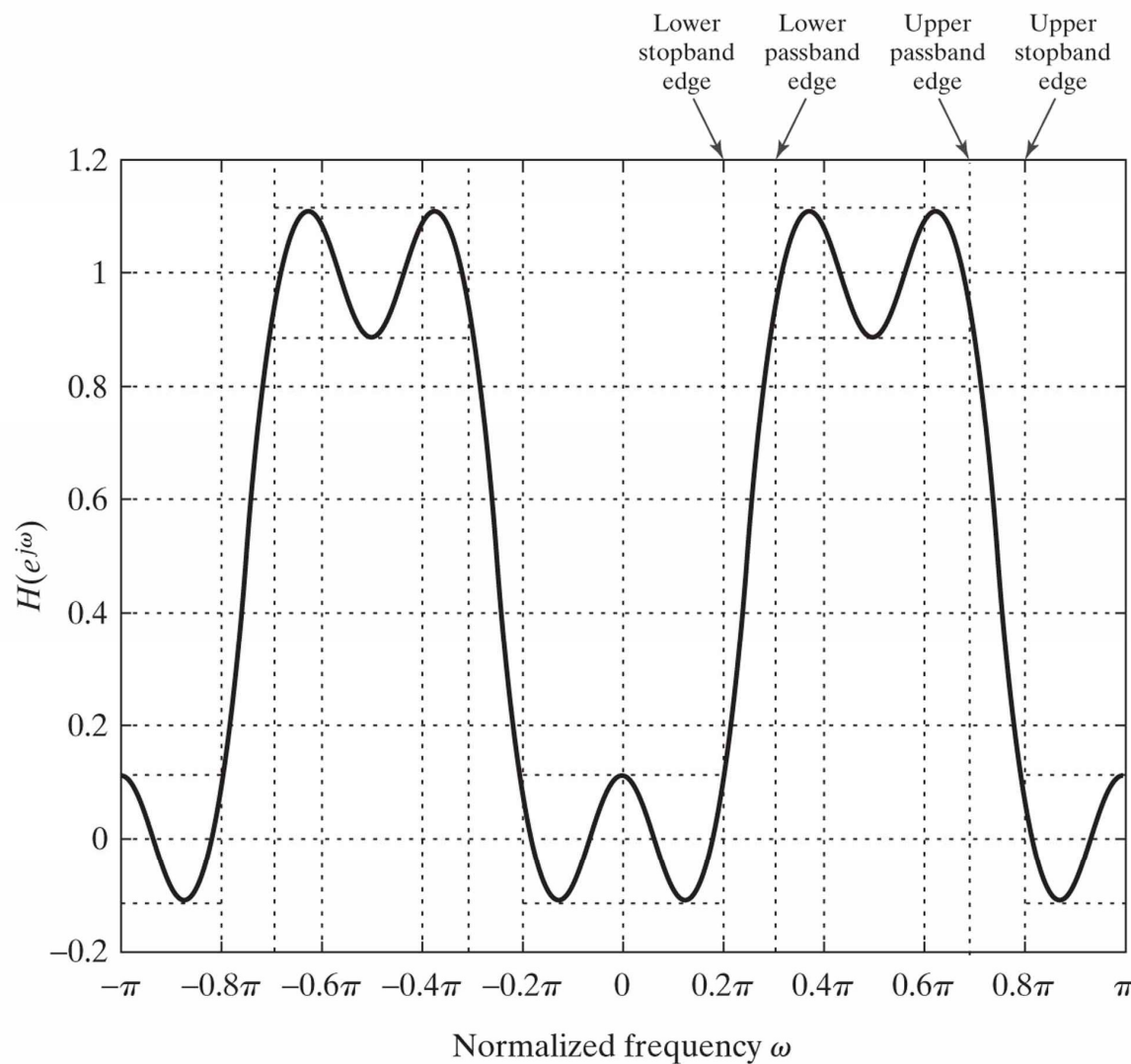


**Figure P7.36**

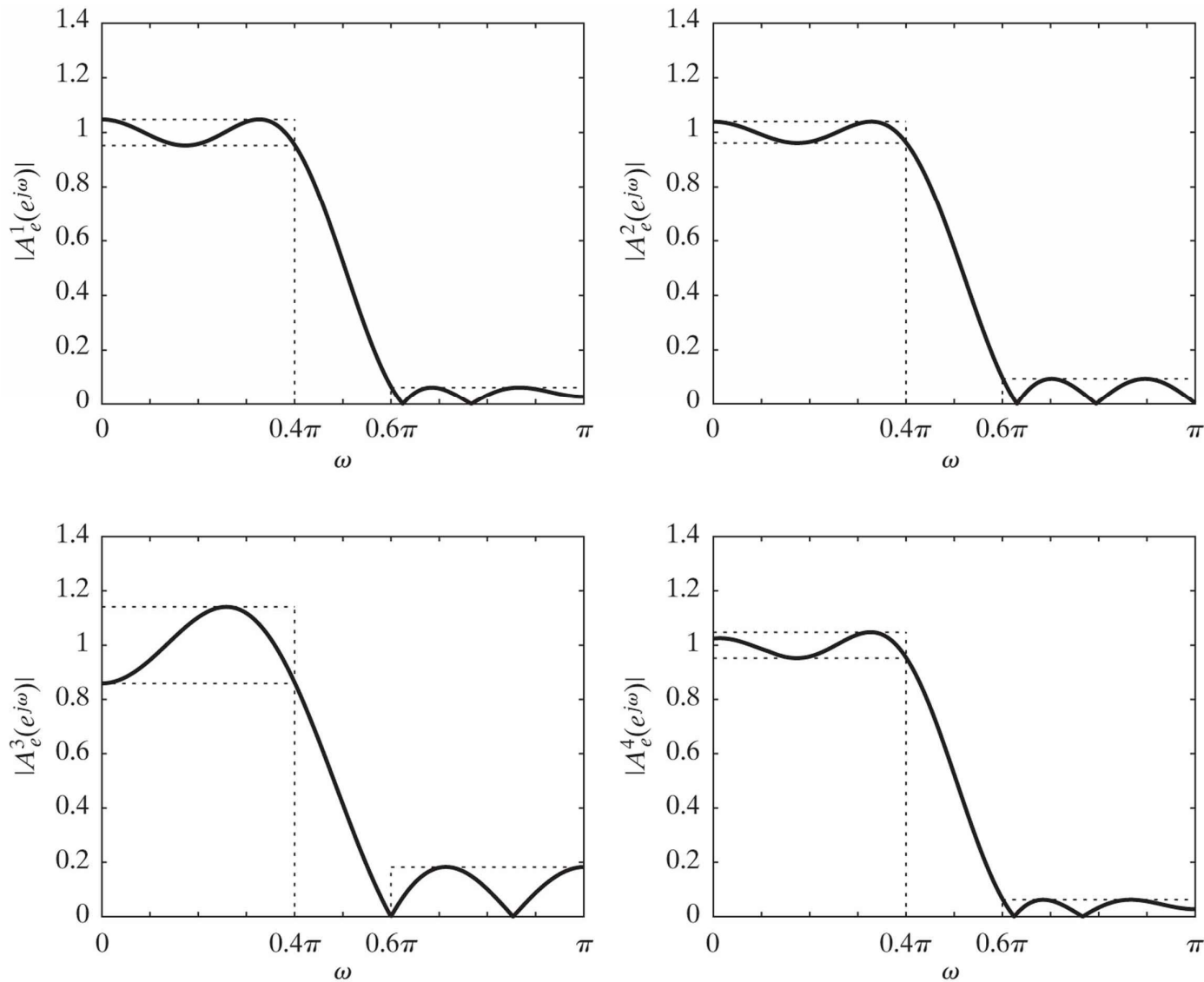


**Figure P7.37**

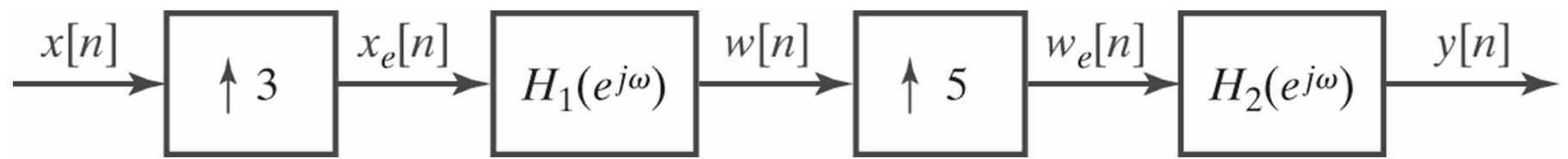


**Figure P7.39**

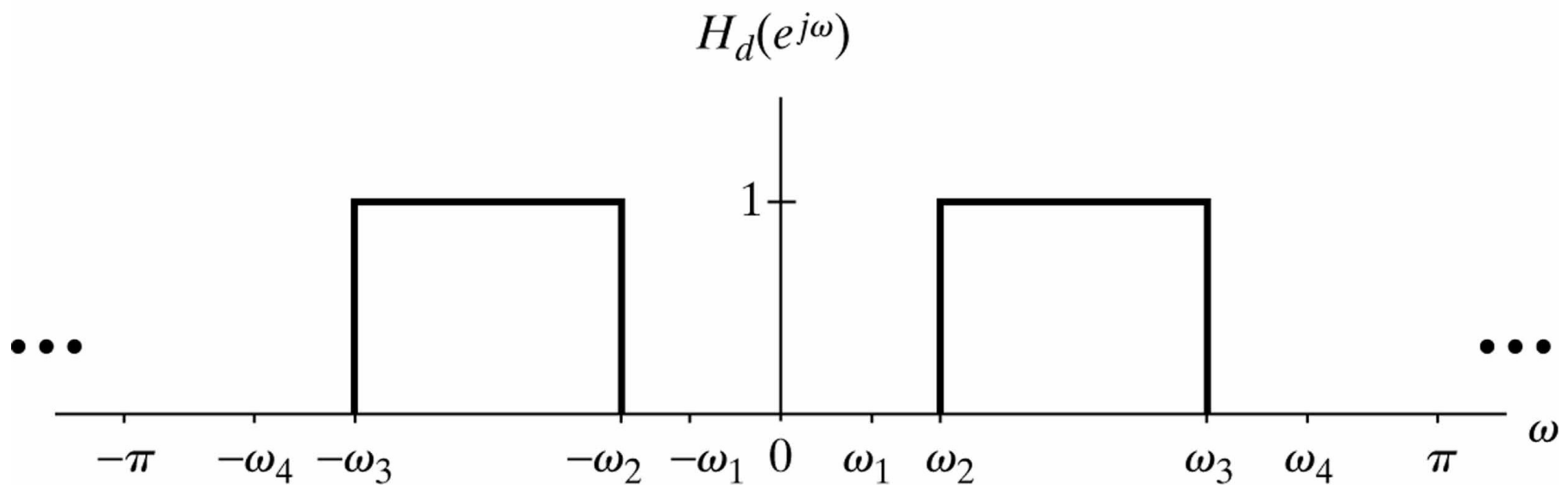


**Figure P7.40-1**

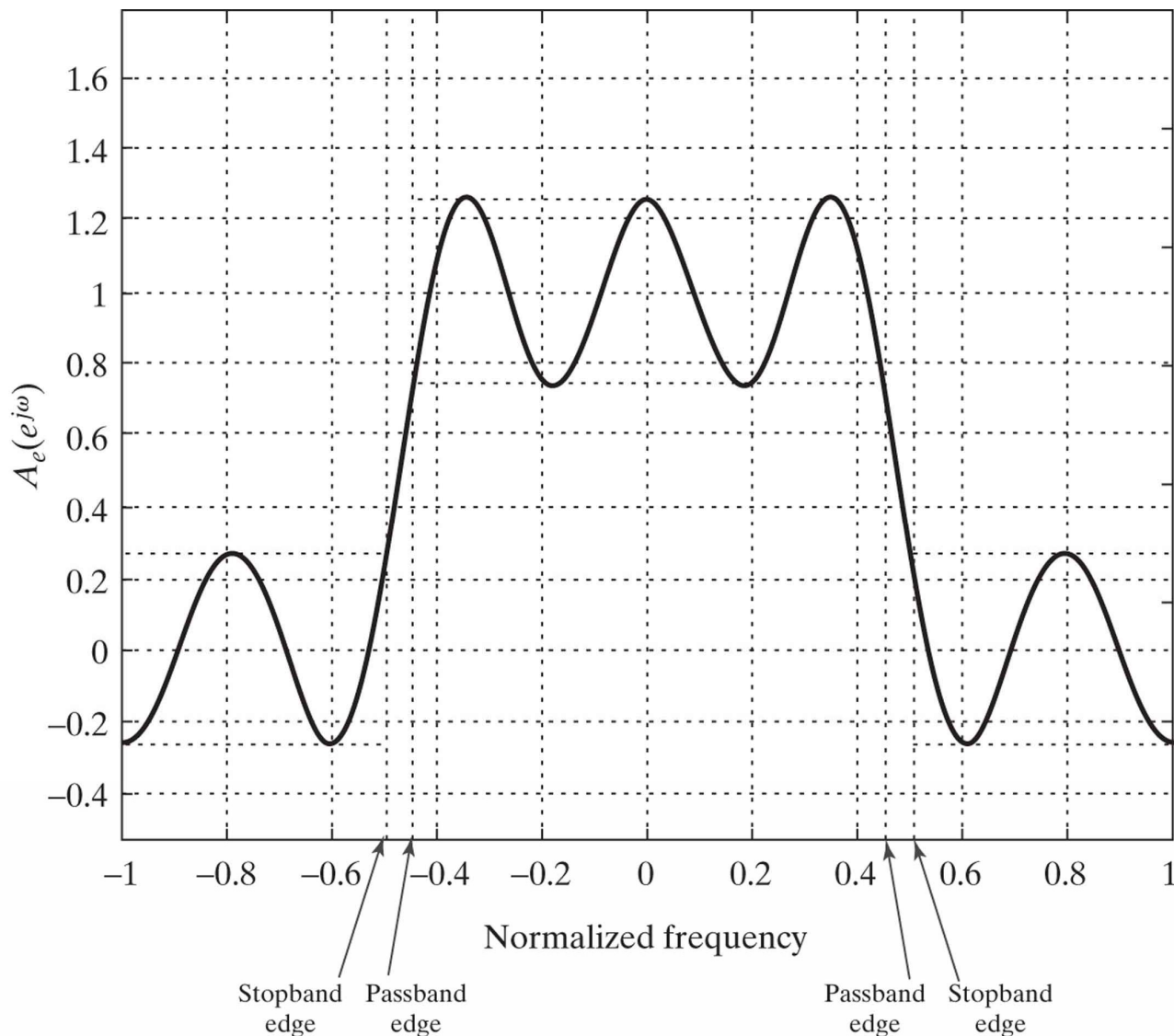


**Figure P7.40-2**

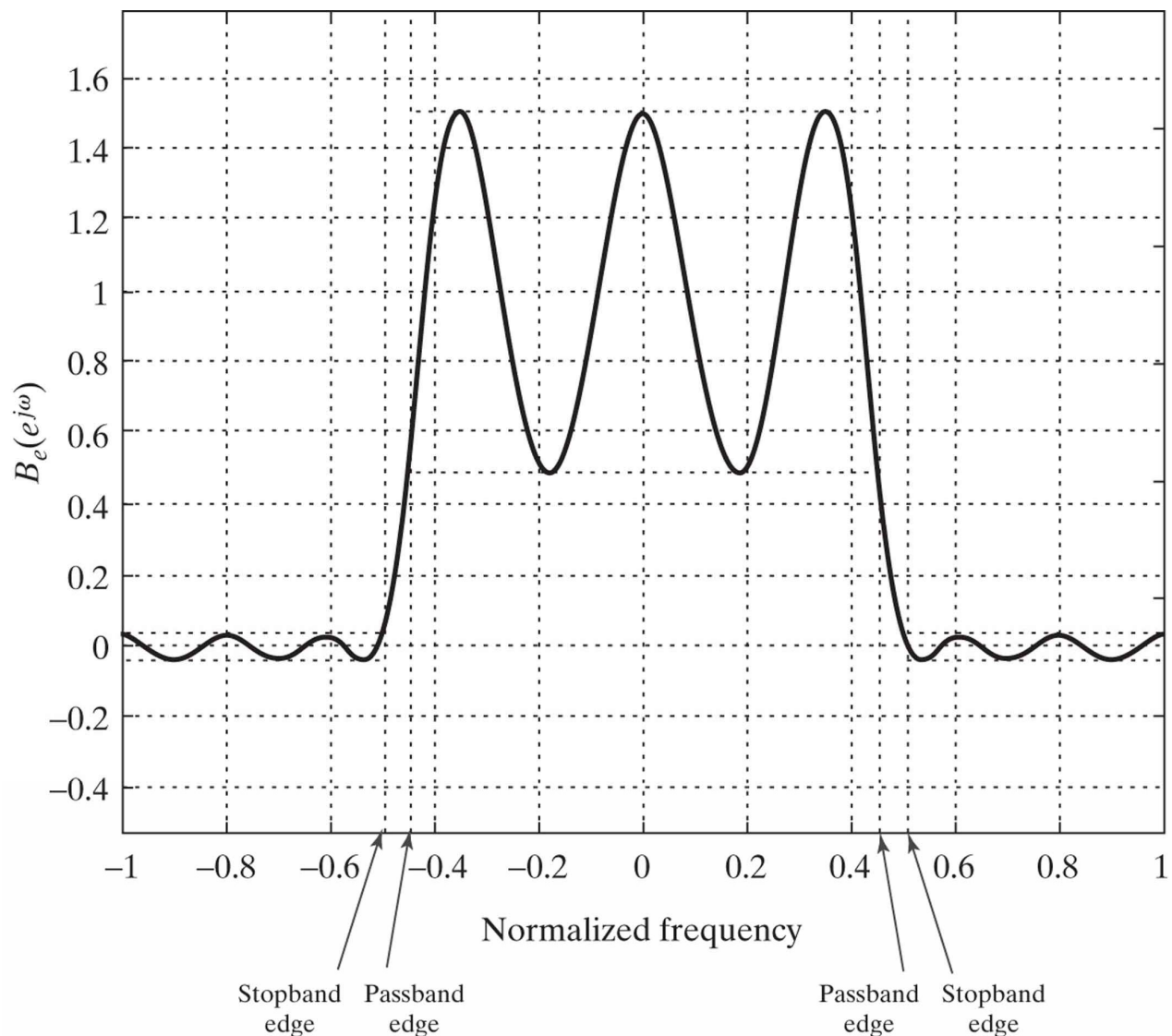


**Figure P7.45**

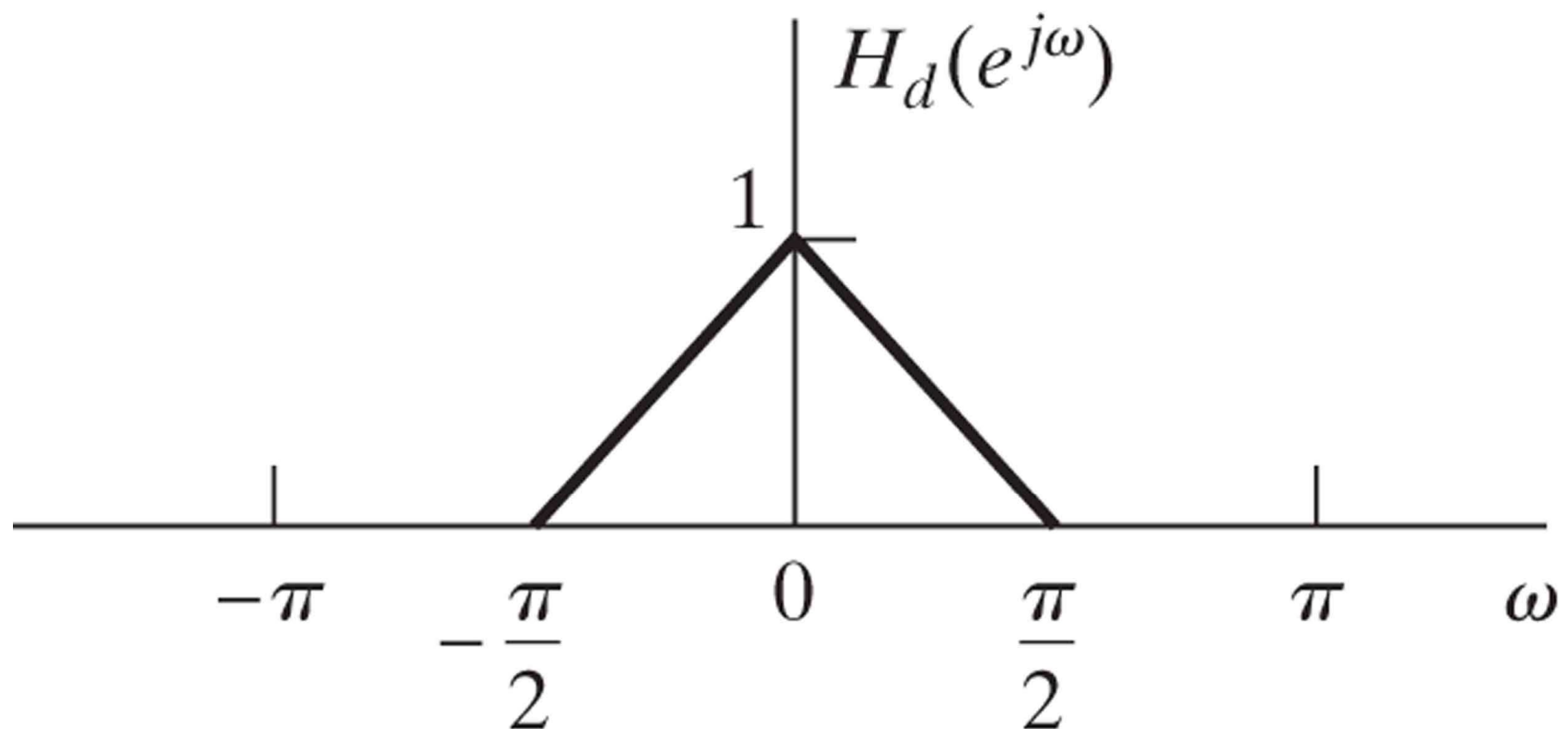


**Figure P7.46**

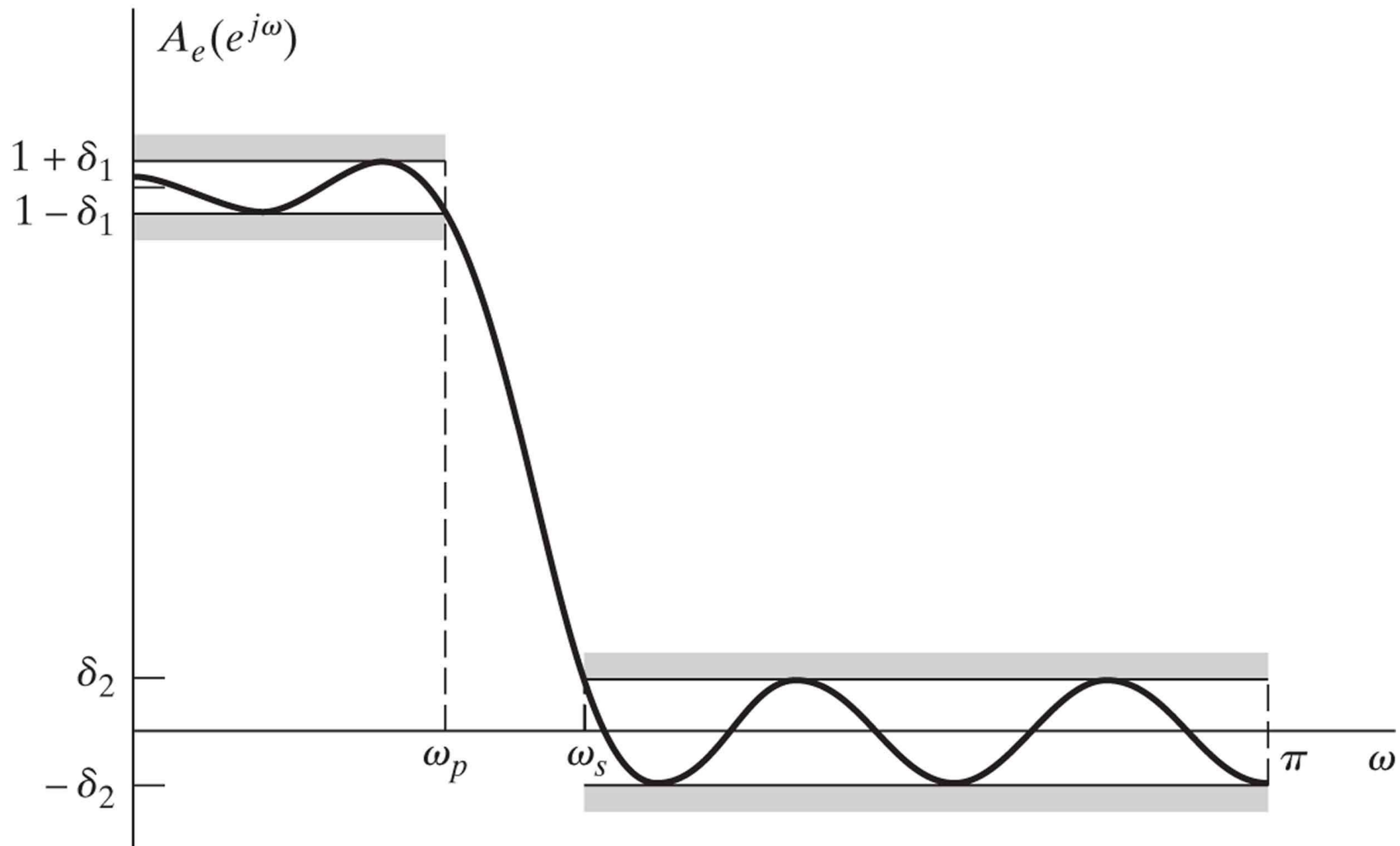


**Figure P7.49**

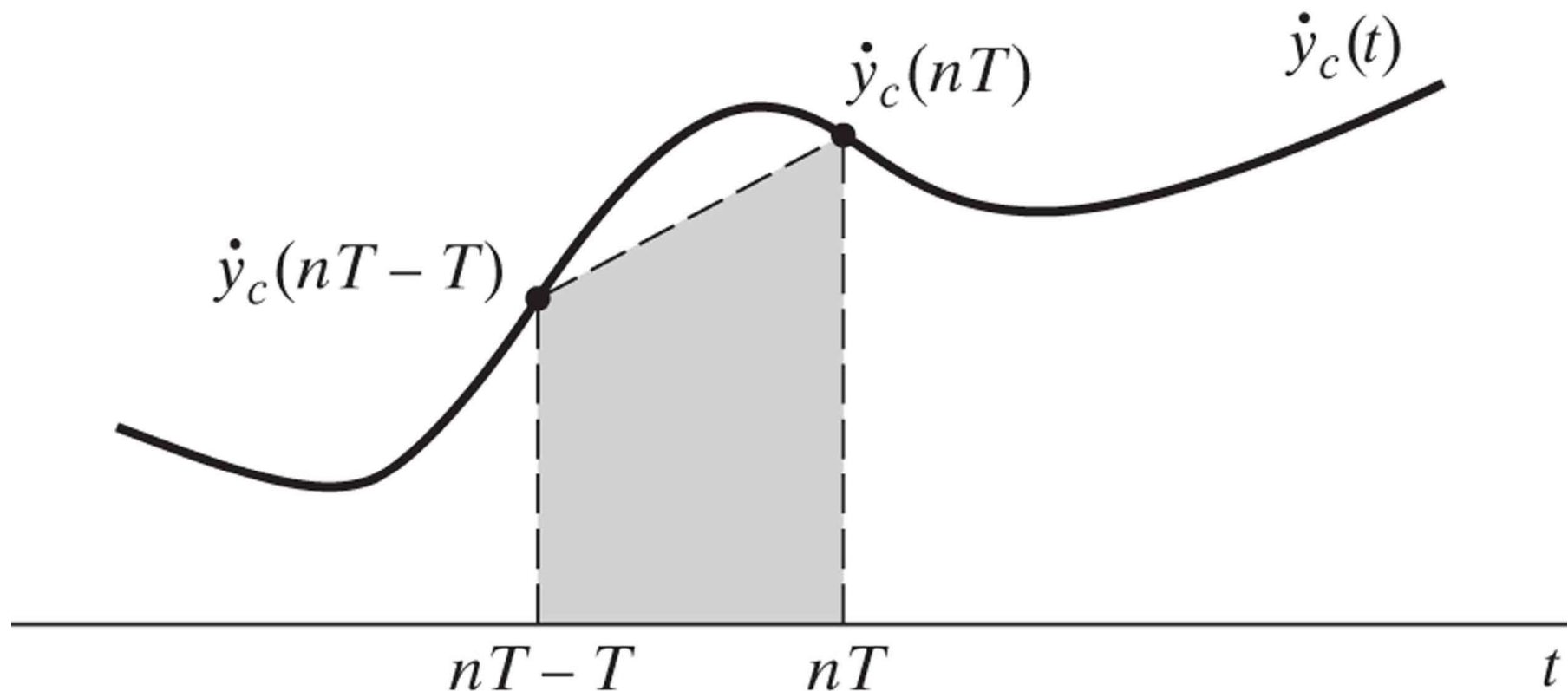


**Figure P7.51-1**



Figure P7.51-2

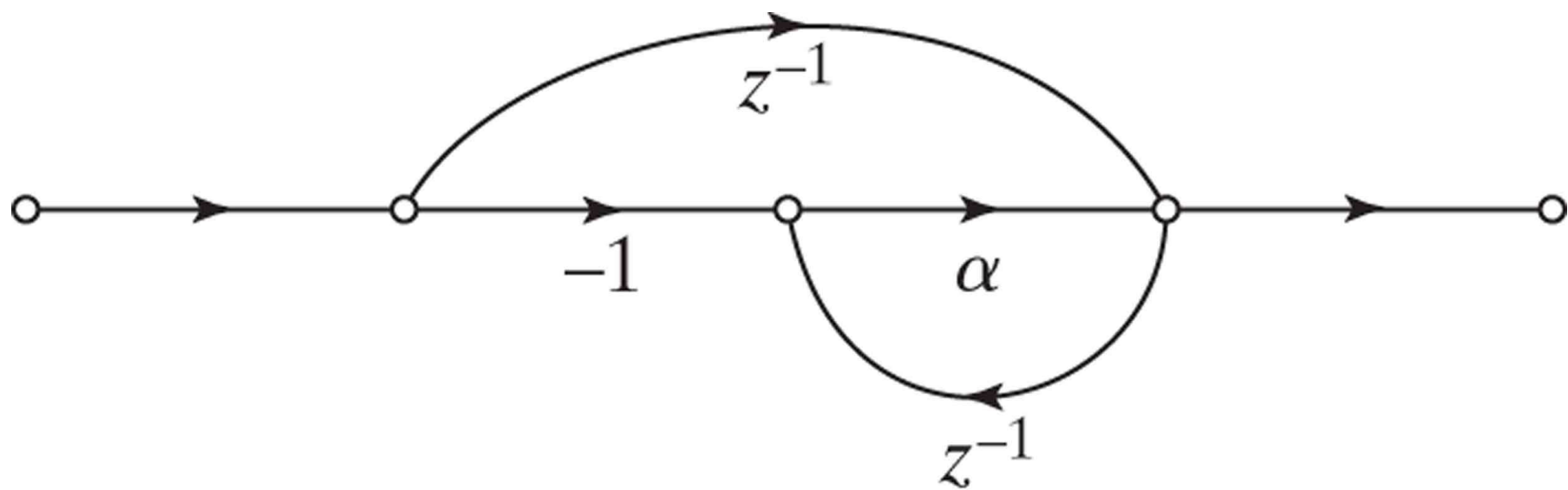


Figure P7.51-3

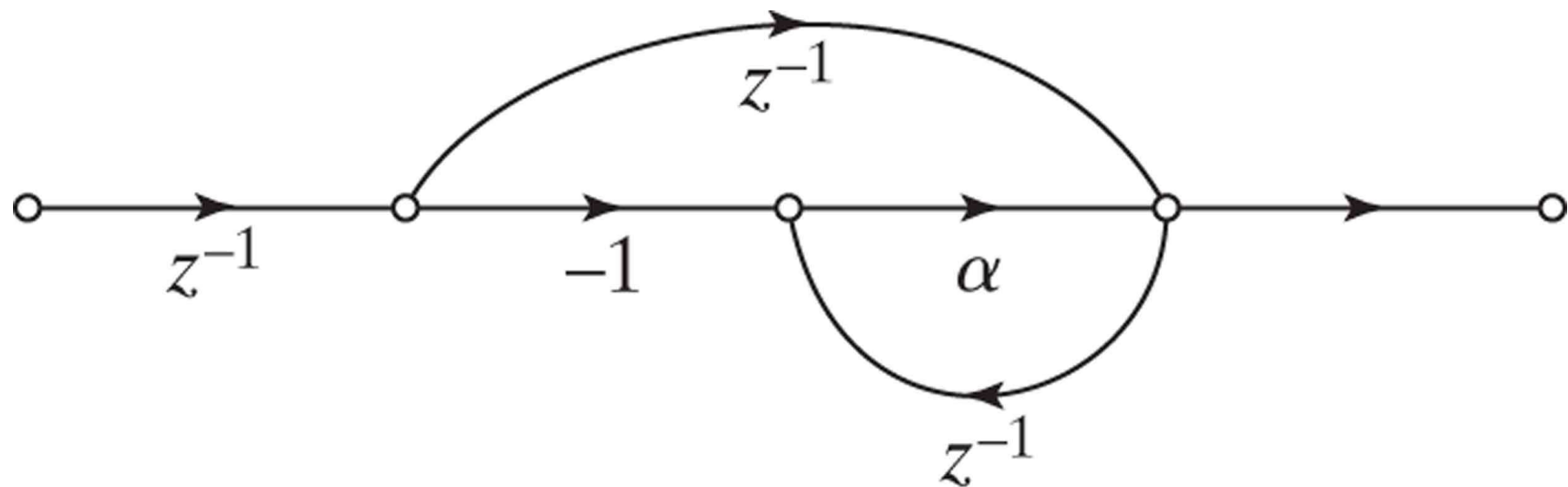
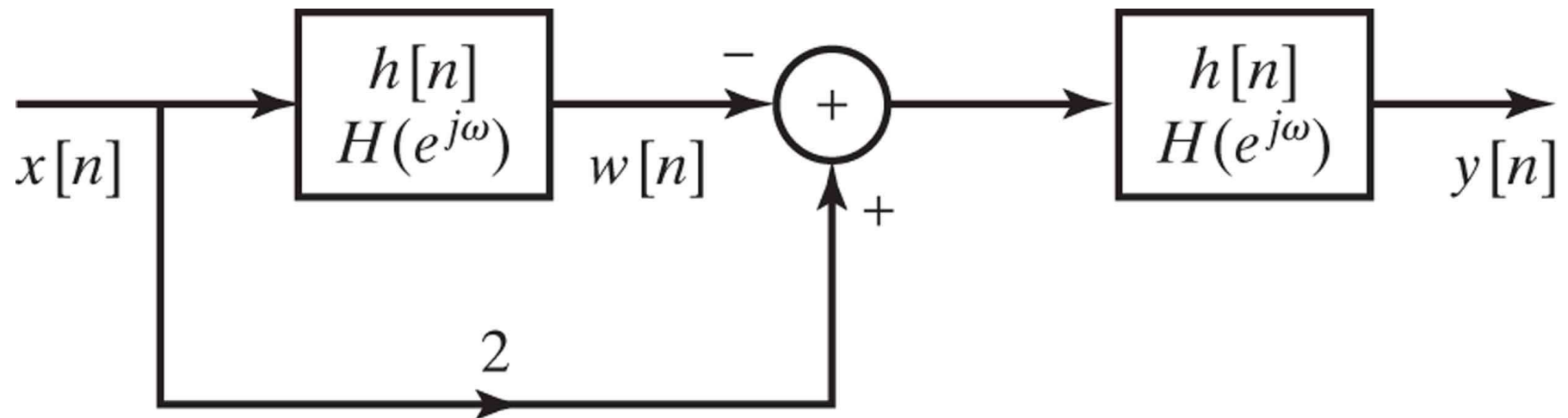
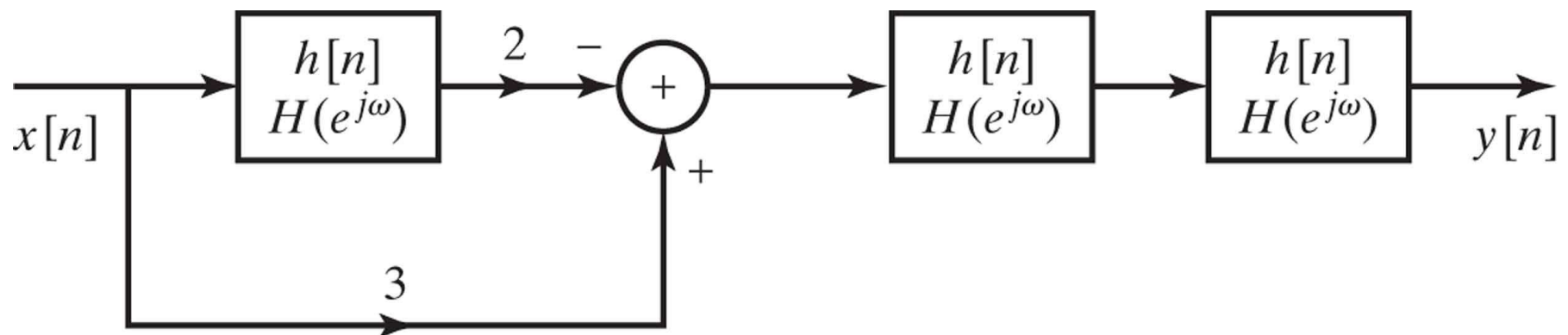


Figure P7.52-1



**Figure P7.52-2**



**Figure P7.54**

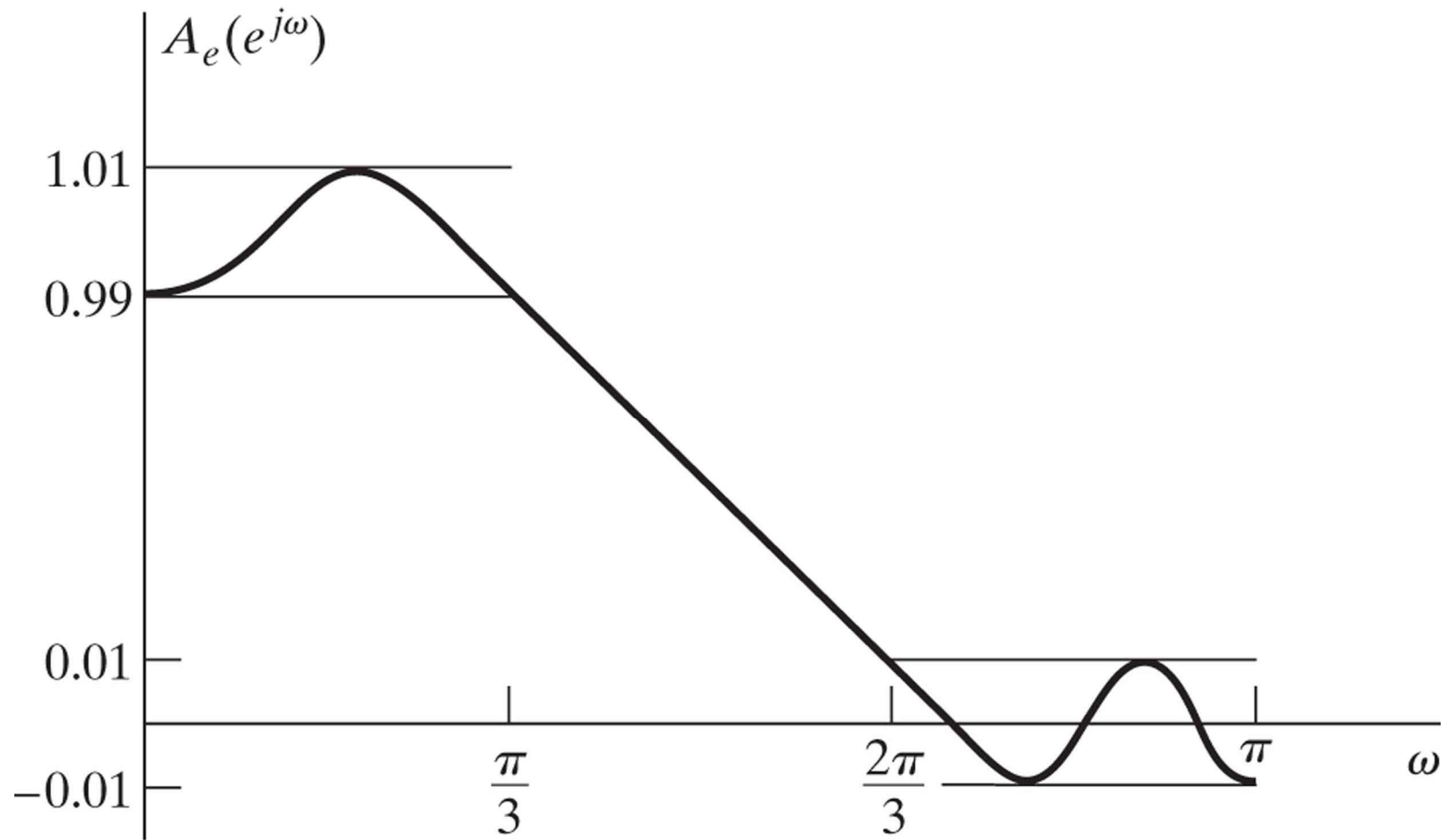


**Figure P7.55**

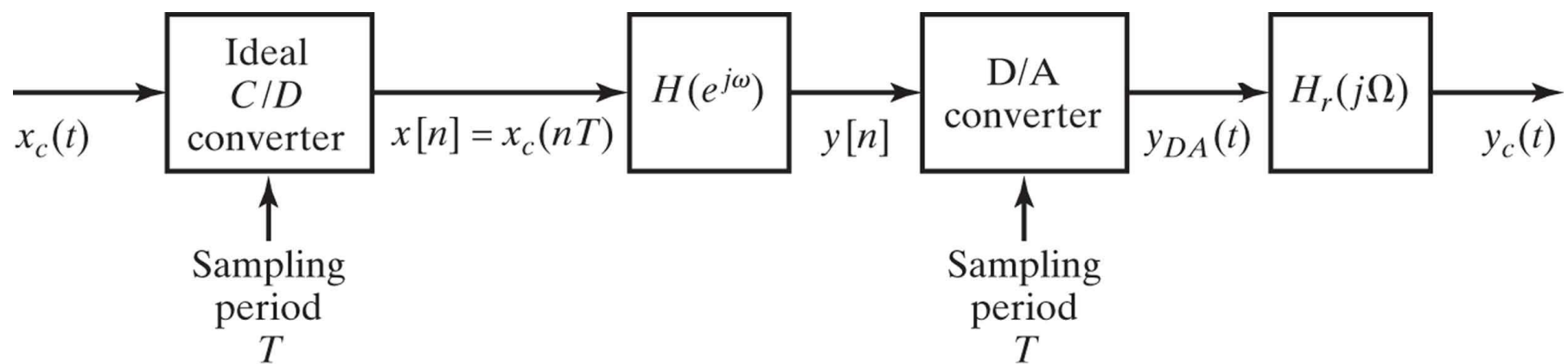
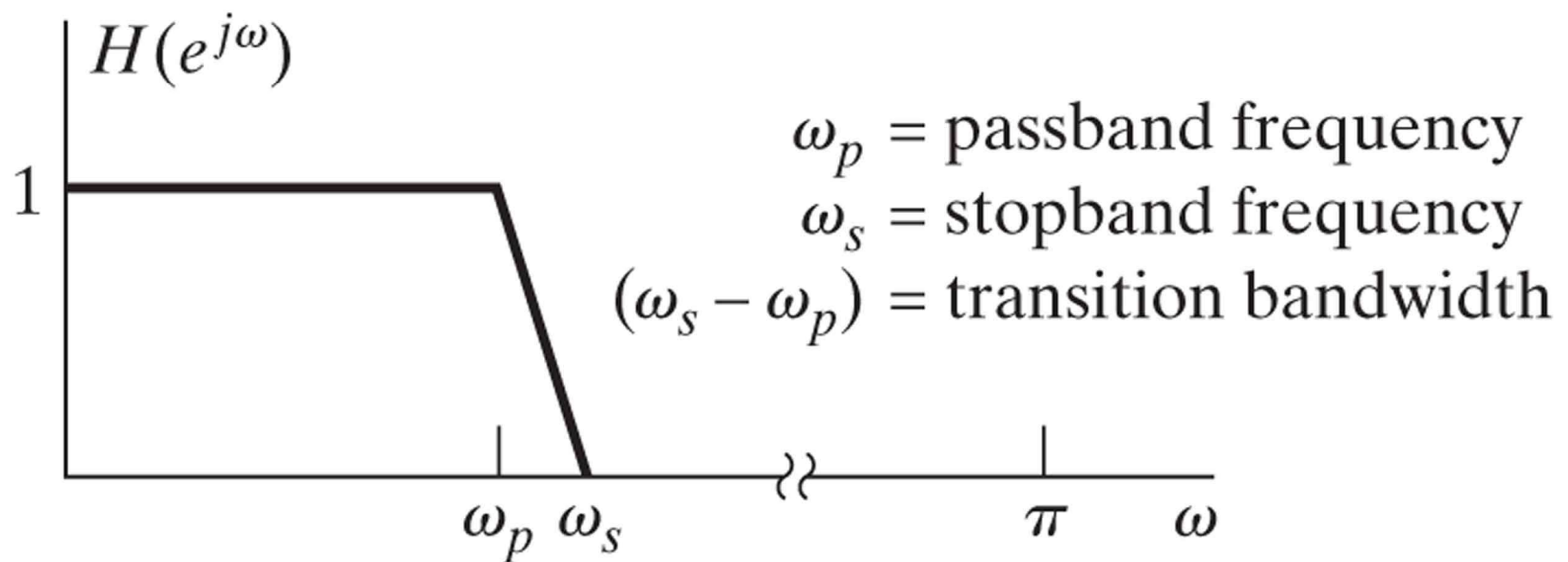
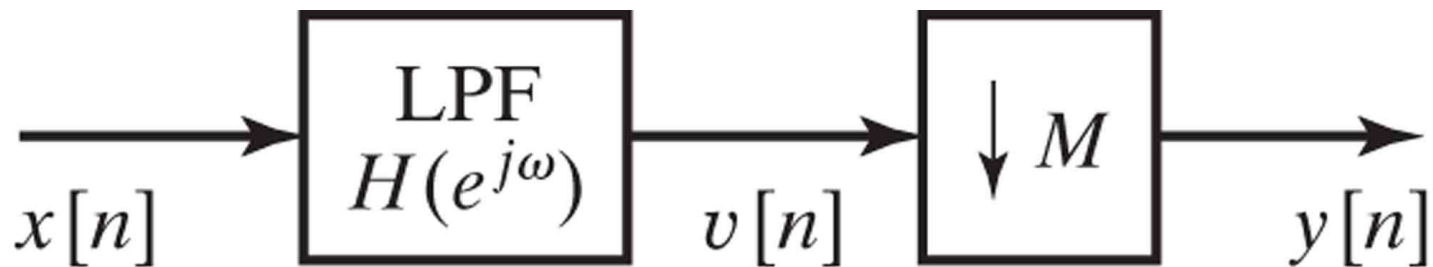
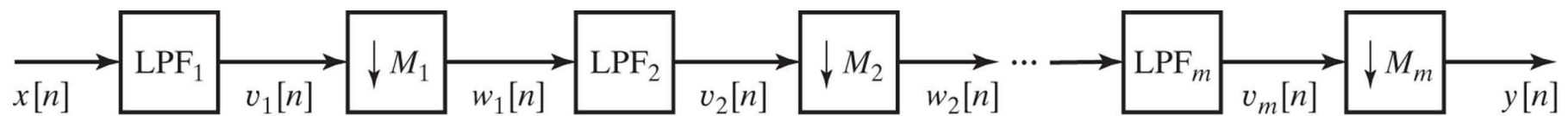


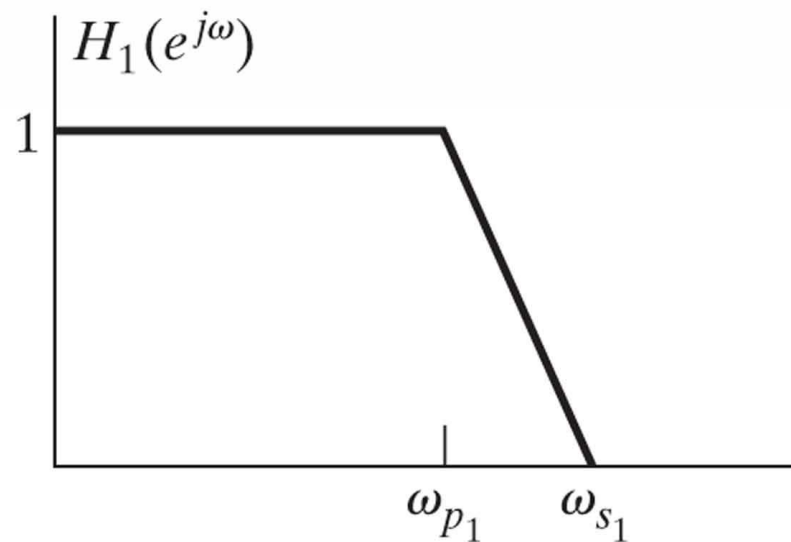
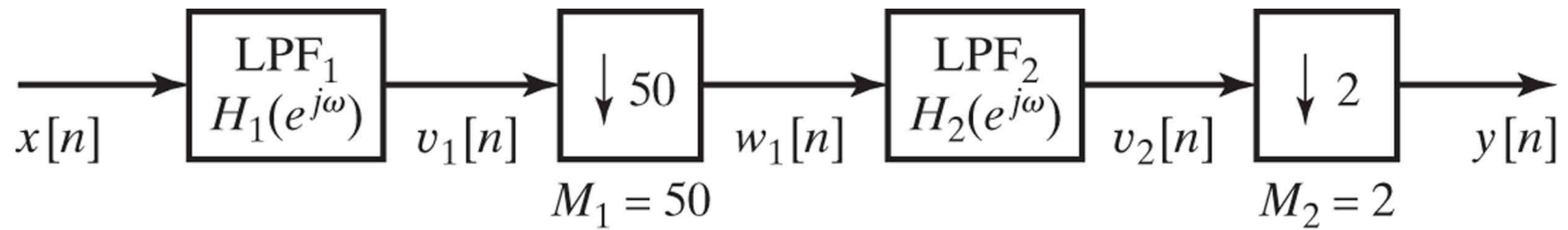
Figure P7.56-1



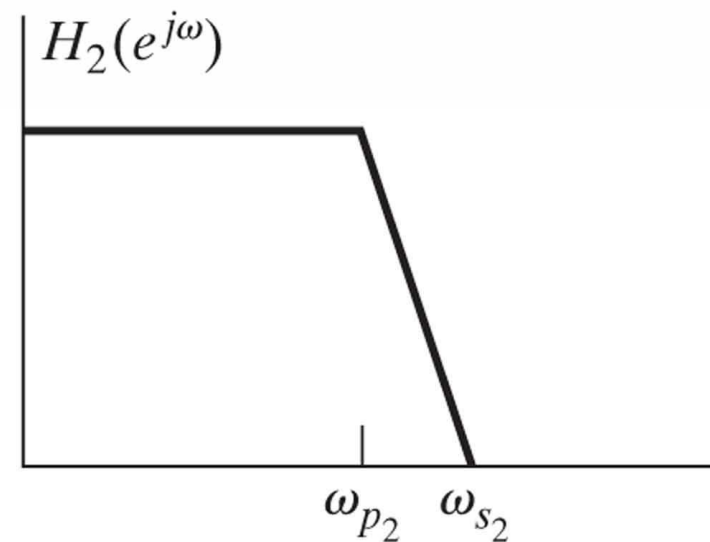
**Figure P7.56-2**



**Figure P7.56-3**



LPF 1



LPF 2

Figure P7.57-1

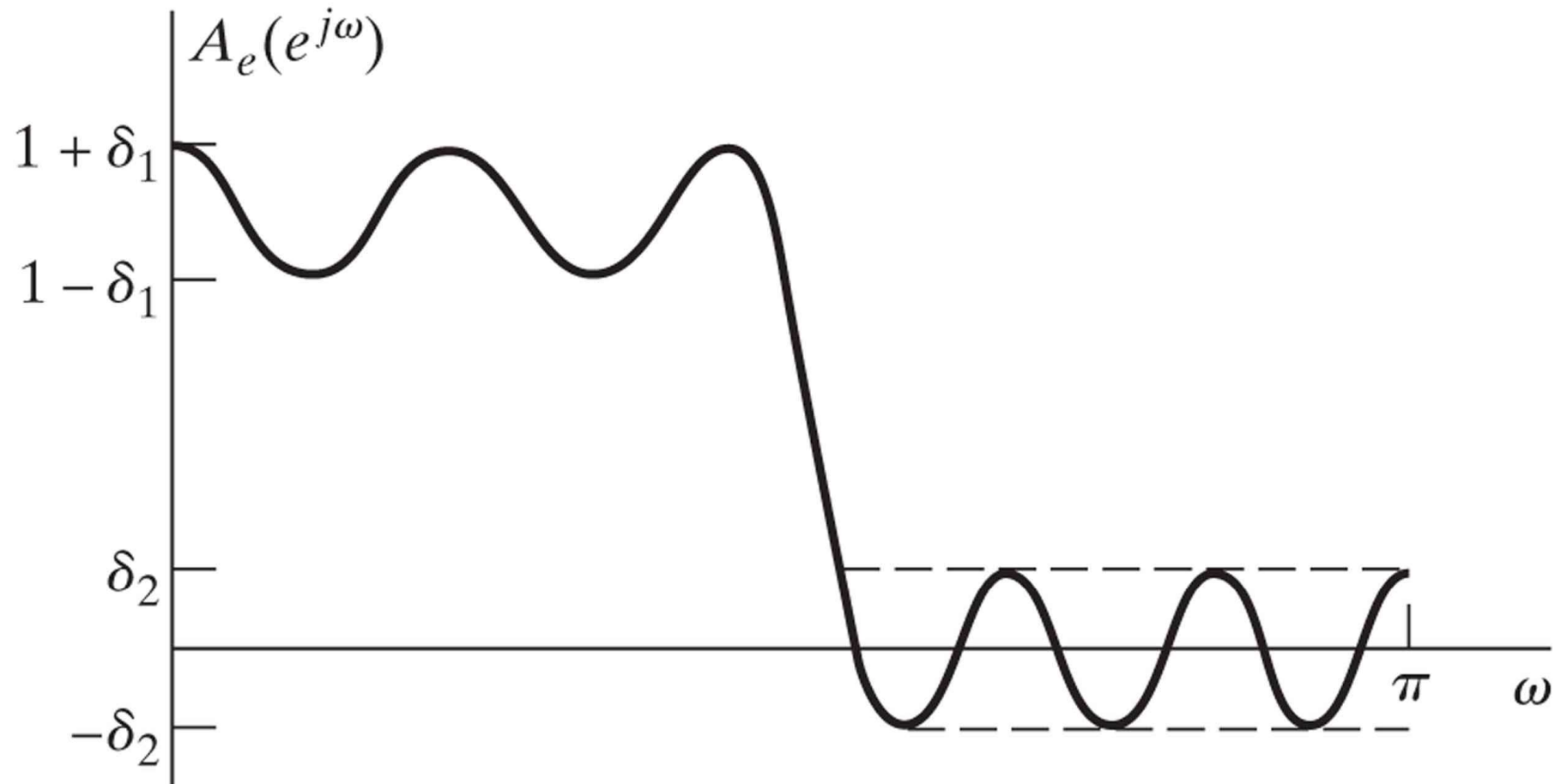
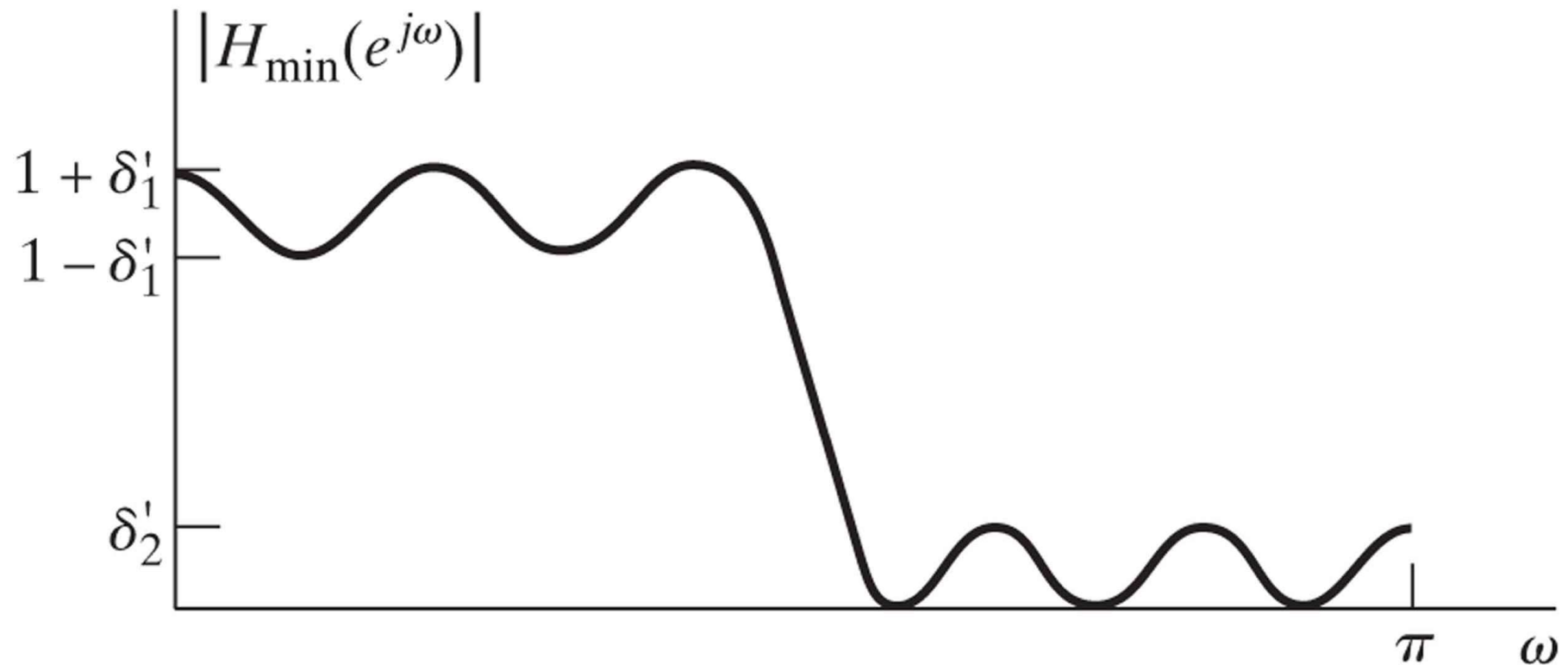
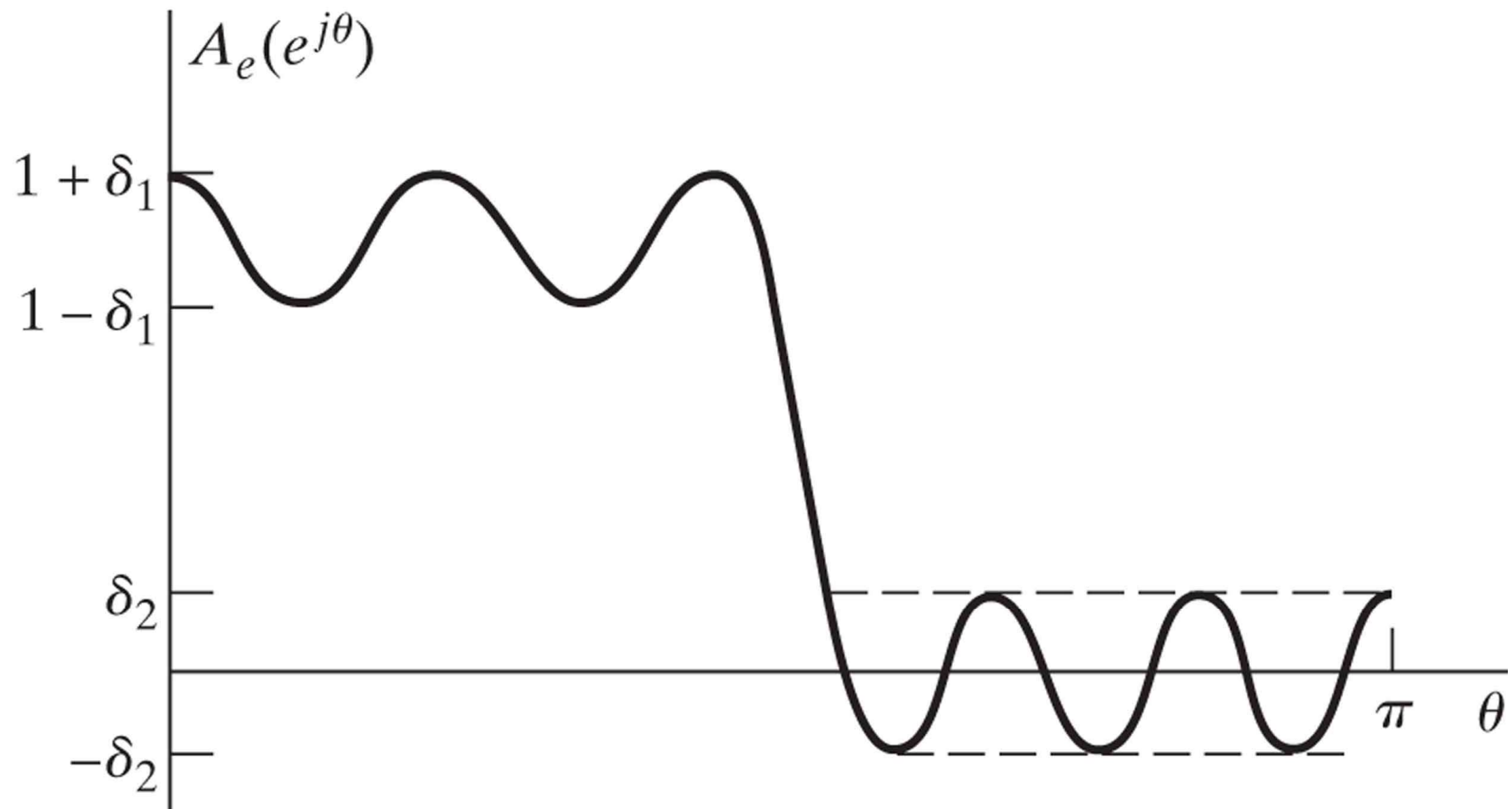


Figure P7.57-2



**Figure P7.59**



**Figure P7.61**

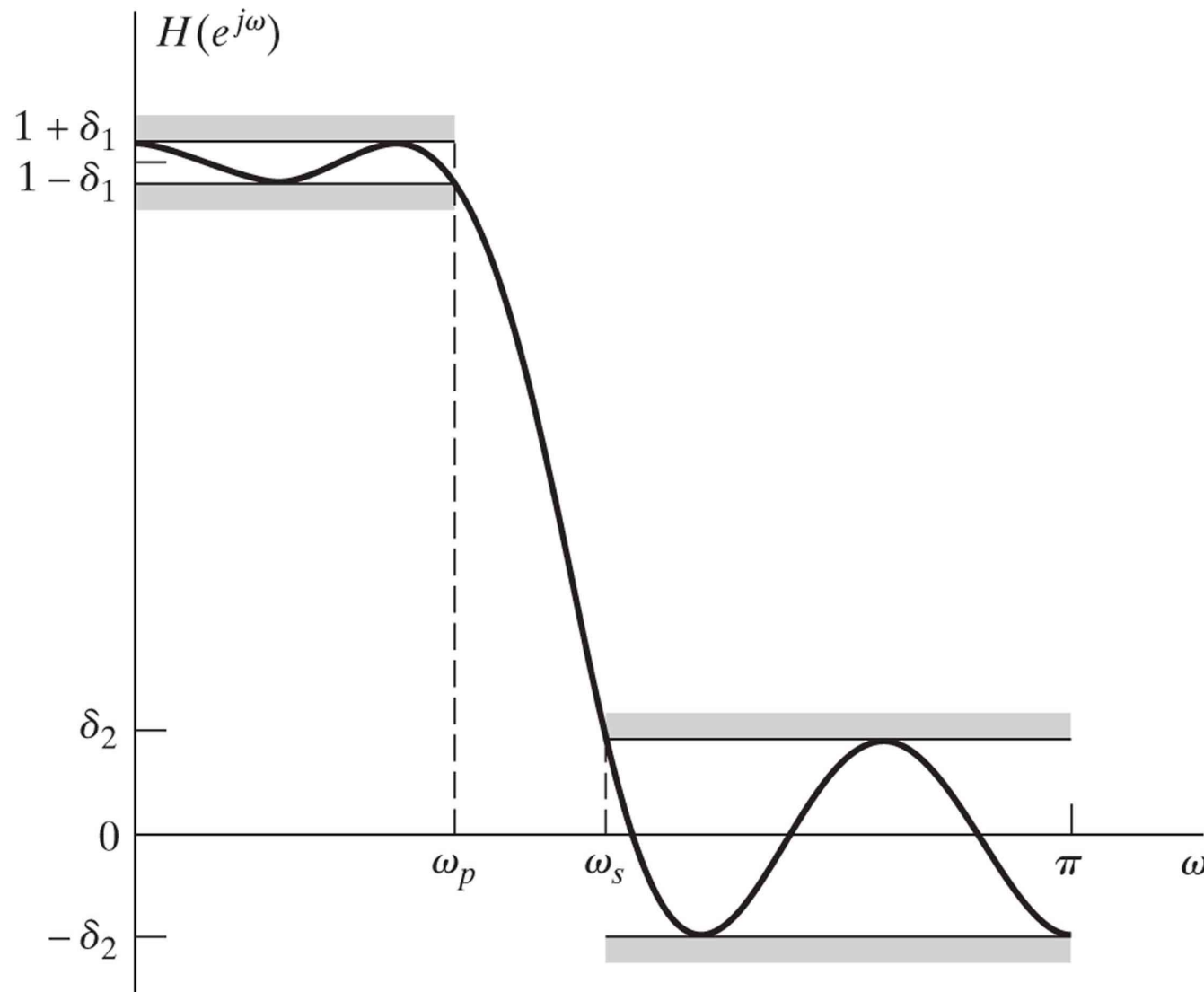


**Figure P7.63**

